

EUROPEAN ORGANISATION FOR NUCLEAR RESEARCH (CERN)



Phys. Rev. D 103, (2021) 112003
DOI: [10.1103/PhysRevD.103.112003](https://doi.org/10.1103/PhysRevD.103.112003)



CERN-EP-2020-201
June 15, 2021

Search for trilepton resonances from chargino and neutralino pair production in $\sqrt{s} = 13$ TeV $p p$ collisions with the ATLAS detector

The ATLAS Collaboration

A search is performed for the electroweak pair production of charginos and associated production of a chargino and neutralino, each of which decays through an R -parity-violating coupling into a lepton and a W , Z , or Higgs boson. The trilepton invariant-mass spectrum is constructed from events with three or more leptons, targeting chargino decays that include an electron or muon and a leptonically decaying Z boson. The analyzed dataset corresponds to an integrated luminosity of 139 fb^{-1} of proton–proton collision data produced by the Large Hadron Collider at a center-of-mass energy of $\sqrt{s} = 13$ TeV and collected by the ATLAS experiment between 2015 and 2018. The data are found to be consistent with predictions from the Standard Model. The results are interpreted as limits at 95% confidence level on model-independent cross sections for processes beyond the Standard Model. Limits are also set on the production of charginos and neutralinos for a Minimal Supersymmetric Standard Model with an approximate $B - L$ symmetry. Charginos and neutralinos with masses between 100 GeV and 1100 GeV are excluded depending on the assumed decay branching fractions into a lepton (electron, muon, or τ -lepton) plus a boson (W , Z , or Higgs).

1 Introduction

The extension of the Standard Model (SM) of particle physics with supersymmetry (SUSY) [1–6] can introduce processes that violate baryon number (B) and lepton number (L) conservation, for instance proton decay. As such processes have not been observed, it is common to introduce an *ad hoc* requirement to conserve R -parity [7], where the R -parity of a particle is defined as $R = (-1)^{3(B-L)+2s}$. Here the B , L , and s are the baryon number, lepton number, and spin of the particle, respectively. All SM particles have $R = 1$ and their SUSY partners have $R = -1$. R -parity conservation (RPC) therefore requires the lightest SUSY particle (LSP) to be stable. In RPC scenarios, a stable LSP must necessarily be neutral in electric and color charge to be compatible with astrophysical data [8, 9].

Theories predicting R -parity violation (RPV) [10, 11] are viable if the interactions that violate $B - L$ conservation have small couplings and violate only one of B or L at tree level, thus preventing rapid proton decay. The benchmark model for this search is a Minimal Supersymmetric Standard Model (MSSM) [12, 13] extension that adds a gauged $U(1)_{B-L}$ [14–18] to the $SU(3)_C \times SU(2)_L \times U(1)_Y$ of the SM and includes three generations of right-handed neutrino supermultiplets. Any one of the right-handed sneutrinos has the correct quantum numbers to spontaneously break the $B - L$ symmetry, and its vacuum expectation value (VEV) introduces L violation only at tree level [17]. The size of the RPV coupling is directly related to the right-handed sneutrino VEV, and therefore to the neutrino sector. As a consequence the RPV coupling is kept small by the small values of the neutrino masses. The LSP may decay into SM particles through the RPV coupling, which allows the LSP to have electric and color charges.

The $B - L$ RPV model predicts unique signatures [19, 20] that are forbidden if R -parity conservation is assumed. In a set of simulations [21, 22] the MSSM parameters were scanned and the exact physical sparticle spectrum was calculated for each simulated point. It was seen [23, 24] that two likely LSP candidates with moderate production cross sections at the Large Hadron Collider (LHC) are the wino-type chargino ($\tilde{\chi}_1^\pm$) and wino-type neutralino ($\tilde{\chi}_1^0$), the SUSY partners of the electroweak gauge fields of the W bosons. Both LSP candidates were found to be nearly mass degenerate with one another for all simulations and therefore both decay primarily via RPV couplings [24]. The RPV coupling was also found by the simulations to be large enough that both the $\tilde{\chi}_1^\pm$ and $\tilde{\chi}_1^0$ decay promptly [24]. Therefore, this search targets prompt decays. In this model the chargino may decay into a Z boson and a charged lepton ($Z\ell$), a Higgs boson and a charged lepton ($H\ell$), or a W boson and a neutrino ($W\nu$), while the neutralino may decay into $W\ell$, $Z\nu$, or $H\nu$, as shown in Figure 1. The $\tilde{\chi}_1^\pm$ and $\tilde{\chi}_1^0$ branching fractions depend on $\tan\beta$, the ratio of the VEVs of the two Higgs fields, and the neutrino mass hierarchy. For example, the branching fractions to electrons are predicted to be small in the normal hierarchy.

This paper presents a search for the electroweak pair production of two charginos ($\tilde{\chi}_1^\pm\tilde{\chi}_1^\mp$) or associated production of a chargino and neutralino ($\tilde{\chi}_1^\pm\tilde{\chi}_1^0$). In contrast to RPC searches, there is no significant missing transverse momentum from an invisible LSP in the event, and all decay products can leave visible energy deposits in the detector. A resonance search in the trilepton mass ($m_{Z\ell}$) is performed in three orthogonal signal regions, all of which target events where the decay of at least one $\tilde{\chi}_1^\pm$ forms a trilepton resonance. One signal region requires four or more leptons and targets events where the second $\tilde{\chi}_1^\pm$ or $\tilde{\chi}_1^0$ (denoted hereafter by $\tilde{\chi}_1^\pm/\tilde{\chi}_1^0$) decay can be fully reconstructed. A second signal region also requires four or more leptons but targets decays of the second $\tilde{\chi}_1^\pm/\tilde{\chi}_1^0$ that include one or more leptons and at least one neutrino. A third signal region requires exactly three leptons, targeting decays of the second $\tilde{\chi}_1^\pm/\tilde{\chi}_1^0$ that include no leptons.

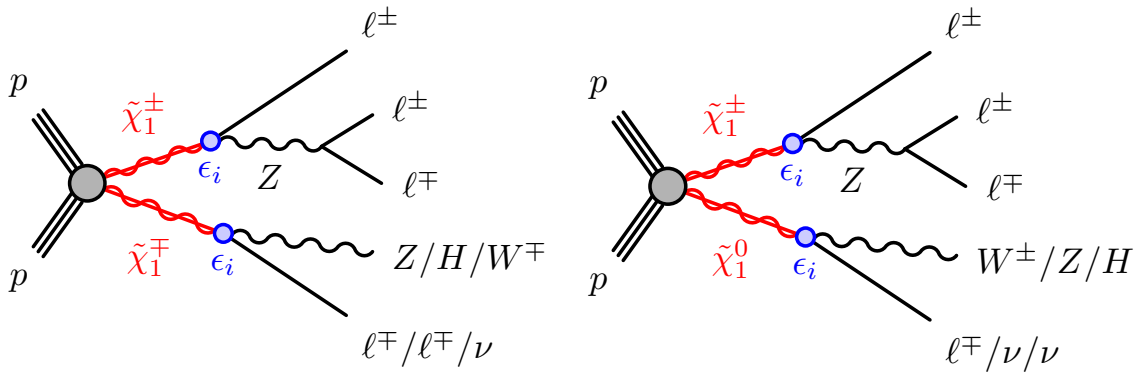


Figure 1: Diagrams of (left) $\tilde{\chi}_1^\pm \tilde{\chi}_1^\mp$ and (right) $\tilde{\chi}_1^\pm \tilde{\chi}_1^0$ production with at least one $\tilde{\chi}_1^\pm \rightarrow Z\ell \rightarrow \ell\ell\ell$ decay. The R -parity-violating coupling ϵ_i allows prompt $\tilde{\chi}_1^\pm$ decays into $Z\ell$, $H\ell$, or $W\nu$ and prompt $\tilde{\chi}_1^0$ decays into $W\ell$, $Z\nu$, or $H\nu$.

Several SM processes with similar final-state particles can contribute to the signal regions, with the largest contributions from the WZ , ZZ , and $t\bar{t}Z$ processes. The expected yields of these processes are estimated using Monte Carlo (MC) simulation that is normalized to data in three highly populated control regions. Additional event selections are applied to reject events from SM processes in the signal regions while maintaining a high selection efficiency for events from the target $\tilde{\chi}_1^\pm \tilde{\chi}_1^\mp$ and $\tilde{\chi}_1^\pm \tilde{\chi}_1^0$ models.

A scan over the possible $\tilde{\chi}_1^\pm$ and $\tilde{\chi}_1^0$ branching fractions to both bosons and leptons is performed when setting model-specific limits. Model-independent limits are also explored in narrow slices of the $m_{Z\ell}$ spectrum, with no assumptions made on the $\tilde{\chi}_1^\pm/\tilde{\chi}_1^0$ branching fractions or decay kinematics of a generic beyond-the-SM process.

Previous searches for the production of wino-type charginos and neutralinos in R -parity-conserving models have targeted final states with three or more leptons via W and Z boson decays and found no significant excess in data over background expectations, with the ATLAS [25, 26] and CMS [27, 28] collaborations setting limits on wino masses of up to 580 GeV and 650 GeV, respectively. Searches have also been performed for trilepton resonances from heavy leptons in type-III seesaw scenarios by the ATLAS [29, 30] and CMS [31] collaborations, but none have attempted to fully reconstruct both decay chains of the charginos and neutralinos. A previous search by ATLAS [32] for events from the $B - L$ RPV model targeted by this analysis focused on the pair production of top squarks [33].

A brief overview of the ATLAS detector is given in Section 2, and a description of the dataset and the MC simulation is presented in Section 3. Details of the reconstruction of the events used in the search are presented in Section 4, and the design of signal regions sensitive to the $B - L$ RPV model is discussed in Section 5. The description of the SM backgrounds and the strategy for their estimation are given in Section 6, followed by an explanation of the systematic uncertainties in Section 7. The results of the search and their interpretation for various $B - L$ RPV model scenarios are presented in Section 8, and the conclusions are given in Section 9.

2 ATLAS detector

The ATLAS detector [34] is a multipurpose particle detector with a nearly 4π coverage in solid angle.¹ It is composed of an inner tracking system covering the pseudorapidity region $|\eta| < 2.5$, electromagnetic and hadronic calorimeters covering $|\eta| < 4.9$, and a muon spectrometer covering $|\eta| < 2.7$.

The inner detector (ID) reconstructs tracks from charged particles using silicon pixel, silicon microstrip, and transition-radiation tracking detectors. The innermost layer of the silicon pixel tracker, the insertable B-layer [35, 36], was installed prior to 2015 at an average radial distance of 3.3 cm from the beamline to improve track reconstruction and the identification of jets initiated by heavy-flavor hadrons. The ID is surrounded by a thin superconducting solenoid providing a 2 T axial magnetic field, facilitating the measurement of charged-particle momenta.

Beyond the solenoid is a high-granularity lead and liquid-argon (LAr) electromagnetic sampling calorimeter covering $|\eta| < 3.2$. Outside the electromagnetic calorimeter are two hadronic calorimeters; a steel and scintillator-tile sampling calorimeter covering $|\eta| < 1.7$ and a copper and LAr endcap calorimeter covering $1.7 < |\eta| < 3.2$. The most forward region of $3.1 < |\eta| < 4.9$ is covered by copper and LAr and tungsten and LAr calorimeters optimized for electromagnetic and hadronic measurements, respectively.

The muon spectrometer (MS) surrounds the calorimeters, identifying and measuring muon tracks through up to three layers of precision tracking and triggering chambers. The MS is interleaved with a system of three superconducting air-core toroidal magnets with eight coils each, with a field integral between 2.0 T m and 6.0 T m across most of the detector.

The ATLAS trigger system consists of a hardware-based first-level (L1) trigger followed by a software-based high-level trigger (HLT) [37]. The L1 and HLT trigger systems are designed to accept events at average rates of 100 kHz and 1 kHz, respectively. Candidate electrons within $|\eta| < 2.5$ are identified by the L1 trigger as compact electromagnetic energy deposits in the electromagnetic calorimeter, and by the HLT using additional fast track reconstruction [38]. Candidate muons within $|\eta| < 2.7$ are identified by the L1 trigger through a coincidence of MS trigger chamber layers and further selected by the HLT using fast reconstruction algorithms with input from the ID and MS.

3 Data and Monte Carlo simulation

The analysis is performed using pp collision data collected by the ATLAS experiment between the years 2015 and 2018. The dataset corresponds to a total integrated luminosity of 139 fb^{-1} after imposing data quality requirements [39]. In this dataset there are, on average, approximately 34 simultaneous pp collisions in each LHC proton bunch crossing.

Monte Carlo simulation is used to model the expected contributions of various SM processes and the $\tilde{\chi}_1^\pm \tilde{\chi}_1^\mp$ and $\tilde{\chi}_1^\pm \tilde{\chi}_1^0$ signal processes targeted by the search. It is used to define and optimize the event selection criteria and to estimate systematic uncertainties in the predictions of event yields. The generators and

¹ ATLAS uses a right-handed coordinate system with its origin at the nominal interaction point (IP) in the center of the detector and the z -axis along the beam pipe. The x -axis points from the IP to the center of the LHC ring, and the y -axis points upwards. Cylindrical coordinates (r, ϕ) are used in the transverse plane, ϕ being the azimuthal angle around the z -axis. The pseudorapidity is defined in terms of the polar angle θ as $\eta = -\ln \tan(\theta/2)$, and the rapidity y is defined as $y = (1/2)\ln[(E + p_z)/(E - p_z)]$, where E is energy and p_z is longitudinal momentum. Angular distance is measured in units of $\Delta R \equiv \sqrt{(\Delta\eta)^2 + (\Delta\phi)^2}$.

Table 1: Details of the MC simulation for each physics process, including the event generator used for matrix element calculation, the generator used for the PS and hadronization, the PS parameter tunes, and the order in α_S of the production cross-section calculations.

Process	Event generator	PS and hadronization	PS tune	Cross section (in QCD)
Diboson, triboson, ($Z+jets$)	SHERPA 2.2	SHERPA 2.2	Default	NLO (NNLO)
$t\bar{t}W, t\bar{t}Z$, (Other top)	MADGRAPH5_aMC@NLO 2	PYTHIA 8	A14	NLO (LO)
$t\bar{t}, (tW), [t\bar{t}H]$	POWHEG-Box v2	PYTHIA 8	A14	NNLO+NNLL (NLO+NNLL) [NLO]
Higgs: ggF, (VBF, VH)	POWHEG-Box v2	PYTHIA 8	AZNLO	NNNLO (NNLO+NNLL)
$\tilde{\chi}_1^\pm \tilde{\chi}_1^\mp, \tilde{\chi}_1^\pm \tilde{\chi}_1^0$	MADGRAPH 2.6	PYTHIA 8	A14	NLO+NLL

parameters used in the MC simulation samples are given below and summarized in Table 1. The expected yields of SM processes are taken directly from MC simulation except for the dominant WZ , ZZ , and $t\bar{t}Z$ backgrounds, which are estimated from MC simulation that is normalized to data in dedicated control regions, as described in Section 6.1. The contribution from events with one or more misidentified or nonprompt (*fake*) leptons is separately predicted using a data-driven method described in Section 6.2.

Diboson, triboson, and $Z+jets$ samples [40, 41] were simulated using the SHERPA 2.2 [42] generator. Triboson and most diboson processes were simulated with SHERPA 2.2.2 while $Z+jets$ and semileptonically decaying diboson processes were simulated with SHERPA 2.2.1. The matrix element calculations were matched to the parton shower (PS) simulation using Catani–Seymour dipole factorization [43, 44]. The matching was performed separately for different jet multiplicities and merged into an inclusive sample using an improved Catani–Krauss–Kuhn–Webber (CKKW) matching procedure [45, 46] extended to next-to-leading-order (NLO) accuracy in QCD using the MEPS@NLO prescription [45–48]. The virtual QCD correction for matrix elements at NLO accuracy was provided by the OPENLOOPS library [49, 50]. The NNPDF3.0NNLO [51] set of parton distribution functions (PDFs) was used together with a dedicated set of tuned PS parameters (tune) developed by the SHERPA authors [44].

The $Z+jets$ (diboson) samples were calculated for up to two (one) additional partons at NLO and up to four (three) additional partons at leading order (LO) in QCD, and the triboson samples were calculated at NLO in QCD for the inclusive processes and at LO in QCD for up to two additional parton emissions. Diboson samples include loop-induced and electroweak production. The diboson and triboson samples do not include Higgs boson contributions. The cross sections calculated by the event generators were used for all samples except for $Z+jets$, which was normalized to a next-to-next-to-leading-order (NNLO) cross-section prediction [52].

The $t\bar{t}$ [53], $t\bar{t}H$ [54], and tW [55] process samples were simulated at NLO in QCD using the POWHEG-Box [56–58] v2 generator and the NNPDF3.0NLO PDF set. The matrix element calculations were interfaced with PYTHIA 8.230 [59] for the PS using the A14 tune [60] and the NNPDF2.3LO PDF set [61]. The h_{damp} parameter² was set to be 1.5 times larger than the top-quark mass following optimization studies using data [62]. The $t\bar{t}$ inclusive production cross section was corrected to the theory prediction calculated at NNLO in QCD and included the resummation of next-to-next-to-leading logarithmic (NNLL) soft-gluon terms calculated with Top++2.0 [63]. The tW inclusive production cross section was corrected to the theory prediction at NLO in QCD with NNLL corrections to the soft-gluon terms [64, 65]. Both samples were generated in the five-flavor scheme, setting all quark masses to zero except for the top quark.

² The h_{damp} parameter controls the transverse momentum p_T of the first additional emission beyond the leading-order Feynman diagram in the PS and therefore regulates the high- p_T emission against which the $t\bar{t}$ system recoils.

The diagram-removal strategy [66] was employed in the tW sample to remove the interference with $t\bar{t}$ production [62].

Other top-quark production processes were simulated with the **MADGRAPH5_aMC@NLO** v2 [67] generator at either NLO in QCD with the NNPDF3.0NLO PDF set or at LO in QCD using the NNPDF2.3LO PDF set. They were interfaced with **PYTHIA** 8 using the A14 tune and the NNPDF2.3LO PDF set. Generator versions **MADGRAPH5_aMC@NLO** v2.3 and **PYTHIA** 8.212 were used for tZ , tWZ , $t\bar{t}Z$, $t\bar{t}W$, and $t\bar{t}WZ$ processes, while versions **MADGRAPH5_aMC@NLO** v2.2 and **PYTHIA** 8.186 were used for $t\bar{t}\gamma$, $t\bar{t}WW$, and four-top processes. These top-quark processes were generated at LO in QCD with the exception of $t\bar{t}Z$, $t\bar{t}W$, and tWZ , which were generated at NLO in QCD.

Higgs boson production via gluon–gluon fusion (ggF) was simulated at NNLO accuracy in QCD using the **POWHEG-Box** v2 NNLOPS program [68] and interfaced with **PYTHIA** 8.212 using the AZNLO tune [69] and PDF4LHC15 NNLO PDF set [70]. The MC prediction was normalized to the next-to-next-to-next-to-leading-order (NNNLO) cross section in QCD plus electroweak corrections at NLO [71, 72].

Higgs boson production via vector-boson fusion (VBF) and Higgs boson production in association with a W or Z boson (VH) were generated using **POWHEG-Box** v2 and interfaced with **PYTHIA** 8.212 using the AZNLO tune and CTEQ6L1 [73] PDF set. The **POWHEG** predictions are accurate to NLO in QCD and were tuned to match calculations including effects due to finite heavy-quark masses and soft-gluon resummations up to NNLL. The MC predictions were normalized to NNLO QCD cross-section calculations with NLO electroweak corrections [74–77].

The $B - L$ RPV $\tilde{\chi}_1^\pm \tilde{\chi}_1^\mp$ and $\tilde{\chi}_1^\pm \tilde{\chi}_1^0$ signal samples were produced using **MADGRAPH5_aMC@NLO** v2.6 and the NNPDF2.3LO PDF set with up to two additional partons calculated at LO in QCD and interfaced with **PYTHIA** 8.230 using the A14 tune and NNPDF2.3LO PDF set. The scale parameter for jet–parton CKKW-L matching was set to a quarter of the $\tilde{\chi}_1^\pm/\tilde{\chi}_1^0$ mass. Samples were generated at masses between 100 GeV and 1500 GeV in steps of 50 GeV. Signals with masses below 100 GeV were not explored as they have been excluded by previous three-lepton searches for charginos and neutralinos [25–31].

Signal events were generated with equal $\tilde{\chi}_1^\pm/\tilde{\chi}_1^0$ branching fractions to each boson (W , Z , or Higgs bosons where kinematically accessible) plus charged-lepton (e , μ , or τ -lepton) channel. In order to explore different assumptions for the $\tilde{\chi}_1^\pm/\tilde{\chi}_1^0$ branching fractions in the analysis, simulated events are reweighted appropriately, assuming that the $\tilde{\chi}_1^\pm$ and $\tilde{\chi}_1^0$ branching fractions change in the same way.

Generated signal events were filtered to have at least three leptons, two of which were associated with a Z boson. Hadronically decaying τ -leptons were not considered by this three-lepton filter for the $\tilde{\chi}_1^\pm \tilde{\chi}_1^0$ events, increasing the useful statistics of the MC sample. The $\tilde{\chi}_1^\pm$ were also required to decay via a Z boson in the $\tilde{\chi}_1^\pm \tilde{\chi}_1^0$ events to increase the number of events with a trilepton resonance. The inclusive production cross sections were calculated assuming mass-degenerate, wino-like $\tilde{\chi}_1^\pm$ and $\tilde{\chi}_1^0$, as predicted by the $B - L$ RPV model [23], and were calculated at NLO in QCD with next-to-leading-logarithmic (NLL) corrections to the soft-gluon terms [78–82]. The cross sections and their uncertainties were derived from an envelope of cross-section predictions using different PDF sets and factorization and renormalization scales [83]. The inclusive cross sections for $\tilde{\chi}_1^\pm \tilde{\chi}_1^\mp$ ($\tilde{\chi}_1^\pm \tilde{\chi}_1^0$) production at a center-of-mass energy of $\sqrt{s} = 13$ TeV range from 11.6 ± 0.5 (22.7 ± 1.0) pb for masses of 100 GeV to 0.040 ± 0.006 (0.080 ± 0.013) fb for masses of 1500 GeV.

The modeling of c - and b -hadron decays in samples generated with **POWHEG-Box** or **MADGRAPH5_aMC@NLO** was performed with **EvtGen** 1.2.0 [84]. Events from all generators were propagated through a full simula-

tion of the ATLAS detector [85] using GEANT4 [86] to model the interactions of particles with the detector. A parameterized simulation of the ATLAS calorimeter [85] was used for faster detector simulation of signal, tW , and $t\bar{t}H$ processes and was found to be in agreement with the full simulation. The effect of multiple interactions in the same and neighboring bunch crossings (pileup) was modeled by overlaying simulated minimum-bias collisions onto each hard-scattering event. The minimum-bias events were generated with PYTHIA 8.210 using the A3 tune [87] and NNPDF2.3LO PDF set. For each simulated hard-scatter process a separate MC sample is generated to reflect the conditions of the 2015+2016, the 2017, and the 2018 datasets. The number of overlaid minimum-bias collisions is sampled for each event according to the distribution of the average number of interactions per bunch crossing measured in that dataset.

4 Event reconstruction

The data events used in the analysis were recorded during stable beam conditions at the LHC and were required to meet data quality criteria. Data events were collected with triggers requiring at least a single electron or a single muon reconstructed by the trigger system, with various lepton- p_T thresholds depending upon the relative quality (including isolation) of the trigger-level leptons [37]. In the analysis, tighter quality and p_T requirements are applied to the fully reconstructed signal leptons, as described below, to ensure the event selection is free from bias in the trigger reconstruction. Each event for which the trigger was activated is required to have at least one electron (muon) with a fully calibrated p_T above 27, 61, or 141 GeV (27.3 or 52.5 GeV), with larger- p_T requirements corresponding to reduced lepton-quality requirements of the trigger. For the 2015 data, the p_T requirement of the analysis for the loosest-quality electron trigger is lowered to 121 GeV. The single-lepton triggers are found to be more than 90% efficient for the signal model with mass of 100 GeV and more than 99% efficient for signal models of mass 300 GeV or higher.

Both the data and MC events are required to have at least one reconstructed vertex that is associated with two or more tracks of transverse momentum $p_T > 500$ MeV. The primary vertex of each event is selected as the vertex with the largest Σp_T^2 of associated tracks [88].

The primary objects considered by this analysis are electrons, muons, and jets. Electron candidates are reconstructed from three-dimensional energy clusters in the electromagnetic calorimeter that are matched to an ID track and calibrated in situ using $Z \rightarrow ee$ decays [89]. Muon candidates in the detector are typically reconstructed from a combined fit of tracks formed in the MS and ID and calibrated in situ using $Z \rightarrow \mu\mu$ and $J/\psi \rightarrow \mu\mu$ decays [90]. Jet candidates are reconstructed from three-dimensional energy clusters formed using both the electromagnetic and hadronic calorimeters [91]. Clusters are grouped using the anti- k_t algorithm [92, 93] with a radius parameter $R = 0.4$. The jet energy scale (JES) and resolution (JER) are first corrected to particle level using MC simulation and then calibrated in situ through $Z+jets$, $\gamma+jets$, and multijet measurements [94].

Two levels of selection criteria are defined for leptons and jets; the looser “baseline” criteria and the tighter “signal” criteria. Baseline objects are used for resolving ambiguities between overlapping objects, calculating the missing transverse momentum ($\mathbf{p}_T^{\text{miss}}$) of an event, and as inputs to the data-driven estimation of *fake*-lepton events. Baseline electrons are required to meet the “loose and B-layer likelihood” quality criteria [89], satisfy $p_T > 10$ GeV, and be within the ID acceptance ($|\eta| < 2.47$) but outside the barrel/endcap transition region of the electromagnetic calorimeter ($1.37 < |\eta| < 1.52$). Baseline muons are required to meet the “medium” quality criteria [90], satisfy $p_T > 10$ GeV, and fall within the MS acceptance ($|\eta| < 2.7$). Each baseline electron or muon is also required to have a trajectory consistent with the primary vertex to suppress pileup. For this purpose, the transverse impact parameter (d_0) of a lepton is

defined as the distance in the transverse plane between the beam-line and the closest point of the associated ID track. The longitudinal impact parameter (z_0) then corresponds to the z -coordinate distance between that point and the primary vertex. A selection of $|z_0 \sin \theta| < 0.5$ mm, where θ is the polar angle of the track, is required for each lepton to ensure it is compatible with the primary vertex.

Baseline jets are required to satisfy $p_T > 20$ GeV and fall within the full calorimeter acceptance ($|\eta| < 4.5$). The identification of baseline jets containing b -hadrons (b -jets) is performed using the MV2 multivariate discriminant built using information from track impact parameters, the presence of displaced secondary vertices, and the reconstructed flight paths of b - and c -hadrons inside the jet [95]. The identification criteria are tuned to an average identification efficiency of 85% as obtained for b -jets in simulated $t\bar{t}$ events, corresponding to rejection factors of 25, 2.7, and 6.1 for jets originating from light quarks and gluons, c -quarks, and τ -leptons, respectively.

While photons are not used directly in the analysis, baseline photons are defined for use in the calculation of $\mathbf{p}_T^{\text{miss}}$. Baseline photons are required to meet the “tight” quality criteria [89], satisfy $p_T > 25$ GeV, and fall within the ID acceptance ($|\eta| < 2.37$) and outside the calorimeter’s transition region ($1.37 < |\eta| < 1.52$).

To aid in the correct reconstruction and identification of leptons and jets an overlap-removal procedure is performed, preventing the reconstruction of a single particle as multiple objects. First, any electron that shares a track with a muon in the ID is removed, as the track is consistent with track segments in the MS. Next, jets are removed if they are within $\Delta R = 0.2$ of a lepton and are either not b -tagged or satisfy $p_T > 100$ GeV, as they are consistent with the energy deposited by an electron shower or muon bremsstrahlung. For the overlap of a jet with a nearby muon, the jet is discarded only if it is associated with fewer than three tracks of $p_T \geq 500$ MeV. Finally, electrons and muons within $\Delta R = 0.4$ of any remaining jets are discarded to reject *fake* leptons originating from hadron decays. In the overlap-removal procedure the calculation of ΔR uses rapidity instead of η to ensure the distance measurement is Lorentz invariant for jets with non-negligible masses.

The $\mathbf{p}_T^{\text{miss}}$ of each event, with magnitude E_T^{miss} , is defined as the negative vector sum of the transverse momenta of all identified baseline objects (electrons, muons, jets, and photons) and an additional soft term [96]. The soft term is constructed from all tracks associated with the primary vertex that are not associated with any baseline object. The $\mathbf{p}_T^{\text{miss}}$ is therefore adjusted to include the full calibration of the reconstructed baseline objects while minimizing any pileup dependence in the soft term.

Tighter “signal” criteria are applied to the final leptons and jets considered by the analysis to ensure a high selection purity and accurate p_T measurement. Any event with a baseline lepton that fails to satisfy the signal criteria is rejected to reduce the contamination from *fake*-lepton events. Signal leptons are required to have $p_T > 12$ GeV and electrons must meet the “medium” quality criteria [89]. At least one of the signal leptons must be identified as having activated a trigger and must pass the larger p_T requirement of that trigger. The track associated with each signal electron or muon must pass a requirement on d_0 and its uncertainty σ_{d_0} such that $|d_0/\sigma_{d_0}| < 5$ (3) for electrons (muons), ensuring the selection of leptons with prompt, well-reconstructed tracks. Finally, signal leptons must be sufficiently isolated from additional detector activity by passing a p_T -dependent “tight” requirement on both calorimeter-based and track-based isolation variables [89, 90]. The calorimeter-based isolation is defined within a cone of size $\Delta R = 0.2$ around the lepton, and the amount of nonassociated calorimeter transverse energy within the cone must be below 6% (15%) of the electron (muon) p_T . The track-based isolation cone size is $\Delta R = 0.2$ for low- p_T electrons and decreases linearly with p_T above 50 GeV as the electron’s shower becomes more collimated. For muons, the size of the track-isolation cone is $\Delta R = 0.3$ for muons with $p_T \leq 33$ GeV and decreases linearly with p_T to $\Delta R = 0.2$ at $p_T = 50$ GeV, improving the selection efficiency for higher- p_T muons.

The track-based isolation only considers nonassociated tracks that are consistent with the primary vertex, and the scalar sum of track p_T (p_T^{iso}) is required to be below 6% (4%) of the electron (muon) p_T . The lepton p_T^{cone} is then defined as the scalar sum of the lepton p_T and p_T^{iso} , and is useful in parameterizing the behavior of *fake* leptons. The muon “tight” isolation requirement is roughly 96% efficient for all p_T and η [90], while for electrons it is 70% efficient at 20 GeV and becomes more than 98% efficient above 100 GeV [89].

Signal jets are required to have $|\eta| < 2.8$, and events are rejected if they contain a jet that fails to meet the “loose” quality criteria [97], reducing contamination from electronic noise bursts and noncollision backgrounds. To suppress jets originating from pileup, jets with $p_T < 120$ GeV and within the ID acceptance ($|\eta| < 2.5$) are required to pass the “medium” working point of the track-based jet vertex tagger [98, 99]. All MC simulation samples are corrected using per-event weights to account for small differences with data in signal-lepton identification, reconstruction, isolation and triggering efficiencies [89, 90], as well as in signal-jet pileup rejection [98] and flavor-identification efficiencies [95].

5 Search strategy

The $B - L$ RPV model allows for many different decay modes of $\tilde{\chi}_1^\pm/\tilde{\chi}_1^0$ and therefore many possible final states. A decay of interest is $\tilde{\chi}_1^\pm \rightarrow Z\ell \rightarrow \ell\ell\ell$ because of the large number of leptons produced from a single resonance. The invariant-mass distribution of the trilepton resonance ($m_{Z\ell}$) is narrow due to the excellent momentum resolution of reconstructed electrons and muons. No SM process naturally produces a three-lepton resonance, leading to a smooth combinatorial background distribution in which a resonance would be distinguishable.

Three orthogonal signal regions (SRs) are developed in Section 5.1 to select $\tilde{\chi}_1^\pm\tilde{\chi}_1^\mp$ and $\tilde{\chi}_1^\pm\tilde{\chi}_1^0$ events with at least one $\tilde{\chi}_1^\pm \rightarrow Z\ell \rightarrow \ell\ell\ell$ decay. Each SR targets different decay scenarios of the second $\tilde{\chi}_1^\pm/\tilde{\chi}_1^0$ through requirements on the number of leptons and reconstructed W , Z , or Higgs bosons. Matching procedures are developed for events with additional leptons or boson candidates to optimally assign the decay products to each $\tilde{\chi}_1^\pm/\tilde{\chi}_1^0$, as described in Section 5.2. The SRs utilize event-wide information to reduce combinatorial backgrounds, as described in Section 5.3.

5.1 Signal regions targeting trilepton decays

Each SR requires at least three signal leptons, two of which are identified as candidate Z boson decay products if they have the same flavor and opposite sign of their electric charge (SFOS) and have an invariant mass $m_{\ell\ell}$ within 10 GeV of the Z boson mass. For events which have more than one SFOS pair, the pair with $m_{\ell\ell}$ closest to the Z mass is chosen. The $m_{Z\ell}$ of the $\tilde{\chi}_1^\pm$ is then reconstructed from the chosen SFOS pair and a third lepton. Deviations of $m_{\ell\ell}$ from the expected Z boson mass of 91.2 GeV can occur due to the imperfect energy reconstruction of leptons, particularly at high p_T . The $m_{Z\ell}$ resolution is therefore improved by shifting the value of $m_{Z\ell}$ by an amount equal to $(91.2 - m_{\ell\ell})$ GeV.

Events are separated into the three SRs according to the number of leptons and the presence of a second reconstructed Z , W , or Higgs boson from the second $\tilde{\chi}_1^\pm/\tilde{\chi}_1^0$ decay. The SRFR region targets events where all decay products are visible and “fully reconstructed”. The SR4 ℓ region targets events with four or more leptons and possible E_T^{miss} , while the SR3 ℓ region targets events with only three visible leptons and substantial E_T^{miss} , with at least one neutrino coming from the decay of the second $\tilde{\chi}_1^\pm/\tilde{\chi}_1^0$. The choice

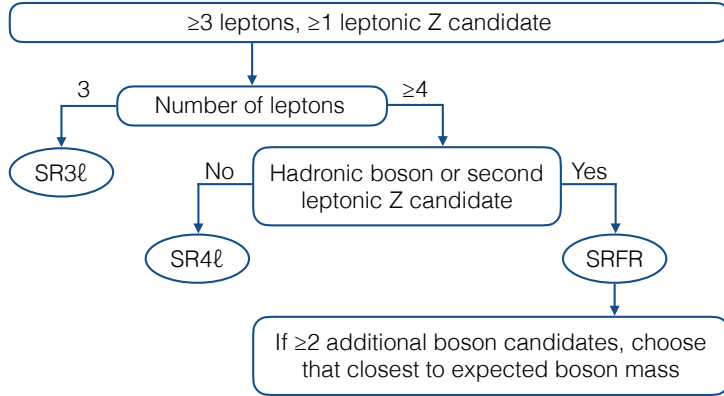


Figure 2: Schematic flow chart describing the assignment of an event to a given signal region.

of SR for an event is described below and summarized in Figure 2. Additional selections to reduce the SM background contributions are subsequently applied in each of the SRs separately, as described in Section 5.3.

To target fully visible events, SRFR requires a fourth lepton and a second reconstructed Z , W , or Higgs boson. Pairs of jets are considered for the second boson if their invariant mass m_{jj} is consistent with that of a W or Z boson, with $71.2 < m_{jj} < 111.2$ GeV. If at least one of the jets is a b -jet, the m_{jj} requirement is loosened to $71.2 < m_{jj} < 150$ GeV to allow for Higgs boson decays. Additional SFOS lepton pairs are also considered for the second boson candidate in events with six or more leptons if their invariant mass is consistent with the Z boson mass, such that $81.2 < m_{\ell\ell} < 101.2$ GeV. If there are multiple candidates for the second boson, the pairing selected is that with invariant mass closest to the Z boson mass, or closest to the Higgs boson mass for pairs that include at least one b -jet.

The SR4 ℓ region targets events in which the decay of the second $\tilde{\chi}_1^\pm/\tilde{\chi}_1^0$ includes one or more leptons but is not fully reconstructed due to the presence of neutrinos. Events with four or more leptons that fail all SRFR requirements are selected by SR4 ℓ . The SR3 ℓ region targets decays of the second $\tilde{\chi}_1^\pm/\tilde{\chi}_1^0$ that include no leptons, requiring exactly three leptons in the event. While each region targets specific $\tilde{\chi}_1^\pm/\tilde{\chi}_1^0$ decay chains, events in which one or more leptons fall outside the detector acceptance or are not reconstructed may still be selected by other regions. For the signal sample with a mass of 500 GeV and democratic $\tilde{\chi}_1^\pm/\tilde{\chi}_1^0$ branching fractions to bosons and leptons, the SRFR, SR4 ℓ , and SR3 ℓ regions have selection efficiencies of 3%, 4%, and 5%, respectively.

Within each SR the search is performed in the $m_{Z\ell}$ spectrum to maximize the discovery sensitivity to a resonance. The binning of the $m_{Z\ell}$ observable was optimized using simulated $\tilde{\chi}_1^\pm\tilde{\chi}_1^\mp$ and $\tilde{\chi}_1^\pm\tilde{\chi}_1^0$ signal samples with reconstructed invariant mass resolutions of around 2%, as measured from the widths of Gaussian fits to the reconstructed invariant mass distributions. The optimized binning accounts for the predicted background expectation. Lower edges are set at

$$m_{Z\ell} = 90, 110, 130, 150, 170, 190, 210, 230, 250, 270, 300, 330, 360, 400, 440, \text{ and } 580 \text{ GeV.} \quad (1)$$

The last bin has no upper edge and includes all events with $m_{Z\ell} > 580$ GeV. The same binning is used for all three SRs, facilitating the discovery of a trilepton resonance that would contribute to all SRs.

5.2 Assignment of leptons and boson candidates to $\tilde{\chi}_1^\pm/\tilde{\chi}_1^0$ decays

The presence of one or more additional leptons from the second $\tilde{\chi}_1^\pm/\tilde{\chi}_1^0$ decay introduces ambiguity in the assignment of a lepton and boson produced directly from a $\tilde{\chi}_1^\pm/\tilde{\chi}_1^0$ decay. A matching procedure is implemented to identify the “direct” leptons that come directly from the $\tilde{\chi}_1^\pm/\tilde{\chi}_1^0$ decays, rather than from the subsequent decay of a boson, and to assign them to each $\tilde{\chi}_1^\pm/\tilde{\chi}_1^0$. The procedure optimizes the sensitivity to signals of various masses by maintaining a high efficiency for the correct assignments while reducing the contamination from SM processes. In SRFR, both the trilepton decay and the fully visible decay of the second $\tilde{\chi}_1^\pm/\tilde{\chi}_1^0$, with reconstructed mass $m_{\tilde{\chi},2}$, are chosen as the groupings that minimize the mass asymmetry between the mass-degenerate $\tilde{\chi}_1^\pm\tilde{\chi}_1^\mp$ or $\tilde{\chi}_1^\pm\tilde{\chi}_1^0$ pair, where $m_{Z\ell}^{\text{asym}}$ is defined as

$$m_{Z\ell}^{\text{asym}} = \frac{|m_{Z\ell} - m_{\tilde{\chi},2}|}{m_{Z\ell} + m_{\tilde{\chi},2}}. \quad (2)$$

The matching efficiency for the signal samples is 60% at 100 GeV and 80% or more for masses of 200 GeV and larger.

The matching procedure for a direct lepton to the Z candidate for all other analysis regions with four or more leptons is developed to optimize the sensitivity of the SR4 ℓ region. Two methods are implemented, and the choice of method exploits the correlation between the true mass of the $\tilde{\chi}_1^\pm/\tilde{\chi}_1^0$ and L_T , the scalar sum of the p_T of all leptons in the event. A method targeting low-mass signals is used when $L_T < 550$ GeV and a method targeting high-mass signals is used when $L_T \geq 550$ GeV. For low-mass signals, the $\tilde{\chi}_1^\pm/\tilde{\chi}_1^0$ can often be produced with a sufficiently large momentum such that the decay products are near to one another, and the lepton that is closest in angular distance ΔR to the reconstructed Z boson is chosen. For high-mass signals, the $\tilde{\chi}_1^\pm/\tilde{\chi}_1^0$ decay products are often produced at a wide angle with respect to each other, and mispairings will produce a $m_{Z\ell}$ that is smaller than the $\tilde{\chi}_1^\pm/\tilde{\chi}_1^0$ mass. Therefore, the lepton that maximizes the reconstructed $m_{Z\ell}$ is chosen. The matching efficiency of this procedure for signal samples with various $\tilde{\chi}_1^\pm/\tilde{\chi}_1^0$ masses is 90% at 100 GeV, 30% at 300 GeV, and 70% at 700 GeV. While a low matching efficiency is seen at 300 GeV due to the use of ΔR matching when the $m_{Z\ell}$ maximization would be preferred, the overall analysis sensitivity is improved by avoiding the $m_{Z\ell}$ maximization of low- L_T backgrounds.

As noted in Section 1, the preferred flavor of the direct lepton(s) is related to the neutrino mass hierarchy. The sensitivity to $\tilde{\chi}_1^\pm\tilde{\chi}_1^\mp$ and $\tilde{\chi}_1^\pm\tilde{\chi}_1^0$ events may therefore be improved by imposing constraints on the flavor of the direct lepton(s), targeting the favored signal decays while rejecting additional SM backgrounds. Two additional sets of SRs are developed that are each identical to the nominal set of three SRs except that they require the direct lepton(s) to be either electron (SRFR $_e$, SR4 ℓ_e , SR3 ℓ_e) or muon (SRFR $_\mu$, SR4 ℓ_μ , SR3 ℓ_μ). These additional “ e ” and “ μ ” channels are used separately from the “inclusive” channel and from one another, and are only used when targeting signal models with high $\tilde{\chi}_1^\pm/\tilde{\chi}_1^0$ branching fractions to either electrons or muons, as discussed in Section 8.2.

5.3 Rejection of combinatorial Standard Model backgrounds

The composition and kinematics of the final-state particles that are produced from the decay chains of the $\tilde{\chi}_1^\pm\tilde{\chi}_1^\mp$ or $\tilde{\chi}_1^\pm\tilde{\chi}_1^0$ processes can be combinatorially reproduced by certain SM processes. The ZZ process has a significant contribution to SRFR and SR4 ℓ when both Z bosons decay leptonically. Events from the ZZ process are rejected if they have exactly four leptons that form two SFOS pairs and the mass $m_{\ell\ell,2}$ of the second pair, the pair not selected for the primary $\tilde{\chi}_1^\pm$ candidate, is within 20 GeV of the Z boson mass.

In SR4 ℓ , which targets decay chains of the second $\tilde{\chi}_1^\pm/\tilde{\chi}_1^0$ with at least one neutrino, the ZZ contribution is further reduced by requiring $E_T^{\text{miss}} > 80$ GeV in events with a second same-flavor lepton pair.

The SM $t\bar{t}Z$ process can also contribute significantly in the SRs, and is identifiable by the presence of two b -jets from the two top-quark decays. Signal events that include a Higgs boson decay may also include two b -jets, with a 72% efficiency of identifying both b -jets using the flavor-tagging algorithm described in Section 4. The b -jets will often be collimated due to the boost of the Higgs boson. Therefore, an additional selection is applied in all SRs that requires the two highest- p_T b -jets, if they are found in the event, to satisfy $\Delta R(b_1, b_2) < 1.5$.

The ZZ, $t\bar{t}Z$, and other SM backgrounds can be further reduced in SRFR by taking advantage of the fully visible decay of the second $\tilde{\chi}_1^\pm/\tilde{\chi}_1^0$. As the $\tilde{\chi}_1^\pm$ and $\tilde{\chi}_1^0$ are expected to be mass-degenerate, the $m_{Z\ell}^{\text{asym}}$ (Eq. (2)) between the $\tilde{\chi}_1^\pm\tilde{\chi}_1^\mp$ or $\tilde{\chi}_1^\pm\tilde{\chi}_1^0$ pair is expected to be small. A requirement of $m_{Z\ell}^{\text{asym}} < 0.1$ in SRFR is effective in rejecting combinatorial backgrounds for which $m_{Z\ell}^{\text{asym}}$ is more evenly distributed.

Events in SR3 ℓ are expected to exhibit a significant E_T^{miss} because the second $\tilde{\chi}_1^\pm/\tilde{\chi}_1^0$ decays directly into a neutrino and a boson, while the subsequent decay of the boson may also produce neutrinos. A requirement of $E_T^{\text{miss}} > 150$ GeV reduces contamination from SM processes with no neutrinos, particularly Z+jets events that include a *fake* lepton. The SM WZ process with fully leptonic decays is also a significant contributor to SR3 ℓ , and contains a single neutrino from the W decay. The measured E_T^{miss} is therefore representative of the p_T of the neutrino, and the transverse mass m_T of the W boson can be reconstructed from the p_T of the lepton and the azimuthal separation $\Delta\phi$ between the lepton and $\mathbf{p}_T^{\text{miss}}$, with

$$m_T = \sqrt{2p_T E_T^{\text{miss}}(1 - \cos(\Delta\phi))}.$$

The m_T of a W boson has a kinematic edge at the W mass, and signal events in SR3 ℓ usually produce lepton– E_T^{miss} pairings with a larger m_T . The minimum m_T of all lepton– E_T^{miss} pairings for which the other two leptons form a SFOS pair, defined as m_T^{min} , is required to be $m_T^{\text{min}} > 125$ GeV in SR3 ℓ . This definition allows WZ events to be rejected even if the incorrect SFOS pair was selected for the Z boson.

6 Background estimation and validation

The MC samples described in Section 3 are used to predict the expected background yield from SM processes. To improve the accuracy of the MC prediction in the unique phase-space of this analysis and to constrain the systematic uncertainties discussed in Section 7, the MC predictions are normalized in control regions (CRs). Each CR is dedicated to the measurement of an important SM process and they are discussed in Section 6.1. A dedicated data-driven estimation is used for the *fake*-lepton background and is discussed in Section 6.2. A fit based on a profile likelihood test statistic [100] is performed on all CRs and SRs simultaneously using the HistFitter package [101] to estimate the final post-fit background prediction and uncertainty.

The CRs are developed to be kinematically similar to the SRs but with a small number of selections inverted, reducing any possible signal contamination and ensuring orthogonality between regions. Validation regions (VRs) between the CRs and SRs are developed to ensure the validity of the extrapolation of the yield normalization across the inverted selections and into the SRs. The regions are developed so that any possible signal contamination from $\tilde{\chi}_1^\pm/\tilde{\chi}_1^0$ with democratic branching fractions to bosons and leptons is typically less than 1% in each CR and less than 5% in each VR. This ensures an accurate estimation of

Table 2: Selection criteria for the various signal, control, and validation regions used in the analysis. All regions require a pair of leptons with the same flavor and opposite sign of their electric charge and with an invariant mass between 81.2 GeV and 101.2 GeV. Additionally, they require a third lepton and a trilepton invariant mass above 90 GeV. The 2nd boson requirement indicates the presence of two additional jets or leptons consistent with a W , Z , or Higgs boson decay. The asterisk (*) in the SR4 ℓ E_T^{miss} requirement indicates that this selection is only considered for events with two pairs of same-flavor leptons. The $\Delta R(b_1, b_2)$ selection is only considered for events with at least two b -jets.

Region	N_{lep}	E_T^{miss} [GeV]	m_T^{\min} [GeV]	2nd boson	2nd leptonic Z ; $ m_{\ell\ell,2} - m_Z $ [GeV]	$N_{b\text{-jet}}$	$\Delta R(b_1, b_2)$	$m_{Z\ell}^{\text{asym}}$
SRFR	≥ 4	-	-	Yes	veto; < 20	-	< 1.5	< 0.1
SR4ℓ	≥ 4	$> 80^*$	-	No	veto; < 20	-	< 1.5	-
CRZZ	$= 4$	-	-	-	require; < 5	-	< 1.5	-
VRZZ	$= 4$	-	-	-	require; $[5, 20]$	-	< 1.5	-
CR $t\bar{t}Z$	≥ 3	> 40	-	-	veto; < 20	≥ 2	> 2.5	-
VR $t\bar{t}Z$	≥ 3	> 40	-	-	veto; < 20	≥ 2	$[1.5, 2.5]$	-
SR3ℓ	$= 3$	> 150	> 125	-	-	-	< 1.5	-
CRWZ	$= 3$	< 80	$[50, 100]$	-	-	-	< 1.5	-
VRE_T^{miss}	$= 3$	> 80	< 100	-	-	-	< 1.5	-
VRm_T^{\min}	$= 3$	< 80	> 125	-	-	-	< 1.5	-
CRFake	$= 3$	< 30	< 30	-	-	-	< 1.5	-
VRFake	$= 3$	$[30, 80]$	< 30	-	-	-	< 1.5	-

the SM backgrounds and an unbiased validation. Any contamination from the signal model in the CRs is accounted for in the fit for completeness. All regions are required to have at least three leptons and one SFOS pair with $m_{\ell\ell}$ within 10 GeV of the Z boson mass. The CRs and VRs are inclusive in $m_{Z\ell}$ as this variable is seen to be well modeled by the MC simulation. A requirement of $m_{Z\ell} > 90$ GeV is made in all regions, corresponding to the lowest $m_{Z\ell}$ probed by the SRs. The selections for the various regions are discussed below and summarized in Table 2.

6.1 Primary backgrounds

The major SM backgrounds that are fitted in dedicated CRs are the WZ , ZZ , and $t\bar{t}Z$ processes. The yields of other SM processes are small and are therefore not normalized by the fit but taken directly from the MC prediction. These include the triboson, Higgs boson, and “Other” background categories, where Other consists almost completely of the tWZ , $t\bar{t}W$, and tZ processes.

The WZ process is dominant in the three-lepton SR3 ℓ , and the CRWZ control region is developed by inverting the E_T^{miss} requirement and selecting events with m_T^{\min} consistent with the presence of a W boson. This removes possible signal contamination from $\tilde{\chi}_1^\pm$ and $\tilde{\chi}_1^0$, which typically have a high E_T^{miss} and m_T^{\min} in SR3 ℓ due to one or more boosted neutrinos. Two VRs, VRE_T^{miss} and VRm_T^{\min} , are designed to test the validity of the WZ normalization in SR3 ℓ using similar E_T^{miss} and m_T^{\min} requirements, respectively. Good data–MC agreement is seen in both VRs, and the E_T^{miss} and m_T^{\min} distributions are shown for CRWZ, VRE_T^{miss} , and VRm_T^{\min} in Figure 3. These distributions have all region selections applied except the variable shown, where the CR or VR selections are indicated by arrows. The exception is the E_T^{miss} distribution in

VRE_T^{miss} , which is shown with all region selections applied. The underflow of the m_T^{min} distribution does not consider events with m_T^{min} below 30 GeV.

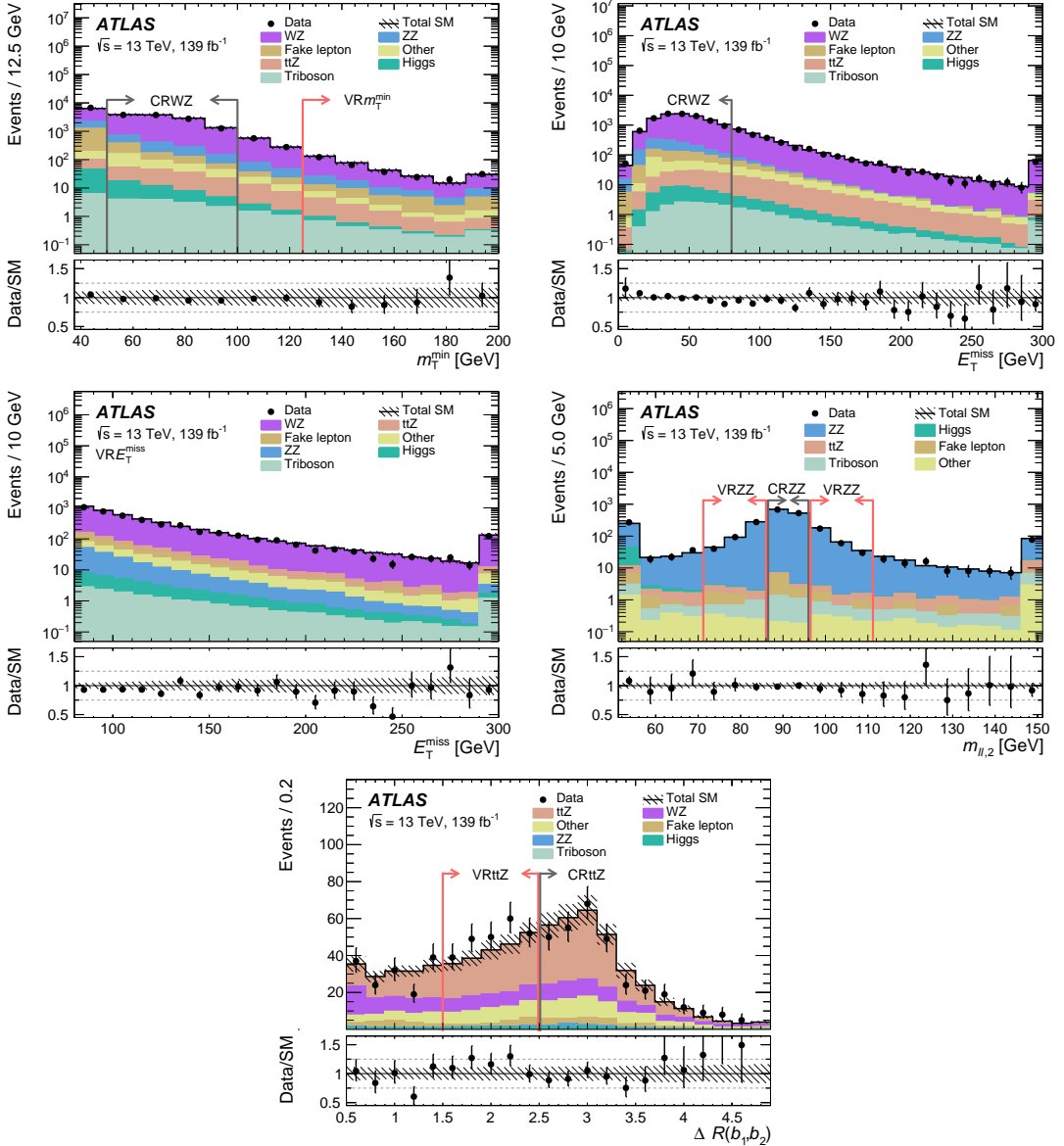


Figure 3: Distributions of the data and post-fit background in the CRs and VRs that are relevant in the extrapolation to the SRs, including (top left) m_T^{min} in CRWZ and VRm_T^{min} , (top right) E_T^{miss} in CRWZ, (middle left) E_T^{miss} in VRE_T^{miss} , (middle right) $m_{ll,2}$ in CRZZ and VRZZ, and (bottom) $\Delta R(b_1, b_2)$ in CR $t\bar{t}Z$ and VR $t\bar{t}Z$. Black (red) arrows indicate the CR (VR) selection on the variable shown, with all other region selections applied. The first (last) bin includes underflow (overflow) events. The “Other” category consists mostly of the tWZ , $t\bar{t}W$, and tZ processes. The hatched bands indicate the combined theoretical, experimental, and MC statistical uncertainties in the background prediction. The bottom panel shows the ratio of the data to the background prediction.

The ZZ and $t\bar{t}Z$ processes are dominant in the four-lepton SR4 ℓ and SRFR regions. A control region for the fully leptonic decay in the ZZ process, CRZZ, is developed by requiring the presence of a second SFOS pair of electrons or muons with an invariant mass $m_{ll,2}$ within 5 GeV of the Z mass. The VRZZ

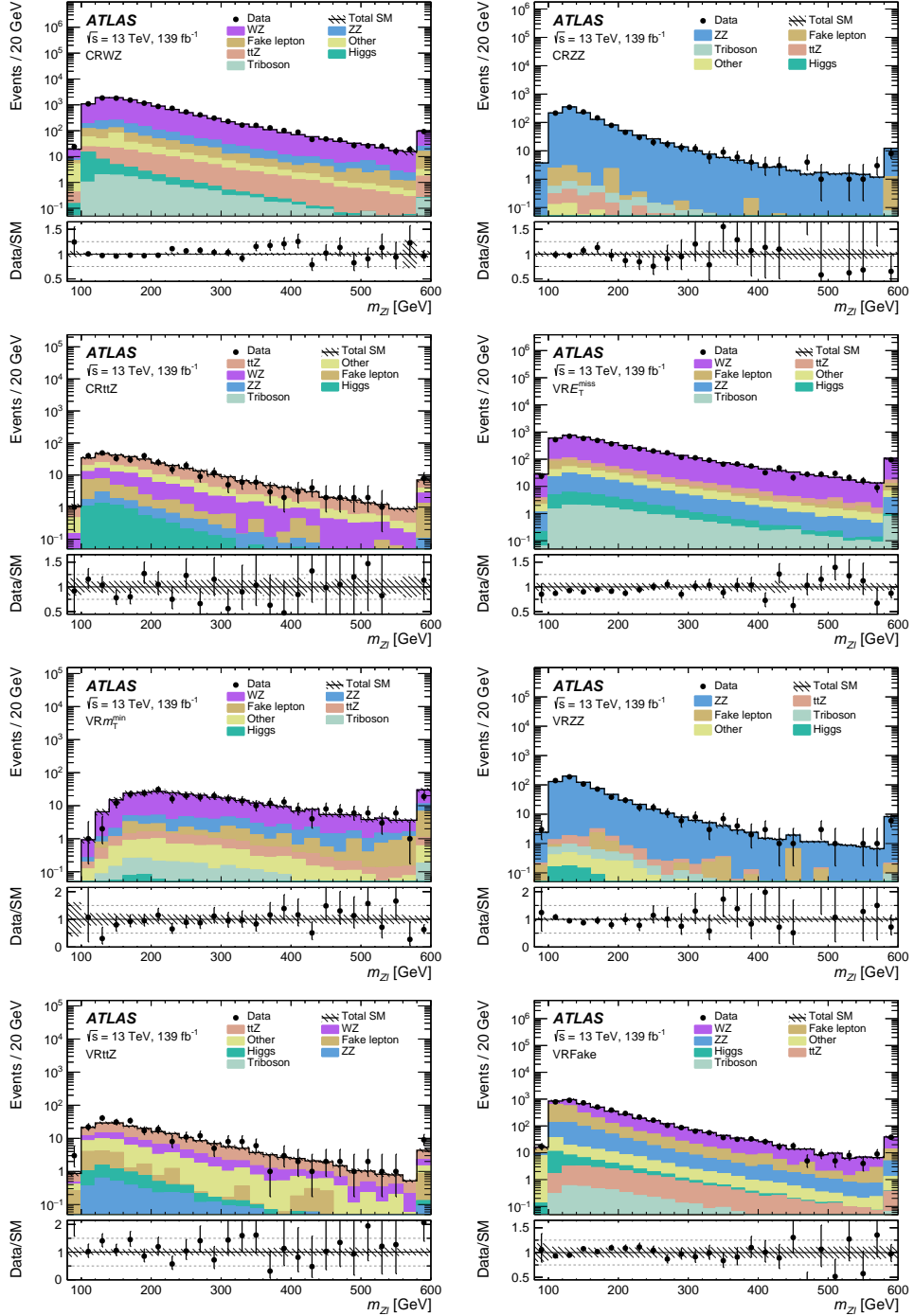


Figure 4: The m_{Z^l} distributions of the data and post-fit background in the (from top left to bottom right) CRWZ, CRZZ, CR $t\bar{Z}$, V $R E_T^{\text{miss}}$, VR m_T^{min} , VRZZ, VR $t\bar{Z}$, and VRFake regions. The last bin includes overflow events. The “Other” category consists mostly of the tWZ , $t\bar{t}W$, and tZ processes. The hatched bands indicate the combined theoretical, experimental, and MC statistical uncertainties in the background prediction. The bottom panel shows the ratio of the data to the background prediction.

validation region has a similar selection, but requires $m_{\ell\ell,2}$ to be between 5 and 20 GeV of the Z mass, falling naturally between the CRZZ requirement and the 20 GeV $m_{\ell\ell,2}$ veto of SR4 ℓ and SRFR. The $m_{\ell\ell,2}$ distribution that includes both CRZZ and VRZZ is shown in Figure 3, and good agreement is seen between data and the post-fit background estimates. Events for which one Z decays into a pair of τ -leptons that both then subsequently decay leptonically are included in this validation region. Good modeling in the three-lepton regions is also expected for such ZZ events when only one τ -lepton decays leptonically, although this process is strongly suppressed by the E_T^{miss} and m_T^{min} requirements.

The control region CR $t\bar{t}Z$ targets the $t\bar{t}Z$ process in the SRs, for which the Z boson decays leptonically and one or both top quarks decay leptonically, and requires at least two b -jets in the event. The $\tilde{\chi}_1^\pm/\tilde{\chi}_1^0$ may also produce two b -jets through the decay of a Higgs boson, but because of the boost of the Higgs boson they are produced back-to-back less often. Therefore, the b -jets in CR $t\bar{t}Z$ are required to be produced with $\Delta R(b_1, b_2) > 2.5$, while the SRs require events with at least two b -jets to satisfy $\Delta R(b_1, b_2) < 1.5$. A requirement of $E_T^{\text{miss}} > 40$ GeV is also imposed to reduce the contamination from the Z +jets process. To increase the number of events in CR $t\bar{t}Z$ the lepton multiplicity requirement is relaxed to $N_\ell \geq 3$, allowing one top quark to decay fully hadronically. The presence or absence of a fourth lepton does not bias the other selections as the ratio of three-lepton to four-lepton events in the $t\bar{t}Z$ sample is well-modeled. The VR $t\bar{t}Z$ validation region is defined with the same selections but requiring $1.5 < \Delta R(b_1, b_2) < 2.5$, falling naturally between CR $t\bar{t}Z$ and the SRs. The $\Delta R(b_1, b_2)$ distribution for both CR $t\bar{t}Z$ and VR $t\bar{t}Z$ is shown in Figure 3. To maintain orthogonality between the $t\bar{t}Z$ regions and the other CRs used in the fit, a requirement of $\Delta R(b_1, b_2) < 1.5$ is applied to all other analysis regions.

The $m_{Z\ell}$ distributions for the CRs and VRs are given in Figure 4. No significant shape disagreement is seen between data and MC simulation, validating the modeling of the backgrounds in $m_{Z\ell}$. The normalization in CRWZ, CRZZ, and CR $t\bar{t}Z$ is therefore performed inclusively in $m_{Z\ell}$ to improve the statistical precision.

The observed event yields in the CRs and VRs are compared with the background estimates and are shown in Figure 5. The CRs are shown with the pre-fit background estimates, and the bottom panel shows the relative disagreement, which is subsequently reduced by the fit. The VRs are shown with the post-fit background estimates, and the bottom panel shows the significance of the disagreement when accounting for all uncertainties. Both the CRs and SRs are included in the fit, with the WZ , ZZ , and $t\bar{t}Z$ normalization factors constrained primarily by the CRs due to their high number of events and purity. The normalization factors of the background-only fit to the CRs and SRs are 1.01 ± 0.03 for the WZ process, 1.12 ± 0.06 for the ZZ process, and 1.05 ± 0.18 for the $t\bar{t}Z$ process.

The data agree well with the post-fit background estimates in all validation regions, giving confidence in the validity of the post-fit background estimation in the SRs. A slight overestimation of almost 2σ is seen in VRE_T^{miss} , and no features are seen in the comparison of data and the post-fit background estimates in the $m_{Z\ell}$ (Figure 4) or E_T^{miss} (Figure 3) distributions of VRE_T^{miss} . A minor excess of data over the background estimation of 1.3σ is seen in VR $t\bar{t}Z$, and good agreement is seen in the shape of the relevant $m_{Z\ell}$ (Figure 4) and $\Delta R(b_1, b_2)$ (Figure 3) distributions.

6.2 Backgrounds from *fake* leptons

Processes that include one or more *fake* leptons are estimated with the data-driven *fake*-factor method [103, 104], avoiding a reliance on MC simulation to model the prompt-lepton quality criteria of *fake* leptons. The modeling is also made difficult by the many sources of *fake*-lepton processes, each of which is kinematically different and provides a relative contribution to the background estimate that is dependent on the analysis

phase-space. The most relevant sources for this analysis include the in-flight decays of heavy-flavor hadrons (HF) and misidentified light-flavor jets or in-flight decays of pions and kaons (LF). The *fake* muons in this analysis are predominantly from HF sources while *fake* electrons are produced from both HF and LF sources, with their relative contribution varying from 2:1 to 1:5 depending upon the analysis region. The pair production of two electrons from the conversion of a prompt photon (Conv) is also considered a *fake*-lepton process but makes a minor contribution. In this analysis the relevant *fake* processes (and their sources) are $Z+jets$ (LF, HF) and $t\bar{t}$ (HF) in the three-lepton regions and WZ (LF) and ZZ (LF, Conv) in the four-lepton regions, with SRFR also having a large contribution from $t\bar{t}Z$ (HF).

Pair-produced electrons are not considered as *fake* leptons if they are produced from the conversion of bremsstrahlung from a prompt electron, such as that from a leptonically decaying Z boson. Events with such electrons are not targeted by the *fake*-factor method but are instead taken directly from MC simulation, which is considered to adequately model such processes. These events are included in the Other category and are a minor contribution in CRWZ and the *fake* measurement and validation regions, described below, and are negligible in all other regions.

A *fake* measurement region CRFake is designed to target the $Z+jets$ process to provide a selection of events enhanced with *fake* leptons from sources representative of those expected in the SRs. The CRFake region is not directly included in the fit, but is used to derive the *fake*-lepton estimation in each analysis region. Events are selected by requiring two signal leptons that form an SFOS pair and with an invariant mass within 10 GeV of the Z boson mass. One of the two signal leptons is required to have fired a single-lepton trigger, thus ensuring no selection bias from *fake* leptons. To enhance the $Z+jets$ purity and reduce prompt-lepton event contamination from the WZ process, CRFake requires $E_T^{\text{miss}} < 30$ GeV and $m_T < 30$ GeV. A third, unpaired baseline lepton is also required in the event and is designated as the *fake* candidate. A requirement on the trilepton invariant mass of $m_{3\ell} > 105$ GeV reduces contamination from

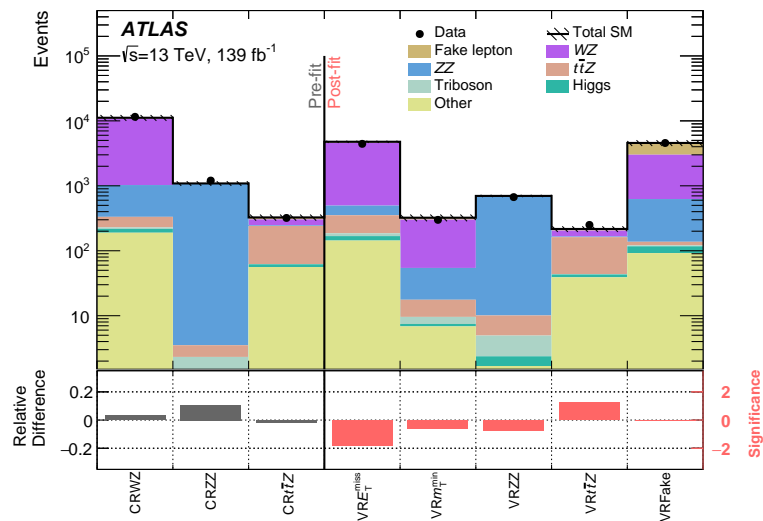


Figure 5: The observed data and the SM background expectation in the CRs (pre-fit) and VRs (post-fit). The “Other” category consists mostly of the tWZ , $t\bar{t}W$, and tZ processes. The hatched bands indicate the combined theoretical, experimental, and MC statistical uncertainties in the background prediction. The bottom panel shows the fractional difference between the observed data and expected yields for the CRs and the significance of the difference for the VRs, computed following the profile likelihood method described in Ref. [102].

the $Z \rightarrow 4\ell$ process.

For all regions, events are split into two populations according to whether the *fake* candidate meets the nominal signal-quality criteria (nom-ID) or fails to meet at least one of the signal-lepton identification, isolation, or impact parameter criteria (anti-ID). The expected contamination by prompt-lepton events from WZ and ZZ processes, as estimated from MC simulation, is subtracted from both populations so that they better represent the yields from *fake*-lepton sources. The *fake* factor is defined as the ratio of the yield of nom-ID to anti-ID events in CRFake and reflects the relative likelihood for a *fake* lepton that meets the baseline criteria to either meet or fail to meet the signal-lepton quality criteria. This ratio has a dependence on the *fake*-lepton source but is fairly independent of the underlying physics process or any additional activity in the event. Therefore, in each analysis region the *fake* factor can be applied to a population of anti-ID events, defined with the same region selections but with one or more signal leptons replaced by anti-ID leptons, to predict the yield of *fake*-lepton events that have passed the selection requirements.

The *fake* factors are derived separately for electron and muon *fake* candidates and are parameterized as a function of p_T^{cone} , which better reflects the p_T of the underlying particle that has produced the *fake* lepton, such as a HF hadron. Additional parameterizations of the *fake* factor were considered, including lepton η , E_T^{miss} , and the b -jet multiplicity of the event, but a two-dimensional parameterization would significantly reduce the statistical precision of the *fake* factors. Alternative parameterizations are instead used to define a systematic uncertainty due to the choice of p_T^{cone} . The statistical uncertainty of each *fake* factor is propagated to an uncertainty in the yield. An uncertainty due to the prompt-lepton subtraction is estimated by varying the subtracted yields of the WZ and ZZ MC simulations up and down by 5%, corresponding to their cross-section uncertainties [105]. For any $m_{Z\ell}$ bin of an SR that does not have an anti-ID event, and therefore has a prediction of zero *fake*-lepton events, an uncertainty is applied corresponding to a yield of 0.32 *fake* events. This represents the largest *fake* estimate possible given a 1σ upward fluctuation in the anti-ID event yield.

To validate the *fake* estimation, a dedicated validation region VRFake is developed closer to the SRs, using the same selections as CRFake but requiring $E_T^{\text{miss}} < 40$ GeV and $30 < m_T < 50$ GeV. Good agreement is seen between data and the post-fit background estimate in VRFake, and for the other VRs, for all observables relevant for the *fake* factor, including the $m_{Z\ell}$ distributions shown in Figure 4. A conservative closure uncertainty of 23% (27%) is applied to the yield of events with electron (muon) *fake* candidates, and is derived so as to cover the most discrepant p_T^{cone} bin observed in VRFake.

The *fake* factor for electrons is sensitive to the relative composition of the *fake* sources, which primarily varies between LF and HF in the analysis regions. To derive an uncertainty in the *fake*-source composition, the MC *fake* factors are measured in MC simulation in CRFake for HF and LF sources separately. The inclusive MC *fake* factors are seen to be reproduced by reweighting the HF and LF MC *fake* factors according to the CRFake composition. Therefore, a composition systematic uncertainty is derived in each analysis region by comparing the inclusive CRFake MC *fake* factors with those calculated from a reweighting of HF and LF MC *fake* factors, according to the composition of that region. The systematic uncertainty is derived using only MC simulation, in order to provide clean sources of HF and LF *fake* electrons, but is applied to the nominal data-driven *fake* factors, and is measured to be at most 53% for the electron *fake* factors in SR4 ℓ .

7 Systematic uncertainties

Uncertainties in the expected signal and background yields account for the statistical uncertainties of the MC samples, the experimental systematic uncertainties in the detector measurements, and the theoretical systematic uncertainties of the MC simulation modeling. The uncertainties of the major backgrounds normalized in the CRs reflect the limited statistical precision of the CRs and the systematic uncertainties in the extrapolation to the signal regions, and an additional uncertainty in the normalization factor from the combined fit is included. The uncertainties related to the data-driven *fake* background estimation are described in detail in Section 6.2.

Systematic uncertainties are treated as Gaussian nuisance parameters in the likelihood while the statistical uncertainties of the MC samples are treated as Poisson nuisance parameters. Unless stated otherwise, each experimental uncertainty is treated as fully correlated across the analysis regions, while each theoretical uncertainty is derived as the relative yield between an analysis region and a control region and is treated as uncorrelated across analysis regions.

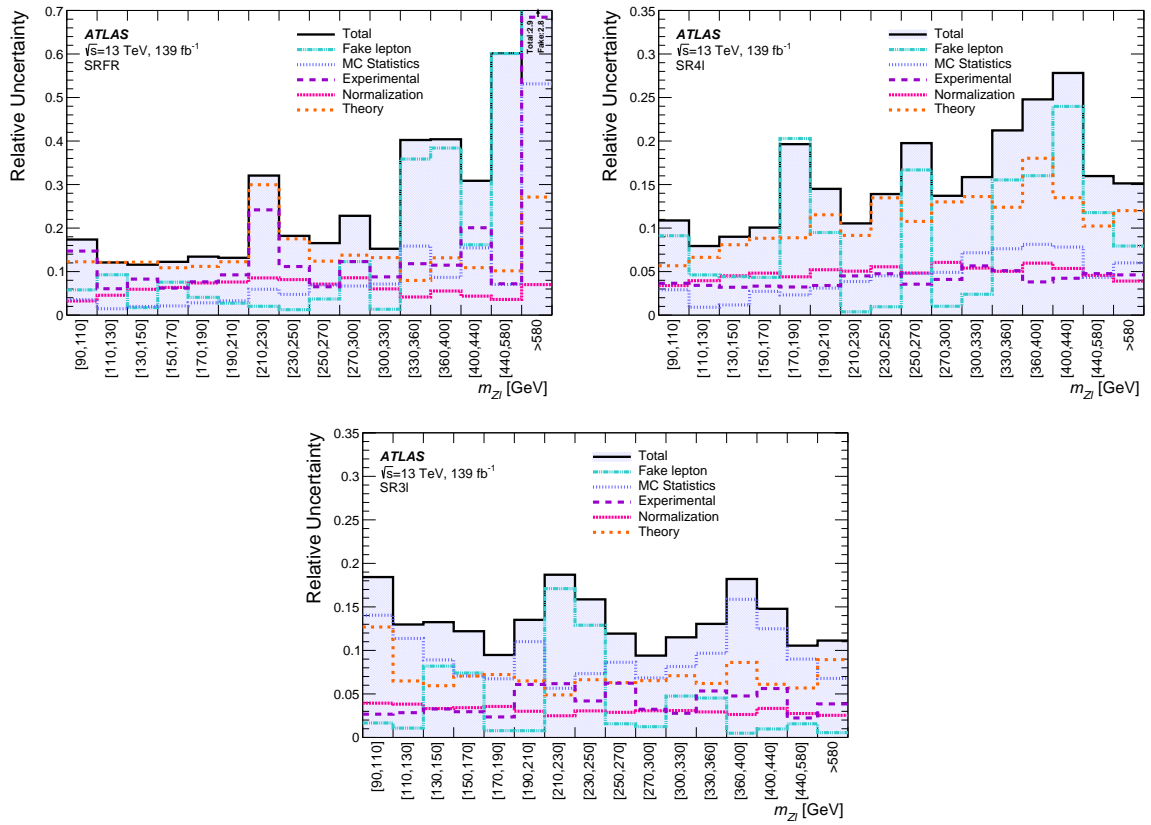


Figure 6: The relative uncertainties in the post-fit SM background prediction as a function of $m_{Z\ell}$ from the background-only fit for the (top left) SRFR, (top right) SR4 ℓ , and (bottom) SR3 ℓ regions. The $m_{Z\ell}$ binning (Eq. (1)) is the same as that used in the fit. Sources of uncertainty are grouped into experimental, theoretical, and MC statistical categories. Separate categories are provided for the *fake* backgrounds and for the normalization procedure of the major WZ , ZZ , and $t\bar{t}Z$ backgrounds. The individual uncertainties can be correlated and do not necessarily contribute in quadrature to the total uncertainty.

A summary of the background uncertainties is shown in Figure 6. Individual uncertainties can be correlated

or anti-correlated, for example between an uncertainty on a major background and the uncertainty on the CR-to-SR normalization procedure for that background. Bin-to-bin fluctuations in the uncertainty of the *fake* background estimation reflect the small anti-ID population and the conservative uncertainties applied when no anti-ID events are seen in the data. The effect of localized fluctuations in one SR is limited as all three SRs contribute to the overall sensitivity. A relative uncertainty of 2.9 is seen in the last $m_{Z\ell}$ bin of SRFR and is driven by a relative uncertainty of 2.8 in the *fake* estimation, reflecting the small post-fit background expectation.

Experimental uncertainties in the detector measurements reflect the accuracy of the kinematic measurements of jets, electrons, muons, and E_T^{miss} . Varying the scale or resolution of the energy or p_T of objects within the uncertainties can cause the migration of events between $m_{Z\ell}$ bins or affect the inclusion of an event in an analysis region. The jet energy scale and resolution uncertainties [94, 106] are a large component of the experimental uncertainty. They are derived as a function of jet p_T and η and account for the flavor and pileup dependencies of the detector energy measurement. Similar scale and resolution uncertainties are included for electrons [89] and muons [90]. These per-object uncertainties are propagated through the E_T^{miss} calculation, with additional uncertainties accounting for the scale and resolution of the E_T^{miss} soft term [96].

Additional experimental uncertainties account for the mismodeling in MC simulation of observables related to the detection of leptons and jets. They include the efficiency of the triggering, identification, reconstruction, and isolation requirements of electrons [89] and muons [90]. They also include the identification and rejection of pileup jets by the jet vertex tagger [98] and the identification of b -jets by the flavor-tagging algorithm [95]. The experimental uncertainty in the combined 2015–2018 integrated luminosity is 1.7% [107], obtained primarily using the luminosity measurements of the LUCID-2 detector [108].

Theoretical uncertainties in the shape of the major diboson, triboson, and $t\bar{t}Z$ backgrounds are derived using MC simulation with varied generator parameters. For the other minor backgrounds a conservative 20% uncertainty is assumed. This value is larger than is typically expected for the minor background processes and the choice has a negligible effect on the final results due to the small contributions of these backgrounds. Uncertainties due to the choice of QCD renormalization and factorization scales [109] are assessed by varying the relevant generator parameters up and down by a factor of two around the nominal values, allowing for both independent and correlated variations of the two scales but prohibiting anti-correlated variations. Each QCD variation is kept separate and is treated as correlated across analysis regions. An uncertainty of 1% due to the chosen value of the strong coupling constant α_S is assessed by varying α_S by ± 0.001 in the generator parameter settings. Uncertainties related to the choice of PDF sets, CT14NNLO [110] or MMHT2014NNLO [111], are derived by taking the envelope of the variation in event yield of 100 propagated uncertainties [70].

Additional theoretical uncertainties are assessed for the major backgrounds. These are related to assumptions made in the event generators and PS models, which can affect both the event kinematics and the cross section of the physics process. For the diboson backgrounds, the SHERPA parameters related to the PS matching scale and resummation scale are varied up and down by a factor of two around the nominal values, and an alternative recoil scheme is studied. For the $t\bar{t}Z$ background, the uncertainties in the hard scatter and in the PS are derived through a comparison with the SHERPA and MADGRAPH5_aMC@NLO +HERWIG7 predictions, respectively. Additional uncertainties in the amount of initial-state radiation (ISR) in the $t\bar{t}Z$ background are assessed by varying the related generator parameters.

For the signal samples, theoretical uncertainties in the cross section are applied, ranging from 4.5% at 100 GeV to 16% at 1500 GeV. Uncertainties related to the QCD scale, PS matching scale, and amount of ISR are derived by varying the related generator parameters of the A14 tune [60].

8 Results

The data are compared with the post-fit background expectations, derived from a background-only profile likelihood fit of all CRs and SRs simultaneously as described in Section 6, and no significant excess is observed. The VRs, shown previously in Figure 5, demonstrate good modeling of the post-fit background expectation in regions kinematically similar to the SRs and for a variety of observables, validating the background-estimation technique. The observed and expected numbers of events in SRFR, SR4 ℓ , and SR3 ℓ are given in Table 3 inclusively in $m_{Z\ell}$ and for the inclusive, e direct-lepton, and μ direct-lepton flavor channels. The background expectation and uncertainty are further split into contributions from each category of SM processes. Separate fits are performed for each flavor channel and for the inclusive channel, and therefore the predicted yields in the e and μ channels may not necessarily add to the inclusive yield. Additionally, the SRFR regions have the same flavor requirement on both direct leptons in an event, and the data and predicted yields in the e and μ channels do not add to the inclusive result.

The $m_{Z\ell}$ distributions in each SR, with binning corresponding to that used in the fit, are shown in Figure 7. The SRs show good agreement in the shape of the $m_{Z\ell}$ distribution between data and the SM expectation, with no significant localized excesses. Three example signals of mass 200, 500, and 800 GeV are included in these figures and peak strongly in their target $m_{Z\ell}$ bin for all three SRs, with the 800 GeV signal only visible in the last $m_{Z\ell}$ bin. Other observables in the SRs relevant for the extrapolation of the yield normalization are shown in Figure 8 and also demonstrate good agreement.

Table 3: The observed yields and post-fit background expectations in SRFR, SR4 ℓ , and SR3 ℓ , shown inclusively and when the direct lepton from a $\tilde{\chi}_1^\pm/\tilde{\chi}_1^0$ decay is required to be an electron or muon. The “Other” category consists mostly of the tWZ , $t\bar{t}W$, and tZ processes. Uncertainties in the background expectation include combined statistical and systematic uncertainties. The individual uncertainties may be correlated and do not necessarily combine in quadrature to give the total background uncertainty.

Region	SRFR	SRFR $_e$	SRFR $_\mu$	SR4 ℓ	SR4 ℓ_e	SR4 ℓ_μ
Observed yield	42	15	17	89	48	41
Expected background yield	39 ± 4	13.7 ± 2.0	15.7 ± 2.5	76 ± 6	35.8 ± 3.5	38.2 ± 2.8
WZ yield	–	–	–	–	–	–
ZZ yield	19 ± 4	7.1 ± 1.7	10.4 ± 2.4	20.9 ± 1.1	9.5 ± 0.6	11.2 ± 0.7
$t\bar{t}Z$ yield	12.2 ± 3.2	2.4 ± 0.7	3.0 ± 0.6	18 ± 6	9.1 ± 3.2	8.5 ± 1.6
Triboson yield	1.3 ± 0.4	0.25 ± 0.09	0.33 ± 0.12	12.2 ± 2.8	5.8 ± 1.4	6.0 ± 1.5
Higgs yield	2.6 ± 0.5	0.72 ± 0.17	1.17 ± 0.25	11.2 ± 2.0	5.3 ± 1.0	5.5 ± 1.1
Other yield	2.1 ± 0.5	0.25 ± 0.17	0.39 ± 0.16	7.9 ± 1.5	4.0 ± 0.8	3.5 ± 0.8
<i>Fake</i> yield	1.3 ± 0.8	3.0 ± 1.5	$0.5^{+0.6}_{-0.5}$	6.4 ± 2.5	2.1 ± 1.1	3.6 ± 1.7
Region	SR3 ℓ	SR3 ℓ_e	SR3 ℓ_μ			
Observed yield	61	28	33			
Expected background yield	54.9 ± 3.3	27.5 ± 2.2	27.4 ± 2.0			
WZ yield	33.6 ± 2.4	16.5 ± 1.7	17.3 ± 1.8			
ZZ yield	0.92 ± 0.27	0.11 ± 0.04	0.77 ± 0.24			
$t\bar{t}Z$ yield	7.5 ± 2.3	4.1 ± 1.3	3.4 ± 0.7			
Triboson yield	5.6 ± 1.5	2.7 ± 0.8	2.6 ± 0.7			
Higgs yield	0.51 ± 0.10	0.25 ± 0.06	0.23 ± 0.05			
Other yield	4.2 ± 0.8	2.0 ± 0.4	2.0 ± 0.4			
<i>Fake</i> yield	2.5 ± 1.2	1.8 ± 1.1	1.0 ± 0.8			

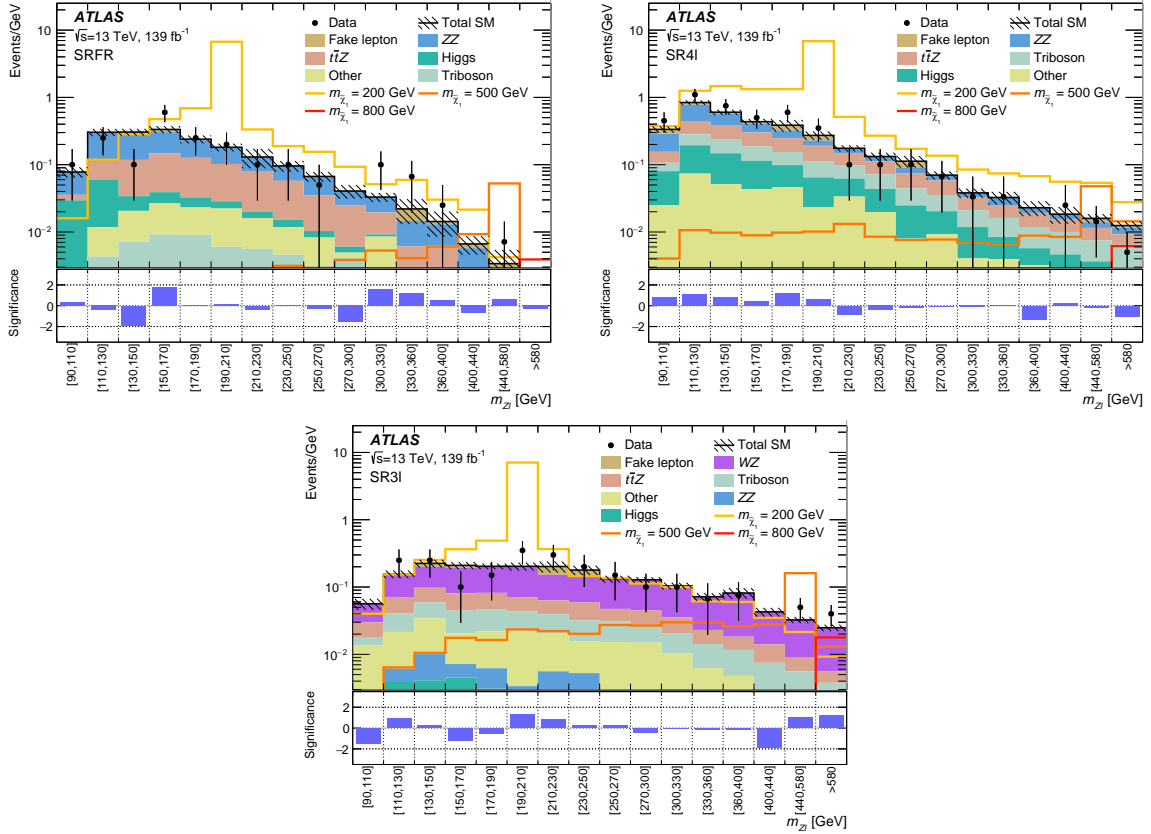


Figure 7: The observed data and post-fit SM background expectation as a function of $m_{Z\ell}$ in (top left) SRFR, (top right) SR4 ℓ , and (bottom) SR3 ℓ . The $m_{Z\ell}$ binning (Eq. (1)) is the same as that used in the fit and the yield is normalized to the bin width, with the last bin normalized using a width of 200 GeV. The “Other” category consists mostly of the tWZ , $t\bar{t}W$, and tZ processes. The hatched bands indicate the combined theoretical, experimental, and MC statistical uncertainties in the background prediction. The bottom panel shows the significance of the differences between the observed data and expected yields, computed following the profile likelihood method described in Ref. [102].

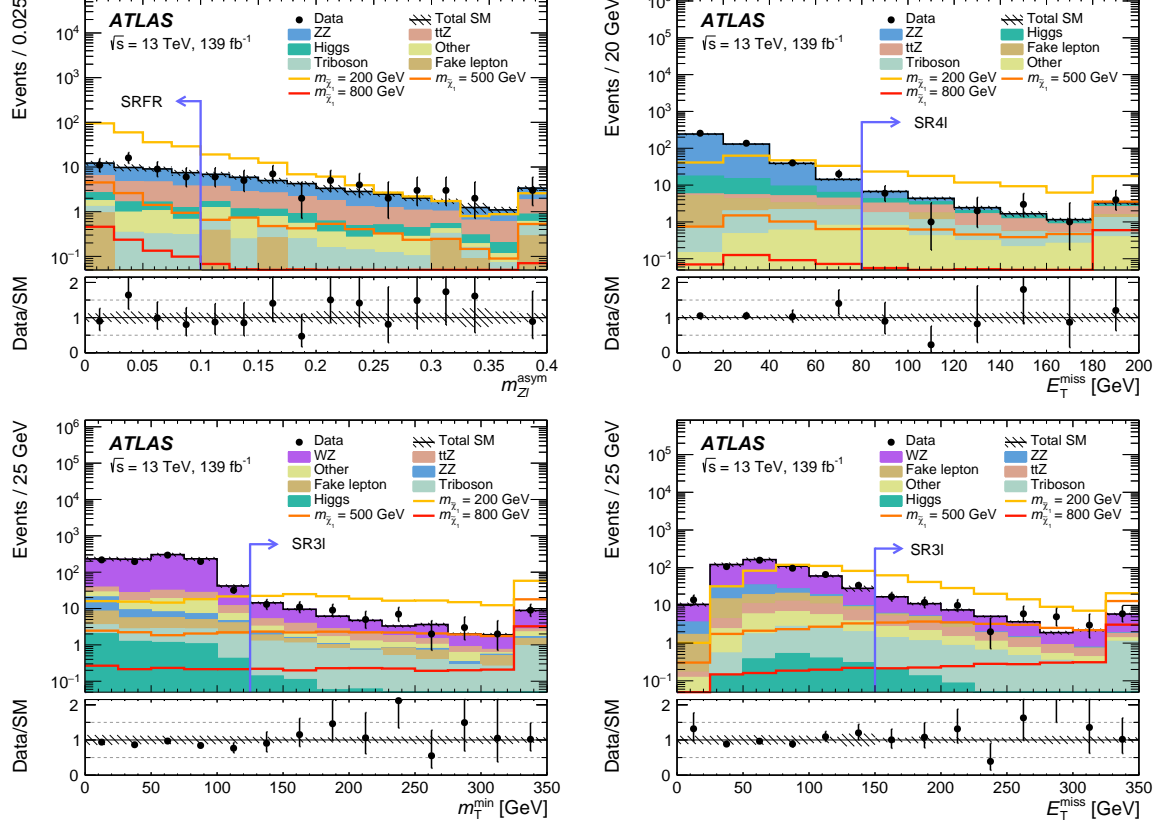


Figure 8: Example kinematic distributions in the signal regions showing the data and the post-fit background expectation, including (top left) $m_{Z\ell}^{\text{asym}}$ in SRFR, (top right) E_T^{miss} in SR4 ℓ , and (bottom left) m_T^{min} and (bottom right) E_T^{miss} in SR3 ℓ . The fit uses all CRs and SRs, and the distributions are shown inclusively in $m_{Z\ell}$. The full event selection for each of the corresponding regions is applied except for the variable shown, where the selection is indicated by a blue arrow. The last bin includes overflow events. The “Other” category consists mostly of the tWZ , $t\bar{t}W$, and tZ processes. The hatched bands indicate the combined theoretical, experimental, and MC statistical uncertainties in the background prediction. The bottom panel shows the ratio of the data to the background prediction.

8.1 Model-independent limits on new physics in inclusive regions

Upper limits are set on the possible visible cross sections of generic beyond-the-SM (BSM) processes in each $m_{Z\ell}$ bin of each SR. These model-independent limits are derived at 95% confidence level (CL) using the CL_s prescription [112], and results are evaluated using pseudo-experiments. A profile likelihood fit is performed on the numbers of observed and expected events in the target $m_{Z\ell}$ bin of one SR and the three CRs, and a generic BSM process is assumed to contribute only to the target $m_{Z\ell}$ bin. In this way no assumption is made concerning the $\tilde{\chi}_1^\pm/\tilde{\chi}_1^0$ branching fractions or $m_{Z\ell}$ shape of the BSM process. No uncertainties in the yield of the BSM process are considered, except for the luminosity uncertainty.

This procedure is repeated for each of the 16 $m_{Z\ell}$ bins in each of the three SRs, with only one SR bin considered for each fit. This differs from the nominal fit strategy which is performed using the three CRs and the 48 $m_{Z\ell}$ bins of the SRs simultaneously, and minor differences from the significances shown in the bottom panel of Figure 7 are seen.

The model-independent limits are summarized in Table 4, which includes for each signal region:

- the number of observed events N_{obs} ,
- the expected number of SM events N_{exp} and the associated uncertainty from a fit to the CRs only,
- the observed limit on the visible cross section $\langle \epsilon \sigma \rangle_{\text{obs}}^{95}$ of the potential BSM process,
- the corresponding observed upper limit on the number of BSM events S_{obs}^{95} ,
- the expected upper limit on the number of BSM events S_{exp}^{95} and the associated uncertainty,
- and the p -value (and associated significance Z) for the SM background alone to fluctuate to at least the number of observed events.

The observed limit $\langle \epsilon \sigma \rangle_{\text{obs}}^{95}$ is defined as the ratio of S_{obs}^{95} to the integrated luminosity, and it incorporates the cross section, acceptance, and selection efficiency of the generic BSM signal. No $m_{Z\ell}$ bin shows a significant excess in all three SRs, in contrast to what would be expected in the presence of a resonance that contributes to all SRs. The largest excess of data over the expected background is seen in SRFR for the $m_{Z\ell}$ region between 150 and 170 GeV, with an associated significance of 2.1σ . This is consistent with the expectation from statistical fluctuations of the SM background when considering 48 independent signal regions.

Table 4: Model-independent results where each row targets one $m_{Z\ell}$ bin of one SR and probes scenarios where a generic beyond-the-SM process is assumed to contribute only to that $m_{Z\ell}$ bin. The first two columns refer to the signal region and $m_{Z\ell}$ bin probed, while the third and fourth columns show the observed (N_{obs}) and expected (N_{exp}) event yields. The expected yields are obtained using a background-only fit of all the CRs, and the errors include statistical and systematic uncertainties. The fifth and sixth columns show the observed 95% CL upper limit on the visible cross section ($\langle \epsilon \sigma \rangle_{\text{obs}}^{95}$) and on the number of signal events (S_{obs}^{95}), while the seventh column shows the expected 95% CL upper limit on the number of signal events (S_{exp}^{95}) with the associated 1σ uncertainties. The last column provides the discovery p -value and significance (Z) of any excess of data above background expectation. Cases for which the observed yield is less than the expected yield are capped at a p -value of 0.5.

Region	Range of $m_{Z\ell}$ [GeV]	N_{obs}	N_{exp}	$\langle \epsilon \sigma \rangle_{\text{obs}}^{95}$ [fb]	S_{obs}^{95}	S_{exp}^{95}	$p(s = 0)$ (Z)
SRFR	[90, 110]	2	1.58 ± 0.32	0.03	4.2	$4.0^{+1.8}_{-0.8}$	0.44 (0.2)
	[110, 130]	5	5.9 ± 1.0	0.04	5.6	$6.7^{+2.3}_{-1.0}$	0.50 (0.0)
	[130, 150]	2	6.0 ± 1.0	0.03	3.8	$6.3^{+2.0}_{-1.0}$	0.50 (0.0)
	[150, 170]	12	6.1 ± 1.0	0.10	14.3	$7.8^{+3.1}_{-1.9}$	0.02 (2.1)
	[170, 190]	5	4.5 ± 0.8	0.05	6.8	$5.8^{+2.2}_{-1.3}$	0.31 (0.5)
	[190, 210]	4	3.4 ± 0.6	0.04	6.2	$5.3^{+2.1}_{-1.2}$	0.28 (0.6)
	[210, 230]	2	2.6 ± 1.5	0.03	4.5	$4.8^{+1.9}_{-0.9}$	0.50 (0.0)
	[230, 250]	2	1.83 ± 0.31	0.03	4.7	$4.1^{+1.6}_{-0.8}$	0.41 (0.2)
	[250, 270]	1	1.25 ± 0.22	0.03	4.0	$3.9^{+1.8}_{-0.9}$	0.50 (0.0)
	[270, 300]	0	1.18 ± 0.32	0.03	3.6	$3.9^{+1.3}_{-0.8}$	0.50 (0.0)
	[300, 330]	3	0.89 ± 0.16	0.05	6.7	$4.2^{+0.8}_{-0.4}$	0.02 (2.0)
	[330, 360]	2	0.52 ± 0.18	0.04	5.6	$3.5^{+0.8}_{-0.2}$	0.03 (1.9)
	[360, 400]	1	0.50 ± 0.19	0.03	4.0	$3.2^{+1.0}_{-0.1}$	0.18 (0.9)
	[400, 440]	0	0.27 ± 0.09	0.02	3.2	$3.1^{+0.8}_{-0.1}$	0.50 (0.0)
	[440, 580]	1	0.29 ± 0.17	0.03	4.4	$3.3^{+1.0}_{-0.1}$	0.12 (1.2)
	>580	0	$0.07^{+0.17}_{-0.07}$	0.02	3.0	$3.1^{+0.1}_{-0.0}$	0.50 (0.0)
SR4 ℓ	[90, 110]	9	6.1 ± 0.7	0.07	9.6	$7.1^{+2.1}_{-1.1}$	0.14 (1.1)
	[110, 130]	22	15.4 ± 1.3	0.12	16.7	$10.0^{+4.4}_{-1.9}$	0.05 (1.6)
	[130, 150]	15	10.9 ± 0.9	0.09	12.8	$8.4^{+3.4}_{-1.8}$	0.09 (1.4)
	[150, 170]	10	7.9 ± 0.8	0.07	10.0	$7.5^{+2.9}_{-1.5}$	0.16 (1.0)
	[170, 190]	12	5.9 ± 0.6	0.10	14.2	$8.5^{+3.4}_{-0.8}$	0.02 (2.0)
	[190, 210]	7	4.9 ± 0.7	0.06	8.3	$6.5^{+1.9}_{-1.5}$	0.15 (1.0)
	[210, 230]	2	3.17 ± 0.33	0.03	4.4	$4.9^{+2.2}_{-1.4}$	0.50 (0.0)
	[230, 250]	2	2.36 ± 0.27	0.03	4.5	$4.5^{+1.9}_{-1.1}$	0.50 (0.0)
	[250, 270]	2	2.1 ± 0.5	0.03	4.9	$4.8^{+1.8}_{-1.2}$	0.50 (0.0)
	[270, 300]	2	1.88 ± 0.21	0.03	4.8	$4.2^{+1.6}_{-1.0}$	0.50 (0.0)
	[300, 330]	1	1.03 ± 0.14	0.03	4.1	$3.6^{+1.6}_{-0.5}$	0.50 (0.0)
	[330, 360]	1	0.88 ± 0.21	0.03	4.0	$3.7^{+1.4}_{-0.7}$	0.26 (0.6)
	[360, 400]	0	0.84 ± 0.20	0.02	3.0	$3.4^{+1.5}_{-0.4}$	0.50 (0.0)
	[400, 440]	1	0.64 ± 0.18	0.03	4.2	$3.2^{+1.1}_{-0.1}$	0.17 (1.0)
	[440, 580]	2	2.0 ± 0.4	0.03	4.7	$4.6^{+1.5}_{-1.4}$	0.50 (0.0)
	>580	1	2.3 ± 0.4	0.03	4.0	$4.7^{+1.7}_{-0.8}$	0.50 (0.0)
SR3 ℓ	[90, 110]	0	1.08 ± 0.18	0.03	4.8	$3.8^{+1.3}_{-0.5}$	0.50 (0.0)
	[110, 130]	5	2.8 ± 0.4	0.06	7.9	$5.6^{+1.7}_{-0.9}$	0.08 (1.4)
	[130, 150]	5	4.1 ± 0.6	0.05	6.7	$5.8^{+2.0}_{-1.2}$	0.26 (0.6)
	[150, 170]	2	4.0 ± 0.6	0.03	4.1	$5.3^{+2.3}_{-1.2}$	0.50 (0.0)
	[170, 190]	3	3.9 ± 0.4	0.03	4.9	$5.2^{+2.4}_{-1.2}$	0.50 (0.0)
	[190, 210]	7	3.7 ± 0.6	0.07	9.1	$6.1^{+2.2}_{-1.9}$	0.10 (1.3)
	[210, 230]	6	3.5 ± 0.7	0.06	8.8	$6.2^{+1.8}_{-1.2}$	0.08 (1.4)
	[230, 250]	4	3.3 ± 0.6	0.04	6.1	$5.3^{+1.7}_{-1.2}$	0.28 (0.6)
	[250, 270]	3	2.5 ± 0.4	0.04	5.1	$4.5^{+1.8}_{-1.2}$	0.36 (0.4)
	[270, 300]	3	3.7 ± 0.4	0.03	4.8	$5.4^{+1.8}_{-1.6}$	0.50 (0.0)
	[300, 330]	3	3.0 ± 0.4	0.04	5.1	$4.9^{+1.8}_{-1.1}$	0.50 (0.0)
	[330, 360]	2	2.06 ± 0.35	0.03	4.8	$4.5^{+1.5}_{-1.4}$	0.50 (0.0)
	[360, 400]	3	3.2 ± 0.7	0.04	5.1	$5.3^{+2.0}_{-1.5}$	0.50 (0.0)
	[400, 440]	0	1.70 ± 0.27	0.02	3.0	$3.7^{+2.0}_{-0.6}$	0.50 (0.0)
	[440, 580]	7	4.3 ± 0.5	0.06	8.7	$6.2^{+1.9}_{-1.3}$	0.09 (1.3)
	>580	8	4.6 ± 0.6	0.07	10.0	$6.5^{+2.3}_{-1.4}$	0.08 (1.4)

8.2 Mass limits on $B - L$ RPV production

Hypothesis tests for the $B - L$ signal models are performed using the same CL_s prescription [112], with exclusion lower limits set on the $\tilde{\chi}_1^\pm/\tilde{\chi}_1^0$ masses for various scenarios of the $\tilde{\chi}_1^\pm/\tilde{\chi}_1^0$ branching fractions using asymptotic formulas [100]. A profile likelihood fit is performed simultaneously to the CRs and all $m_{Z\ell}$ bins of the three SRs, benefiting from the contribution of a signal model to a small number of $m_{Z\ell}$ bins coherently across SRFR, SR4 ℓ , and SR3 ℓ . The signal strength is represented by a single parameter of interest and coherently scales the signal yield across all regions.

The sensitivity to the signal models is dependent on the $\tilde{\chi}_1^\pm/\tilde{\chi}_1^0$ branching fractions to each lepton and boson type, and a scan is performed over various combinations. The contributions from the $\tilde{\chi}_1^\pm\tilde{\chi}_1^\mp$ and $\tilde{\chi}_1^\pm\tilde{\chi}_1^0$ processes are treated together, and the $\tilde{\chi}_1^\pm/\tilde{\chi}_1^0$ branching fractions are treated as fully correlated. Four scenarios are considered for the $\tilde{\chi}_1^\pm/\tilde{\chi}_1^0$ branching fractions to leptons: the scenario with equal branching fractions to e , μ , and τ -leptons and the three scenarios with 100% branching fractions to a single lepton type.

For each leptonic scenario, the $\tilde{\chi}_1^\pm/\tilde{\chi}_1^0$ branching fractions to W , Z , and Higgs bosons are scanned at 10% intervals. A 0% branching fraction to Z bosons is not explored and is replaced by a 1% branching fraction in the scans. No significant difference in sensitivity is seen for the relative $\tilde{\chi}_1^\pm/\tilde{\chi}_1^0$ branching fractions to W or Higgs bosons, with the sensitivity dominated by the branching fraction to Z bosons, which produces the target trilepton resonances. The three SRs contribute roughly equally to the overall sensitivity of the search, with a minor increase in sensitivity to Higgs boson decays from SRFR offset by a similar increase in sensitivity to W boson decays from SR4 ℓ .

The expected and observed mass-exclusion contours as a function of the $\tilde{\chi}_1^\pm/\tilde{\chi}_1^0$ branching fraction to Z bosons are shown in Figure 9 for each of the four lepton-flavor scenarios. The $\tilde{\chi}_1^\pm/\tilde{\chi}_1^0$ branching fractions to W and Higgs bosons are set to be equal here. Limits are set for signal masses above 100 GeV, and agreement within the uncertainties is seen between the observed and expected limits. The observed limit is slightly weaker than the expected limit due to the minor excesses seen at low $m_{Z\ell}$ in SR4 ℓ and in some high $m_{Z\ell}$ bins in SRFR and SR3 ℓ .

The observed mass exclusions are strongest when the $\tilde{\chi}_1^\pm/\tilde{\chi}_1^0$ branching fraction to Z bosons is largest, reaching 1100 GeV and 1050 GeV for the e and μ channels, respectively. The limit is slightly reduced to 975 GeV when no assumption is made about the flavor of the directly produced lepton, and is weakest at 625 GeV when only $\tilde{\chi}_1^\pm/\tilde{\chi}_1^0$ decays into τ -leptons are allowed. The observed mass limit becomes significantly reduced when the $\tilde{\chi}_1^\pm/\tilde{\chi}_1^0$ branching fraction to Z bosons falls below 20%, reaching 375 GeV in the μ channel and 350 GeV in the e channel when the branching fraction reaches 1%. No limits are set when requiring decays into τ -leptons for branching fractions to Z bosons below 11%.

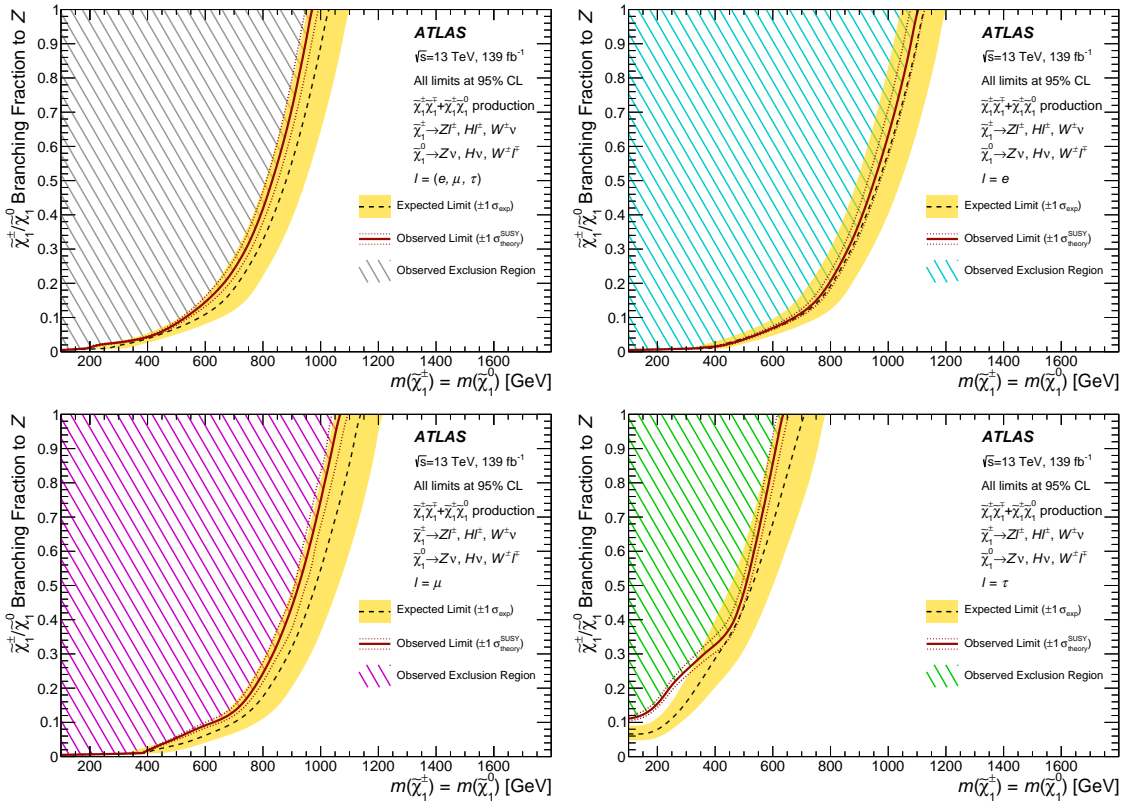


Figure 9: Exclusion curves for the simplified model of $\tilde{\chi}_1^\pm \tilde{\chi}_1^\mp + \tilde{\chi}_1^\pm \tilde{\chi}_1^0$ production as a function of $\tilde{\chi}_1^\pm/\tilde{\chi}_1^0$ mass and branching fraction to Z bosons. Curves are derived separately when requiring that the charged-lepton decays of $\tilde{\chi}_1^\pm/\tilde{\chi}_1^0$ are into (top left) any leptons with equal probability, (top right) electrons only, (bottom left) muons only, or (bottom right) τ -leptons only. The expected 95% CL exclusion (dashed black line) is shown with $\pm 1 \sigma_{\text{exp}}$ variations (shaded yellow band) from systematic and statistical uncertainties in the expected yields. The observed 95% CL exclusion (solid red line) is shown with $\pm 1 \sigma_{\text{theory}}^{\text{SUSY}}$ variations (dotted red lines) from cross-section uncertainties for the signal models. The phase-space excluded by the search is shown in the hatched regions. The sum of the $\tilde{\chi}_1^\pm/\tilde{\chi}_1^0$ branching fractions to W , Z , and Higgs bosons is unity for each point, and the branching fractions to W and Higgs bosons are chosen so as to be equal everywhere.

9 Conclusions

This paper presents a search for wino-type $\tilde{\chi}_1^\pm \tilde{\chi}_1^\mp$ and $\tilde{\chi}_1^\pm \tilde{\chi}_1^0$ production where each $\tilde{\chi}_1^\pm/\tilde{\chi}_1^0$ decays via an RPV coupling into a W , Z , or Higgs boson and a lepton. The dataset corresponds to an integrated luminosity of 139 fb^{-1} of proton–proton collision data produced at a center-of-mass energy of $\sqrt{s} = 13 \text{ TeV}$ and collected by the ATLAS experiment at the LHC between 2015 and 2018. This search primarily targets the three-lepton decay of a $\tilde{\chi}_1^\pm$ and is the first ATLAS analysis using $\sqrt{s} = 13 \text{ TeV}$ data to search for a resonance in the $m_{Z\ell}$ spectrum. Three signal regions are defined that target events with three or more leptons and missing transverse momentum or with two fully reconstructed $\tilde{\chi}_1^\pm/\tilde{\chi}_1^0$ decays. The observed event yields are found to be in agreement with Standard Model expectations, with no significant excess seen in the $m_{Z\ell}$ distributions of the signal regions.

Model-independent limits are set at a 95% confidence level for each $m_{Z\ell}$ bin in each signal region. The largest excess of data over the expectation in the 48 model-independent regions is found to be 2.1σ . No

trend is seen in the distribution of data excesses in $m_{Z\ell}$ bins across the three signal regions. Model-specific lower limits are also set on the $\tilde{\chi}_1^\pm/\tilde{\chi}_1^0$ masses for various decay branching fractions into a lepton (electron, muon, or τ -lepton) plus a boson (W , Z , or Higgs), reflecting sensitivity to the neutrino mass hierarchy and the MSSM parameters of the $B - L$ RPV theory. For scenarios with large $\tilde{\chi}_1^\pm/\tilde{\chi}_1^0$ branching fractions to Z bosons, lower limits on the $\tilde{\chi}_1^\pm/\tilde{\chi}_1^0$ masses are set at 625 GeV, 1050 GeV, and 1100 GeV for 100% branching fractions to a Z boson plus a τ -lepton, muon, or electron, respectively.

Acknowledgments

We thank CERN for the very successful operation of the LHC, as well as the support staff from our institutions without whom ATLAS could not be operated efficiently.

We acknowledge the support of ANPCyT, Argentina; YerPhI, Armenia; ARC, Australia; BMWFW and FWF, Austria; ANAS, Azerbaijan; SSTC, Belarus; CNPq and FAPESP, Brazil; NSERC, NRC and CFI, Canada; CERN; ANID, Chile; CAS, MOST and NSFC, China; COLCIENCIAS, Colombia; MSMT CR, MPO CR and VSC CR, Czech Republic; DNRF and DNSRC, Denmark; IN2P3-CNRS and CEA-DRF/IRFU, France; SRNSFG, Georgia; BMBF, HGF and MPG, Germany; GSRT, Greece; RGC and Hong Kong SAR, China; ISF and Benoziyo Center, Israel; INFN, Italy; MEXT and JSPS, Japan; CNRST, Morocco; NWO, Netherlands; RCN, Norway; MNiSW and NCN, Poland; FCT, Portugal; MNE/IFA, Romania; JINR; MES of Russia and NRC KI, Russian Federation; MESTD, Serbia; MSSR, Slovakia; ARRS and MIZŠ, Slovenia; DST/NRF, South Africa; MICINN, Spain; SRC and Wallenberg Foundation, Sweden; SERI, SNSF and Cantons of Bern and Geneva, Switzerland; MOST, Taiwan; TAEK, Turkey; STFC, United Kingdom; DOE and NSF, United States of America. In addition, individual groups and members have received support from BCKDF, CANARIE, Compute Canada, CRC and IVADO, Canada; Beijing Municipal Science & Technology Commission, China; COST, ERC, ERDF, Horizon 2020 and Marie Skłodowska-Curie Actions, European Union; Investissements d’Avenir Labex, Investissements d’Avenir Idex and ANR, France; DFG and AvH Foundation, Germany; Herakleitos, Thales and Aristeia programmes co-financed by EU-ESF and the Greek NSRF, Greece; BSF-NSF and GIF, Israel; La Caixa Banking Foundation, CERCA Programme Generalitat de Catalunya and PROMETEO and GenT Programmes Generalitat Valenciana, Spain; Göran Gustafssons Stiftelse, Sweden; The Royal Society and Leverhulme Trust, United Kingdom.

The crucial computing support from all WLCG partners is acknowledged gratefully, in particular from CERN, the ATLAS Tier-1 facilities at TRIUMF (Canada), NDGF (Denmark, Norway, Sweden), CC-IN2P3 (France), KIT/GridKA (Germany), INFN-CNAF (Italy), NL-T1 (Netherlands), PIC (Spain), ASGC (Taiwan), RAL (UK) and BNL (USA), the Tier-2 facilities worldwide and large non-WLCG resource providers. Major contributors of computing resources are listed in Ref. [113].

References

- [1] Y. Golfand and E. Likhtman, *Extension of the Algebra of Poincare Group Generators and Violation of P Invariance*, JETP Lett. **13** (1971) 323, [Pisma Zh. Eksp. Teor. Fiz. **13** (1971) 452].
- [2] D. Volkov and V. Akulov, *Is the neutrino a goldstone particle?* Phys. Lett. B **46** (1973) 109.
- [3] J. Wess and B. Zumino, *Supergauge transformations in four dimensions*, Nucl. Phys. B **70** (1974) 39.
- [4] J. Wess and B. Zumino, *Supergauge invariant extension of quantum electrodynamics*, Nucl. Phys. B **78** (1974) 1.
- [5] S. Ferrara and B. Zumino, *Supergauge invariant Yang-Mills theories*, Nucl. Phys. B **79** (1974) 413.
- [6] A. Salam and J. Strathdee, *Super-symmetry and non-Abelian gauges*, Phys. Lett. B **51** (1974) 353.
- [7] G. R. Farrar and P. Fayet, *Phenomenology of the production, decay, and detection of new hadronic states associated with supersymmetry*, Phys. Lett. B **76** (1978) 575.
- [8] J. Ellis, J. Hagelin, D. V. Nanopoulos, K. A. Olive, and M. Srednicki, *Supersymmetric relics from the big bang*, Nucl. Phys. B **238** (1984) 453.
- [9] M. Pospelov, *Particle physics catalysis of thermal Big Bang Nucleosynthesis*, Phys. Rev. Lett. **98** (2007) 231301, arXiv: [hep-ph/0605215](#).
- [10] H. K. Dreiner, *An introduction to explicit R-parity violation*, Adv. Ser. Direct. High Energy Phys. **21** (2010) 565, arXiv: [hep-ph/9707435](#).
- [11] R. Barbier et al., *R-parity violating supersymmetry*, Phys. Rept. **420** (2005) 1, arXiv: [hep-ph/0406039](#).
- [12] P. Fayet, *Supersymmetry and weak, electromagnetic and strong interactions*, Phys. Lett. B **64** (1976) 159.
- [13] P. Fayet, *Spontaneously broken supersymmetric theories of weak, electromagnetic and strong interactions*, Phys. Lett. B **69** (1977) 489.
- [14] V. Barger, P. Fileviez Perez, and S. Spinner, *Minimal Gauged $U(1)_{B-L}$ Model with Spontaneous R-Parity Violation*, Phys. Rev. Lett. **102** (2009) 181802, arXiv: [0812.3661 \[hep-ph\]](#).
- [15] L. L. Everett, P. Fileviez Perez, and S. Spinner, *The right side of TeV scale spontaneous R-Parity violation*, Phys. Rev. D **80** (2009) 055007, arXiv: [0906.4095 \[hep-ph\]](#).
- [16] V. Braun, Y.-H. He, B. A. Ovrut, and T. Panett, *A heterotic standard model*, Phys. Lett. B **618** (2005) 252, arXiv: [hep-th/0501070](#).
- [17] R. Deen, B. A. Ovrut, and A. Purves, *The minimal SUSY $B - L$ model: simultaneous Wilson lines and string thresholds*, JHEP **07** (2016) 043, arXiv: [1604.08588 \[hep-ph\]](#).
- [18] P. Fileviez Perez and S. Spinner, *Spontaneous R-Parity breaking and left-right symmetry*, Phys. Lett. B **673** (2009) 251, arXiv: [0811.3424 \[hep-ph\]](#).
- [19] P. Fileviez Perez and S. Spinner, *The Minimal Theory for R-parity Violation at the LHC*, JHEP **04** (2012) 118, arXiv: [1201.5923 \[hep-ph\]](#).
- [20] P. Fileviez Perez and S. Spinner, *Supersymmetry at the LHC and the Theory of R-parity*, Phys. Lett. B **728** (2014) 489, arXiv: [1308.0524 \[hep-ph\]](#).
- [21] B. A. Ovrut, A. Purves, and S. Spinner, *A statistical analysis of the minimal SUSY $B - L$ theory*, Mod. Phys. Lett. A **30** (2015) 1550085, arXiv: [1412.6103 \[hep-ph\]](#).

- [22] B. A. Ovrut, A. Purves, and S. Spinner, *The minimal SUSY $B - L$ model: from the unification scale to the LHC*, JHEP **06** (2015) 182, arXiv: [1503.01473 \[hep-ph\]](#).
- [23] S. Dumitru, B. A. Ovrut, and A. Purves, *The R -parity violating decays of charginos and neutralinos in the $B-L$ MSSM*, JHEP **02** (2019) 124, arXiv: [1810.11035 \[hep-ph\]](#).
- [24] S. Dumitru, B. A. Ovrut, and A. Purves, *R -parity violating decays of wino chargino and wino neutralino LSPs and NLSPs at the LHC*, JHEP **06** (2019) 100, arXiv: [1811.05581 \[hep-ph\]](#).
- [25] ATLAS Collaboration, *Search for electroweak production of supersymmetric particles in final states with two or three leptons at $\sqrt{s} = 13$ TeV with the ATLAS detector*, Eur. Phys. J. C **78** (2018) 995, arXiv: [1803.02762 \[hep-ex\]](#).
- [26] ATLAS Collaboration, *Search for direct production of charginos and neutralinos in events with three leptons and missing transverse momentum in $\sqrt{s} = 8$ TeV pp collisions with the ATLAS detector*, JHEP **04** (2014) 169, arXiv: [1402.7029 \[hep-ex\]](#).
- [27] CMS Collaboration, *Search for electroweak production of charginos and neutralinos in multilepton final states in proton–proton collisions at $\sqrt{s} = 13$ TeV*, JHEP **03** (2018) 166, arXiv: [1709.05406 \[hep-ex\]](#).
- [28] CMS Collaboration, *Combined search for electroweak production of charginos and neutralinos in proton–proton collisions at $\sqrt{s} = 13$ TeV*, JHEP **03** (2018) 160, arXiv: [1801.03957 \[hep-ex\]](#).
- [29] ATLAS Collaboration, *Search for type-III seesaw heavy leptons in pp collisions at $\sqrt{s} = 8$ TeV with the ATLAS Detector*, Phys. Rev. D **92** (2015) 032001, arXiv: [1506.01839 \[hep-ex\]](#).
- [30] ATLAS Collaboration, *Search for heavy lepton resonances decaying to a Z boson and a lepton in pp collisions at $\sqrt{s} = 8$ TeV with the ATLAS detector*, JHEP **09** (2015) 108, arXiv: [1506.01291 \[hep-ex\]](#).
- [31] CMS Collaboration, *Search for Evidence of the Type-III Seesaw Mechanism in Multilepton Final States in Proton–Proton Collisions at $\sqrt{s} = 13$ TeV*, Phys. Rev. Lett. **119** (2017) 221802, arXiv: [1708.07962 \[hep-ex\]](#).
- [32] ATLAS Collaboration, *Search for $B-L$ R -parity-violating top squarks in $\sqrt{s} = 13$ TeV pp collisions with the ATLAS experiment*, Phys. Rev. D **97** (2018) 032003, arXiv: [1710.05544 \[hep-ex\]](#).
- [33] Z. Marshall, B. A. Ovrut, A. Purves, and S. Spinner, *LSP squark decays at the LHC and the neutrino mass hierarchy*, Phys. Rev. D **90** (2014) 015034, arXiv: [1402.5434 \[hep-ph\]](#).
- [34] ATLAS Collaboration, *The ATLAS Experiment at the CERN Large Hadron Collider*, JINST **3** (2008) S08003.
- [35] ATLAS Collaboration, *ATLAS Insertable B-Layer Technical Design Report*, ATLAS-TDR-19, 2010, URL: <https://cds.cern.ch/record/1291633>, *ATLAS Insertable B-Layer Technical Design Report Addendum*, ATLAS-TDR-19-ADD-1, 2012, URL: <https://cds.cern.ch/record/1451888>.
- [36] B. Abbott et al., *Production and integration of the ATLAS Insertable B-Layer*, JINST **13** (2018) T05008, arXiv: [1803.00844 \[physics.ins-det\]](#).
- [37] ATLAS Collaboration, *Performance of the ATLAS trigger system in 2015*, Eur. Phys. J. C **77** (2017) 317, arXiv: [1611.09661 \[hep-ex\]](#).
- [38] ATLAS Collaboration, *Performance of electron and photon triggers in ATLAS during LHC Run 2*, Eur. Phys. J. C **80** (2020) 47, arXiv: [1909.00761 \[hep-ex\]](#).

- [39] ATLAS Collaboration, *ATLAS data quality operations and performance for 2015–2018 data-taking*, *JINST* **15** (2020) P04003, arXiv: [1911.04632 \[physics.ins-det\]](#).
- [40] ATLAS Collaboration, *Multi-Boson Simulation for 13 TeV ATLAS Analyses*, ATL-PHYS-PUB-2017-005, 2017, URL: <https://cds.cern.ch/record/2261933>.
- [41] ATLAS Collaboration, *ATLAS simulation of boson plus jets processes in Run 2*, ATL-PHYS-PUB-2017-006, 2017, URL: <https://cds.cern.ch/record/2261937>.
- [42] E. Bothmann et al., *Event Generation with Sherpa 2.2*, (2019), arXiv: [1905.09127 \[hep-ph\]](#).
- [43] T. Gleisberg and S. Höche, *Comix, a new matrix element generator*, *JHEP* **12** (2008) 039, arXiv: [0808.3674 \[hep-ph\]](#).
- [44] S. Schumann and F. Krauss, *A parton shower algorithm based on Catani–Seymour dipole factorisation*, *JHEP* **03** (2008) 038, arXiv: [0709.1027 \[hep-ph\]](#).
- [45] S. Catani, F. Krauss, R. Kuhn, and B. R. Webber, *QCD matrix elements + parton showers*, *JHEP* **11** (2001) 063, arXiv: [hep-ph/0109231](#).
- [46] S. Höche, F. Krauss, S. Schumann, and F. Siegert, *QCD matrix elements and truncated showers*, *JHEP* **05** (2009) 053, arXiv: [0903.1219 \[hep-ph\]](#).
- [47] S. Höche, F. Krauss, M. Schönherr, and F. Siegert, *A critical appraisal of NLO+PS matching methods*, *JHEP* **09** (2012) 049, arXiv: [1111.1220 \[hep-ph\]](#).
- [48] S. Höche, F. Krauss, M. Schönherr, and F. Siegert, *QCD matrix elements + parton showers. The NLO case*, *JHEP* **04** (2013) 027, arXiv: [1207.5030 \[hep-ph\]](#).
- [49] F. Cascioli, P. Maierhöfer, and S. Pozzorini, *Scattering Amplitudes with Open Loops*, *Phys. Rev. Lett.* **108** (2012) 111601, arXiv: [1111.5206 \[hep-ph\]](#).
- [50] A. Denner, S. Dittmaier, and L. Hofer, *Collier: a fortran-based Complex One-Loop Library in Extended Regularizations*, *Comput. Phys. Commun.* **212** (2017) 220, arXiv: [1604.06792 \[hep-ph\]](#).
- [51] R. D. Ball et al., *Parton distributions for the LHC run II*, *JHEP* **04** (2015) 040, arXiv: [1410.8849 \[hep-ph\]](#).
- [52] C. Anastasiou, L. J. Dixon, K. Melnikov, and F. Petriello, *High precision QCD at hadron colliders: Electroweak gauge boson rapidity distributions at NNLO*, *Phys. Rev. D* **69** (2004) 094008, arXiv: [hep-ph/0312266](#).
- [53] S. Frixione et al., *A positive-weight next-to-leading-order Monte Carlo for heavy flavour hadroproduction*, *JHEP* **09** (2007) 126, arXiv: [0707.3088 \[hep-ph\]](#).
- [54] H. B. Hartanto, B. Jager, L. Reina, and D. Wackerlo, *Higgs boson production in association with top quarks in the POWHEG BOX*, *Phys. Rev. D* **91** (2015) 094003, arXiv: [1501.04498 \[hep-ph\]](#).
- [55] E. Re, *Single-top Wt-channel production matched with parton showers using the POWHEG method*, *Eur. Phys. J. C* **71** (2011) 1547, arXiv: [1009.2450 \[hep-ph\]](#).
- [56] P. Nason, *A new method for combining NLO QCD with shower Monte Carlo algorithms*, *JHEP* **11** (2004) 040, arXiv: [hep-ph/0409146](#).
- [57] S. Frixione, P. Nason, and C. Oleari, *Matching NLO QCD computations with parton shower simulations: the POWHEG method*, *JHEP* **11** (2007) 070, arXiv: [0709.2092 \[hep-ph\]](#).

- [58] S. Alioli, P. Nason, C. Oleari, and E. Re, *A general framework for implementing NLO calculations in shower Monte Carlo programs: the POWHEG BOX*, *JHEP* **06** (2010) 043, arXiv: [1002.2581 \[hep-ph\]](#).
- [59] T. Sjöstrand et al., *An introduction to PYTHIA 8.2*, *Comput. Phys. Commun.* **191** (2015) 159, arXiv: [1410.3012 \[hep-ph\]](#).
- [60] ATLAS Collaboration, *ATLAS Pythia 8 tunes to 7 TeV data*, ATL-PHYS-PUB-2014-021, 2014, URL: <https://cds.cern.ch/record/1966419>.
- [61] R. D. Ball et al., *Parton distributions with LHC data*, *Nucl. Phys. B* **867** (2013) 244, arXiv: [1207.1303 \[hep-ph\]](#).
- [62] ATLAS Collaboration, *Studies on top-quark Monte Carlo modelling for Top2016*, ATL-PHYS-PUB-2016-020, 2016, URL: <https://cds.cern.ch/record/2216168>.
- [63] M. Czakon and A. Mitov, *Top++: A program for the calculation of the top-pair cross-section at hadron colliders*, *Comput. Phys. Commun.* **185** (2014) 2930, arXiv: [1112.5675 \[hep-ph\]](#).
- [64] M. Aliev et al., *HATHOR: HAdronic Top and Heavy quarks crOss section calculatoR*, *Comput. Phys. Commun.* **182** (2011) 1034, arXiv: [1007.1327 \[hep-ph\]](#).
- [65] P. Kant et al., *HatHor for single top-quark production: Updated predictions and uncertainty estimates for single top-quark production in hadronic collisions*, *Comput. Phys. Commun.* **191** (2015) 74, arXiv: [1406.4403 \[hep-ph\]](#).
- [66] S. Frixione, E. Laenen, P. Motylinski, C. White, and B. R. Webber, *Single-top hadroproduction in association with a W boson*, *JHEP* **07** (2008) 029, arXiv: [0805.3067 \[hep-ph\]](#).
- [67] J. Alwall et al., *The automated computation of tree-level and next-to-leading order differential cross sections, and their matching to parton shower simulations*, *JHEP* **07** (2014) 079, arXiv: [1405.0301 \[hep-ph\]](#).
- [68] K. Hamilton, P. Nason, E. Re, and G. Zanderighi, *NNLOPS simulation of Higgs boson production*, *JHEP* **10** (2013) 222, arXiv: [1309.0017 \[hep-ph\]](#).
- [69] ATLAS Collaboration, *Measurement of the Z/γ^* boson transverse momentum distribution in pp collisions at $\sqrt{s} = 7$ TeV with the ATLAS detector*, *JHEP* **09** (2014) 145, arXiv: [1406.3660 \[hep-ex\]](#).
- [70] J. Butterworth et al., *PDF4LHC recommendations for LHC Run II*, *J. Phys. G* **43** (2016) 023001, arXiv: [1510.03865 \[hep-ph\]](#).
- [71] U. Aglietti, R. Bonciani, G. Degrassi, and A. Vicini, *Two-loop light fermion contribution to Higgs production and decays*, *Phys. Lett. B* **595** (2004) 432, arXiv: [hep-ph/0404071](#).
- [72] S. Actis, G. Passarino, C. Sturm, and S. Uccirati, *NLO electroweak corrections to Higgs boson production at hadron colliders*, *Phys. Lett. B* **670** (2008) 12, arXiv: [0809.1301 \[hep-ph\]](#).
- [73] J. Pumplin et al., *New Generation of Parton Distributions with Uncertainties from Global QCD Analysis*, *JHEP* **07** (2002) 012, arXiv: [hep-ph/0201195](#).
- [74] M. Ciccolini, A. Denner, and S. Dittmaier, *Strong and electroweak corrections to the production of Higgs + 2 jets via weak interactions at the Large Hadron Collider*, *Phys. Rev. Lett.* **99** (2007) 161803, arXiv: [0707.0381 \[hep-ph\]](#).
- [75] T. Han and S. Willenbrock, *QCD correction to the $pp \rightarrow WH$ and ZH total cross sections*, *Phys. Lett. B* **273** (1991) 167.

- [76] O. Brein, A. Djouadi, and R. Harlander, *NNLO QCD corrections to the Higgs-strahlung processes at hadron colliders*, Phys. Lett. B **579** (2004) 149, arXiv: [hep-ph/0307206](#).
- [77] M. L. Ciccolini, S. Dittmaier, and M. Krämer, *Electroweak radiative corrections to associated WH and ZH production at hadron colliders*, Phys. Rev. D **68** (2003) 073003, arXiv: [hep-ph/0306234](#).
- [78] W. Beenakker et al., *The Production of Charginos/Neutralinos and Sleptons at Hadron Colliders*, Phys. Rev. Lett. **83** (1999) 3780, arXiv: [hep-ph/9906298](#), Erratum: Phys. Rev. Lett. **100** (2008) 029901.
- [79] J. Debove, B. Fuks, and M. Klasen, *Threshold resummation for gaugino pair production at hadron colliders*, Nucl. Phys. B **842** (2011) 51, arXiv: [1005.2909 \[hep-ph\]](#).
- [80] B. Fuks, M. Klasen, D. R. Lamprea, and M. Rothering, *Gaugino production in proton-proton collisions at a center-of-mass energy of 8 TeV*, JHEP **10** (2012) 081, arXiv: [1207.2159 \[hep-ph\]](#).
- [81] B. Fuks, M. Klasen, D. R. Lamprea, and M. Rothering, *Precision predictions for electroweak superpartner production at hadron colliders with RESUMMINO*, Eur. Phys. J. C **73** (2013) 2480, arXiv: [1304.0790 \[hep-ph\]](#).
- [82] J. Fiaschi and M. Klasen, *Neutralino-chargino pair production at NLO+NLL with resummation-improved parton density functions for LHC Run II*, Phys. Rev. D **98** (2018) 055014, arXiv: [1805.11322 \[hep-ph\]](#).
- [83] C. Borschensky et al., *Squark and gluino production cross sections in pp collisions at $\sqrt{s} = 13, 14, 33$ and 100 TeV*, Eur. Phys. J. C **74** (2014) 3174, arXiv: [1407.5066 \[hep-ph\]](#).
- [84] D. J. Lange, *The EvtGen particle decay simulation package*, Nucl. Instrum. Meth. A **462** (2001) 152.
- [85] ATLAS Collaboration, *The ATLAS Simulation Infrastructure*, Eur. Phys. J. C **70** (2010) 823, arXiv: [1005.4568 \[physics.ins-det\]](#).
- [86] S. Agostinelli et al., *GEANT4 – a simulation toolkit*, Nucl. Instrum. Meth. A **506** (2003) 250.
- [87] ATLAS Collaboration, *The Pythia 8 A3 tune description of ATLAS minimum bias and inelastic measurements incorporating the Donnachie–Landshoff diffractive model*, ATL-PHYS-PUB-2016-017, 2016, url: <https://cds.cern.ch/record/2206965>.
- [88] ATLAS Collaboration, *Vertex Reconstruction Performance of the ATLAS Detector at $\sqrt{s} = 13$ TeV*, ATL-PHYS-PUB-2015-026, 2015, url: <https://cds.cern.ch/record/2037717>.
- [89] ATLAS Collaboration, *Electron and photon performance measurements with the ATLAS detector using the 2015–2017 LHC proton–proton collision data*, JINST **14** (2019) P12006, arXiv: [1908.00005 \[hep-ex\]](#).
- [90] ATLAS Collaboration, *Muon reconstruction performance of the ATLAS detector in proton–proton collision data at $\sqrt{s} = 13$ TeV*, Eur. Phys. J. C **76** (2016) 292, arXiv: [1603.05598 \[hep-ex\]](#).
- [91] ATLAS Collaboration, *Topological cell clustering in the ATLAS calorimeters and its performance in LHC Run 1*, Eur. Phys. J. C **77** (2017) 490, arXiv: [1603.02934 \[hep-ex\]](#).
- [92] M. Cacciari, G. P. Salam, and G. Soyez, *FastJet user manual*, Eur. Phys. J. C **72** (2012) 1896, arXiv: [1111.6097 \[hep-ph\]](#).
- [93] M. Cacciari, G. P. Salam, and G. Soyez, *The anti- k_t jet clustering algorithm*, JHEP **04** (2008) 063, arXiv: [0802.1189 \[hep-ph\]](#).
- [94] ATLAS Collaboration, *Jet energy scale measurements and their systematic uncertainties in proton–proton collisions at $\sqrt{s} = 13$ TeV with the ATLAS detector*, Phys. Rev. D **96** (2017) 072002, arXiv: [1703.09665 \[hep-ex\]](#).

- [95] ATLAS Collaboration, *ATLAS b-jet identification performance and efficiency measurement with $t\bar{t}$ events in pp collisions at $\sqrt{s} = 13 \text{ TeV}$* , *Eur. Phys. J. C* **79** (2019) 970, arXiv: [1907.05120 \[hep-ex\]](#).
- [96] ATLAS Collaboration, *Performance of missing transverse momentum reconstruction with the ATLAS detector using proton–proton collisions at $\sqrt{s} = 13 \text{ TeV}$* , *Eur. Phys. J. C* **78** (2018) 903, arXiv: [1802.08168 \[hep-ex\]](#).
- [97] ATLAS Collaboration, *Selection of jets produced in 13 TeV proton–proton collisions with the ATLAS detector*, ATLAS-CONF-2015-029, 2015, URL: <https://cds.cern.ch/record/2037702>.
- [98] ATLAS Collaboration, *Performance of pile-up mitigation techniques for jets in pp collisions at $\sqrt{s} = 8 \text{ TeV}$ using the ATLAS detector*, *Eur. Phys. J. C* **76** (2016) 581, arXiv: [1510.03823 \[hep-ex\]](#).
- [99] ATLAS Collaboration, *Tagging and suppression of pileup jets with the ATLAS detector*, ATLAS-CONF-2014-018, 2014, URL: <https://cds.cern.ch/record/1700870>.
- [100] G. Cowan, K. Cranmer, E. Gross, and O. Vitells, *Asymptotic formulae for likelihood-based tests of new physics*, *Eur. Phys. J. C* **71** (2011) 1554, arXiv: [1007.1727 \[physics.data-an\]](#), Erratum: *Eur. Phys. J. C* **73** (2013) 2501.
- [101] M. Baak et al., *HistFitter software framework for statistical data analysis*, *Eur. Phys. J. C* **75** (2015) 153, arXiv: [1410.1280 \[hep-ex\]](#).
- [102] R. D. Cousins, J. T. Linnemann, and J. Tucker, *Evaluation of three methods for calculating statistical significance when incorporating a systematic uncertainty into a test of the background-only hypothesis for a Poisson process*, *Nucl. Instrum. Meth. A* **595** (2008) 480, arXiv: [physics/0702156 \[physics.data-an\]](#).
- [103] ATLAS Collaboration, *Measurement of the WW cross section in $\sqrt{s} = 7 \text{ TeV}$ pp collisions with the ATLAS detector and limits on anomalous gauge couplings*, *Phys. Lett. B* **712** (2012) 289, arXiv: [1203.6232 \[hep-ex\]](#).
- [104] ATLAS Collaboration, *Prospects for Higgs boson searches using the $H \rightarrow WW^{(*)} \rightarrow \ell\nu\ell\nu$ decay mode with the ATLAS detector at 10 TeV*, ATL-PHYS-PUB-2010-005, 2010, URL: <https://cds.cern.ch/record/1270568>.
- [105] ATLAS Collaboration, *Measurement of $W^\pm Z$ production cross sections and gauge boson polarisation in pp collisions at $\sqrt{s} = 13 \text{ TeV}$ with the ATLAS detector*, *Eur. Phys. J. C* **79** (2019) 535, arXiv: [1902.05759 \[hep-ex\]](#).
- [106] ATLAS Collaboration, *Jet energy resolution in proton–proton collisions at $\sqrt{s} = 7 \text{ TeV}$ recorded in 2010 with the ATLAS detector*, *Eur. Phys. J. C* **73** (2013) 2306, arXiv: [1210.6210 \[hep-ex\]](#).
- [107] ATLAS Collaboration, *Luminosity determination in pp collisions at $\sqrt{s} = 13 \text{ TeV}$ using the ATLAS detector at the LHC*, ATLAS-CONF-2019-021, 2019, URL: <https://cds.cern.ch/record/2677054>.
- [108] G. Avoni et al., *The new LUCID-2 detector for luminosity measurement and monitoring in ATLAS*, *JINST* **13** (2018) P07017.
- [109] E. Bothmann, M. Schönherr, and S. Schumann, *Reweighting QCD matrix-element and parton-shower calculations*, *Eur. Phys. J. C* **76** (2016) 590, arXiv: [1606.08753 \[hep-ph\]](#).
- [110] S. Dulat et al., *New parton distribution functions from a global analysis of quantum chromodynamics*, *Phys. Rev. D* **93** (2016) 033006, arXiv: [1506.07443 \[hep-ph\]](#).

- [111] L. Harland-Lang, A. Martin, P. Motylinski, and R. Thorne, *Parton distributions in the LHC era: MMHT 2014 PDFs*, *Eur. Phys. J. C* **75** (2015) 204, arXiv: [1412.3989 \[hep-ph\]](https://arxiv.org/abs/1412.3989).
- [112] A. L. Read, *Presentation of search results: the CL_S technique*, *J. Phys. G* **28** (2002) 2693.
- [113] ATLAS Collaboration, *ATLAS Computing Acknowledgements*, ATL-SOFT-PUB-2020-001, URL: <https://cds.cern.ch/record/2717821>.

The ATLAS Collaboration

G. Aad¹⁰², B. Abbott¹²⁸, D.C. Abbott¹⁰³, A. Abed Abud³⁶, K. Abeling⁵³, D.K. Abhayasinghe⁹⁴, S.H. Abidi¹⁶⁷, O.S. AbouZeid⁴⁰, N.L. Abraham¹⁵⁶, H. Abramowicz¹⁶¹, H. Abreu¹⁶⁰, Y. Abulaiti⁶, B.S. Acharya^{67a,67b,n}, B. Achkar⁵³, L. Adam¹⁰⁰, C. Adam Bourdarios⁵, L. Adamczyk^{84a}, L. Adamek¹⁶⁷, J. Adelman¹²¹, M. Adersberger¹¹⁴, A. Adiguzel^{12c,ae}, S. Adorni⁵⁴, T. Adye¹⁴³, A.A. Affolder¹⁴⁵, Y. Afik¹⁶⁰, C. Agapopoulou⁶⁵, M.N. Agaras³⁸, A. Aggarwal¹¹⁹, C. Agheorghiesei^{27c}, J.A. Aguilar-Saavedra^{139f,139a,ad}, A. Ahmad³⁶, F. Ahmadov⁸⁰, W.S. Ahmed¹⁰⁴, X. Ai¹⁸, G. Aielli^{74a,74b}, S. Akatsuka⁸⁶, M. Akbiyik¹⁰⁰, T.P.A. Åkesson⁹⁷, E. Akilli⁵⁴, A.V. Akimov¹¹¹, K. Al Khoury⁶⁵, G.L. Alberghini^{23b,23a}, J. Albert¹⁷⁶, M.J. Alconada Verzini¹⁶¹, S. Alderweireldt³⁶, M. Aleksa³⁶, I.N. Aleksandrov⁸⁰, C. Alexa^{27b}, T. Alexopoulos¹⁰, A. Alfonsi¹²⁰, F. Alfonsi^{23b,23a}, M. Alhoob¹²⁸, B. Ali¹⁴¹, S. Ali¹⁵⁸, M. Aliev¹⁶⁶, G. Alimonti^{69a}, C. Allaire³⁶, B.M.M. Allbrooke¹⁵⁶, B.W. Allen¹³¹, P.P. Allport²¹, A. Aloisio^{70a,70b}, F. Alonso⁸⁹, C. Alpigiani¹⁴⁸, E. Alunno Camelia^{74a,74b}, M. Alvarez Estevez⁹⁹, M.G. Alviggi^{70a,70b}, Y. Amaral Coutinho^{81b}, A. Ambler¹⁰⁴, L. Ambroz¹³⁴, C. Amelung²⁶, D. Amidei¹⁰⁶, S.P. Amor Dos Santos^{139a}, S. Amoroso⁴⁶, C.S. Amrouche⁵⁴, F. An⁷⁹, C. Anastopoulos¹⁴⁹, N. Andari¹⁴⁴, T. Andeen¹¹, J.K. Anders²⁰, S.Y. Andrean^{45a,45b}, A. Andreazza^{69a,69b}, V. Andrei^{61a}, C.R. Anelli¹⁷⁶, S. Angelidakis⁹, A. Angerami³⁹, A.V. Anisenkov^{122b,122a}, A. Annovi^{72a}, C. Antel⁵⁴, M.T. Anthony¹⁴⁹, E. Antipov¹²⁹, M. Antonelli⁵¹, D.J.A. Antrim¹⁷¹, F. Anulli^{73a}, M. Aoki⁸², J.A. Aparisi Pozo¹⁷⁴, M.A. Aparo¹⁵⁶, L. Aperio Bella⁴⁶, N. Aranzabal³⁶, V. Araujo Ferraz^{81a}, R. Araujo Pereira^{81b}, C. Arcangeletti⁵¹, A.T.H. Arce⁴⁹, F.A. Arduh⁸⁹, J.-F. Arguin¹¹⁰, S. Argyropoulos⁵², J.-H. Arling⁴⁶, A.J. Armbruster³⁶, A. Armstrong¹⁷¹, O. Arnaez¹⁶⁷, H. Arnold¹²⁰, Z.P. Arrubarrena Tame¹¹⁴, G. Artoni¹³⁴, K. Asai¹²⁶, S. Asai¹⁶³, T. Asawatavonvanich¹⁶⁵, N.A. Asbah⁵⁹, E.M. Asimakopoulou¹⁷², L. Asquith¹⁵⁶, J. Assahsah^{35e}, K. Assamagan²⁹, R. Astalos^{28a}, R.J. Atkin^{33a}, M. Atkinson¹⁷³, N.B. Atlay¹⁹, H. Atmani⁶⁵, K. Augsten¹⁴¹, V.A. Austrup¹⁸², G. Avolio³⁶, M.K. Ayoub^{15a}, G. Azuelos^{110,am}, H. Bachacou¹⁴⁴, K. Bachas¹⁶², M. Backes¹³⁴, F. Backman^{45a,45b}, P. Bagnaia^{73a,73b}, H. Bahrasemani¹⁵², A.J. Bailey¹⁷⁴, V.R. Bailey¹⁷³, J.T. Baines¹⁴³, C. Bakalis¹⁰, O.K. Baker¹⁸³, P.J. Bakker¹²⁰, E. Bakos¹⁶, D. Bakshi Gupta⁸, S. Balaji¹⁵⁷, E.M. Baldin^{122b,122a}, P. Balek¹⁸⁰, F. Balli¹⁴⁴, W.K. Balunas¹³⁴, J. Balz¹⁰⁰, E. Banas⁸⁵, M. Bandieramonte¹³⁸, A. Bandyopadhyay²⁴, Sw. Banerjee^{181,i}, L. Barak¹⁶¹, W.M. Barbe³⁸, E.L. Barberio¹⁰⁵, D. Barberis^{55b,55a}, M. Barbero¹⁰², G. Barbour⁹⁵, T. Barillari¹¹⁵, M.-S. Barisits³⁶, J. Barkeloo¹³¹, T. Barklow¹⁵³, R. Barnea¹⁶⁰, B.M. Barnett¹⁴³, R.M. Barnett¹⁸, Z. Barnovska-Blenessy^{60a}, A. Baroncelli^{60a}, G. Barone²⁹, A.J. Barr¹³⁴, L. Barranco Navarro^{45a,45b}, F. Barreiro⁹⁹, J. Barreiro Guimarães da Costa^{15a}, U. Barron¹⁶¹, S. Barsov¹³⁷, F. Bartels^{61a}, R. Bartoldus¹⁵³, G. Bartolini¹⁰², A.E. Barton⁹⁰, P. Bartos^{28a}, A. Basalaev⁴⁶, A. Basan¹⁰⁰, A. Bassalat^{65,aj}, M.J. Basso¹⁶⁷, R.L. Bates⁵⁷, S. Batlamous^{35f}, J.R. Batley³², B. Batool¹⁵¹, M. Battaglia¹⁴⁵, M. Baucé^{73a,73b}, F. Bauer^{144,*}, K.T. Bauer¹⁷¹, P. Bauer²⁴, H.S. Bawa³¹, A. Bayirli^{12c}, J.B. Beacham⁴⁹, T. Beau¹³⁵, P.H. Beauchemin¹⁷⁰, F. Becherer⁵², P. Bechtle²⁴, H.C. Beck⁵³, H.P. Beck^{20,p}, K. Becker¹⁷⁸, C. Becot⁴⁶, A. Beddall^{12d}, A.J. Beddall^{12a}, V.A. Bednyakov⁸⁰, M. Bedognetti¹²⁰, C.P. Bee¹⁵⁵, T.A. Beermann¹⁸², M. Begalli^{81b}, M. Begel²⁹, A. Behera¹⁵⁵, J.K. Behr⁴⁶, F. Beisiegel²⁴, M. Belfkir⁵, A.S. Bell⁹⁵, G. Bella¹⁶¹, L. Bellagamba^{23b}, A. Bellerive³⁴, P. Bellos⁹, K. Beloborodov^{122b,122a}, K. Belotskiy¹¹², N.L. Belyaev¹¹², D. Benchekroun^{35a}, N. Benekos¹⁰, Y. Benhammou¹⁶¹, D.P. Benjamin⁶, M. Benoit⁵⁴, J.R. Bensinger²⁶, S. Bentvelsen¹²⁰, L. Beresford¹³⁴, M. Beretta⁵¹, D. Berge¹⁹, E. Bergeaas Kuutmann¹⁷², N. Berger⁵, B. Bergmann¹⁴¹, L.J. Bergsten²⁶, J. Beringer¹⁸, S. Berlendis⁷, G. Bernardi¹³⁵, C. Bernius¹⁵³, F.U. Bernlochner²⁴, T. Berry⁹⁴, P. Berta¹⁰⁰, C. Bertella^{15a}, A. Berthold⁴⁸, I.A. Bertram⁹⁰, O. Bessidskaia Bylund¹⁸², N. Besson¹⁴⁴, A. Bethani¹⁰¹, S. Bethke¹¹⁵, A. Betti⁴², A.J. Bevan⁹³, J. Beyer¹¹⁵, D.S. Bhattacharya¹⁷⁷, P. Bhattacharai²⁶, V.S. Bhopatkar⁶, R. Bi¹³⁸, R.M. Bianchi¹³⁸, O. Biebel¹¹⁴, D. Biedermann¹⁹, R. Bielski³⁶, K. Bierwagen¹⁰⁰, N.V. Biesuz^{72a,72b}, M. Biglietti^{75a}, T.R.V. Billoud¹¹⁰,

M. Bindi⁵³, A. Bingul^{12d}, C. Bini^{73a,73b}, S. Biondi^{23b,23a}, C.J. Birch-sykes¹⁰¹, M. Birman¹⁸⁰, T. Bisanz³⁶, J.P. Biswal³, D. Biswas^{181,i}, A. Bitadze¹⁰¹, C. Bittrich⁴⁸, K. Bjørke¹³³, T. Blazek^{28a}, I. Bloch⁴⁶, C. Blocker²⁶, A. Blue⁵⁷, U. Blumenschein⁹³, G.J. Bobbink¹²⁰, V.S. Bobrovnikov^{122b,122a}, S.S. Bocchetta⁹⁷, D. Bogavac¹⁴, A.G. Bogdanchikov^{122b,122a}, C. Bohm^{45a}, V. Boisvert⁹⁴, P. Bokan⁵³, T. Bold^{84a}, A.E. Bolz^{61b}, M. Bomben¹³⁵, M. Bona⁹³, J.S. Bonilla¹³¹, M. Boonekamp¹⁴⁴, C.D. Booth⁹⁴, A.G. Borbély⁵⁷, H.M. Borecka-Bielska⁹¹, L.S. Borgna⁹⁵, A. Borisov¹²³, G. Borissov⁹⁰, D. Bortoletto¹³⁴, D. Boscherini^{23b}, M. Bosman¹⁴, J.D. Bossio Sola¹⁰⁴, K. Bouaouda^{35a}, J. Boudreau¹³⁸, E.V. Bouhova-Thacker⁹⁰, D. Boumediene³⁸, S.K. Boutle⁵⁷, A. Boveia¹²⁷, J. Boyd³⁶, D. Boye^{33c}, I.R. Boyko⁸⁰, A.J. Bozson⁹⁴, J. Bracinik²¹, N. Brahimi^{60d,60c}, G. Brandt¹⁸², O. Brandt³², F. Braren⁴⁶, B. Brau¹⁰³, J.E. Brau¹³¹, W.D. Breaden Madden⁵⁷, K. Brendlinger⁴⁶, R. Brener¹⁶⁰, L. Brenner³⁶, R. Brenner¹⁷², S. Bressler¹⁸⁰, B. Brickwedde¹⁰⁰, D.L. Briglin²¹, D. Britton⁵⁷, D. Britzger¹¹⁵, I. Brock²⁴, R. Brock¹⁰⁷, G. Brooijmans³⁹, W.K. Brooks^{146d}, E. Brost²⁹, P.A. Bruckman de Renstrom⁸⁵, B. Brüers⁴⁶, D. Bruncko^{28b}, A. Bruni^{23b}, G. Bruni^{23b}, L.S. Bruni¹²⁰, S. Bruno^{74a,74b}, M. Bruschi^{23b}, N. Bruscino^{73a,73b}, L. Bryngemark¹⁵³, T. Buanes¹⁷, Q. Buat¹⁵⁵, P. Buchholz¹⁵¹, A.G. Buckley⁵⁷, I.A. Budagov⁸⁰, M.K. Bugge¹³³, F. Bührer⁵², O. Bulekov¹¹², B.A. Bullard⁵⁹, T.J. Burch¹²¹, S. Burdin⁹¹, C.D. Burgard¹²⁰, A.M. Burger¹²⁹, B. Burghgrave⁸, J.T.P. Burr⁴⁶, C.D. Burton¹¹, J.C. Burzynski¹⁰³, V. Büscher¹⁰⁰, E. Buschmann⁵³, P.J. Bussey⁵⁷, J.M. Butler²⁵, C.M. Buttar⁵⁷, J.M. Butterworth⁹⁵, P. Butt³⁶, W. Buttinger³⁶, C.J. Buxo Vazquez¹⁰⁷, A. Buzatu¹⁵⁸, A.R. Buzykaev^{122b,122a}, G. Cabras^{23b,23a}, S. Cabrera Urbán¹⁷⁴, D. Caforio⁵⁶, H. Cai¹³⁸, V.M.M. Cairo¹⁵³, O. Cakir^{4a}, N. Calace³⁶, P. Calafiura¹⁸, G. Calderini¹³⁵, P. Calfayan⁶⁶, G. Callea⁵⁷, L.P. Caloba^{81b}, A. Caltabiano^{74a,74b}, S. Calvente Lopez⁹⁹, D. Calvet³⁸, S. Calvet³⁸, T.P. Calvet¹⁰², M. Calvetti^{72a,72b}, R. Camacho Toro¹³⁵, S. Camarda³⁶, D. Camarero Munoz⁹⁹, P. Camarri^{74a,74b}, M.T. Camerlingo^{75a,75b}, D. Cameron¹³³, C. Camincher³⁶, S. Campana³⁶, M. Campanelli⁹⁵, A. Camplani⁴⁰, V. Canale^{70a,70b}, A. Canesse¹⁰⁴, M. Cano Bret⁷⁸, J. Cantero¹²⁹, T. Cao¹⁶¹, Y. Cao¹⁷³, M.D.M. Capeans Garrido³⁶, M. Capua^{41b,41a}, R. Cardarelli^{74a}, F. Cardillo¹⁴⁹, G. Carducci^{41b,41a}, I. Carli¹⁴², T. Carli³⁶, G. Carlino^{70a}, B.T. Carlson¹³⁸, E.M. Carlson^{176,168a}, L. Carminati^{69a,69b}, R.M.D. Carney¹⁵³, S. Caron¹¹⁹, E. Carquin^{146d}, S. Carrá⁴⁶, G. Carratta^{23b,23a}, J.W.S. Carter¹⁶⁷, T.M. Carter⁵⁰, M.P. Casado^{14,f}, A.F. Casha¹⁶⁷, F.L. Castillo¹⁷⁴, L. Castillo Garcia¹⁴, V. Castillo Gimenez¹⁷⁴, N.F. Castro^{139a,139e}, A. Catinaccio³⁶, J.R. Catmore¹³³, A. Cattai³⁶, V. Cavaliere²⁹, V. Cavasinni^{72a,72b}, E. Celebi^{12b}, F. Celli¹³⁴, K. Cerny¹³⁰, A.S. Cerqueira^{81a}, A. Cerri¹⁵⁶, L. Cerrito^{74a,74b}, F. Cerutti¹⁸, A. Cervelli^{23b,23a}, S.A. Cetin^{12b}, Z. Chadi^{35a}, D. Chakraborty¹²¹, J. Chan¹⁸¹, W.S. Chan¹²⁰, W.Y. Chan⁹¹, J.D. Chapman³², B. Chargeishvili^{159b}, D.G. Charlton²¹, T.P. Charman⁹³, C.C. Chau³⁴, S. Che¹²⁷, S. Chekanov⁶, S.V. Chekulaev^{168a}, G.A. Chelkov^{80,ah}, B. Chen⁷⁹, C. Chen^{60a}, C.H. Chen⁷⁹, H. Chen²⁹, J. Chen^{60a}, J. Chen³⁹, J. Chen²⁶, S. Chen¹³⁶, S.J. Chen^{15c}, X. Chen^{15b}, Y. Chen^{60a}, Y-H. Chen⁴⁶, H.C. Cheng^{63a}, H.J. Cheng^{15a}, A. Cheplakov⁸⁰, E. Cheremushkina¹²³, R. Cherkouoi El Moursli^{35f}, E. Cheu⁷, K. Cheung⁶⁴, T.J.A. Chevaléries¹⁴⁴, L. Chevalier¹⁴⁴, V. Chiarella⁵¹, G. Chiarelli^{72a}, G. Chiodini^{68a}, A.S. Chisholm²¹, A. Chitan^{27b}, I. Chiu¹⁶³, Y.H. Chiu¹⁷⁶, M.V. Chizhov⁸⁰, K. Choi¹¹, A.R. Chomont^{73a,73b}, Y.S. Chow¹²⁰, L.D. Christopher^{33f}, M.C. Chu^{63a}, X. Chu^{15a,15d}, J. Chudoba¹⁴⁰, J.J. Chwastowski⁸⁵, L. Chytka¹³⁰, D. Cieri¹¹⁵, K.M. Ciesla⁸⁵, D. Cinca⁴⁷, V. Cindro⁹², I.A. Cioară^{27b}, A. Ciocio¹⁸, F. Ciroto^{70a,70b}, Z.H. Citron^{180,j}, M. Citterio^{69a}, D.A. Ciubotaru^{27b}, B.M. Ciungu¹⁶⁷, A. Clark⁵⁴, M.R. Clark³⁹, P.J. Clark⁵⁰, S.E. Clawson¹⁰¹, C. Clement^{45a,45b}, Y. Coadou¹⁰², M. Cobal^{67a,67c}, A. Coccaro^{55b}, J. Cochran⁷⁹, R. Coelho Lopes De Sa¹⁰³, H. Cohen¹⁶¹, A.E.C. Coimbra³⁶, B. Cole³⁹, A.P. Colijn¹²⁰, J. Collot⁵⁸, P. Conde Muiño^{139a,139h}, S.H. Connell^{133c}, I.A. Connally⁵⁷, S. Constantinescu^{27b}, F. Conventi^{70a,an}, A.M. Cooper-Sarkar¹³⁴, F. Cormier¹⁷⁵, K.J.R. Cormier¹⁶⁷, L.D. Corpe⁹⁵, M. Corradi^{73a,73b}, E.E. Corrigan⁹⁷, F. Corriveau^{104,ab}, M.J. Costa¹⁷⁴, F. Costanza⁵, D. Costanzo¹⁴⁹, G. Cowan⁹⁴, J.W. Cowley³², J. Crane¹⁰¹, K. Cranmer¹²⁵, R.A. Creager¹³⁶, S. Crépé-Renaudin⁵⁸, F. Crescioli¹³⁵, M. Cristinziani²⁴, V. Croft¹⁷⁰, G. Crosetti^{41b,41a}, A. Cueto⁵, T. Cuhadar Donszelmann¹⁷¹, H. Cui^{15a,15d}, A.R. Cukierman¹⁵³, W.R. Cunningham⁵⁷,

S. Czekierda⁸⁵, P. Czodrowski³⁶, M.M. Czurylo^{61b}, M.J. Da Cunha Sargedas De Sousa^{60b},
 J.V. Da Fonseca Pinto^{81b}, C. Da Via¹⁰¹, W. Dabrowski^{84a}, F. Dachs³⁶, T. Dado⁴⁷, S. Dahbi^{33f}, T. Dai¹⁰⁶,
 C. Dallapiccola¹⁰³, M. Dam⁴⁰, G. D'amen²⁹, V. D'Amico^{75a,75b}, J. Damp¹⁰⁰, J.R. Dandoy¹³⁶,
 M.F. Daneri³⁰, M. Danninger¹⁵², V. Dao³⁶, G. Darbo^{55b}, O. Dartsi⁵, A. Dattagupta¹³¹, T. Daubney⁴⁶,
 S. D'Auria^{69a,69b}, C. David^{168b}, T. Davidek¹⁴², D.R. Davis⁴⁹, I. Dawson¹⁴⁹, K. De⁸, R. De Asmundis^{70a},
 M. De Beurs¹²⁰, S. De Castro^{23b,23a}, N. De Groot¹¹⁹, P. de Jong¹²⁰, H. De la Torre¹⁰⁷, A. De Maria^{15c},
 D. De Pedis^{73a}, A. De Salvo^{73a}, U. De Sanctis^{74a,74b}, M. De Santis^{74a,74b}, A. De Santo¹⁵⁶,
 J.B. De Vivie De Regie⁶⁵, C. Debenedetti¹⁴⁵, D.V. Dedovich⁸⁰, A.M. Deiana⁴², J. Del Peso⁹⁹,
 Y. Delabat Diaz⁴⁶, D. Delgove⁶⁵, F. Deliot¹⁴⁴, C.M. Delitzsch⁷, M. Della Pietra^{70a,70b}, D. Della Volpe⁵⁴,
 A. Dell'Acqua³⁶, L. Dell'Asta^{74a,74b}, M. Delmastro⁵, C. Delporte⁶⁵, P.A. Delsart⁵⁸, D.A. DeMarco¹⁶⁷,
 S. Demers¹⁸³, M. Demichev⁸⁰, G. Demontigny¹¹⁰, S.P. Denisov¹²³, L. D'Eramo¹²¹, D. Derendarz⁸⁵,
 J.E. Derkaoui^{35e}, F. Derue¹³⁵, P. Dervan⁹¹, K. Desch²⁴, K. Dette¹⁶⁷, C. Deutsch²⁴, M.R. Devesa³⁰,
 P.O. Deviveiros³⁶, F.A. Di Bello^{73a,73b}, A. Di Ciaccio^{74a,74b}, L. Di Ciaccio⁵, W.K. Di Clemente¹³⁶,
 C. Di Donato^{70a,70b}, A. Di Girolamo³⁶, G. Di Gregorio^{72a,72b}, B. Di Micco^{75a,75b}, R. Di Nardo^{75a,75b},
 K.F. Di Petrillo⁵⁹, R. Di Sipio¹⁶⁷, C. Diaconu¹⁰², F.A. Dias¹²⁰, T. Dias Do Vale^{139a}, M.A. Diaz^{146a},
 F.G. Diaz Capriles²⁴, J. Dickinson¹⁸, M. Didenko¹⁶⁶, E.B. Diehl¹⁰⁶, J. Dietrich¹⁹, S. Díez Cornell⁴⁶,
 C. Diez Pardos¹⁵¹, A. Dimitrievska¹⁸, W. Ding^{15b}, J. Dingfelder²⁴, S.J. Dittmeier^{61b}, F. Dittus³⁶,
 F. Djama¹⁰², T. Djobava^{159b}, J.I. Djuvsland¹⁷, M.A.B. Do Vale¹⁴⁷, M. Dobre^{27b}, D. Dodsworth²⁶,
 C. Doglioni⁹⁷, J. Dolejsi¹⁴², Z. Dolezal¹⁴², M. Donadelli^{81c}, B. Dong^{60c}, J. Donini³⁸, A. D'onofrio^{15c},
 M. D'Onofrio⁹¹, J. Dopke¹⁴³, A. Doria^{70a}, M.T. Dova⁸⁹, A.T. Doyle⁵⁷, E. Drechsler¹⁵², E. Dreyer¹⁵²,
 T. Dreyer⁵³, A.S. Drobac¹⁷⁰, D. Du^{60b}, T.A. du Pree¹²⁰, Y. Duan^{60d}, F. Dubinin¹¹¹, M. Dubovsky^{28a},
 A. Dubreuil⁵⁴, E. Duchovni¹⁸⁰, G. Duckeck¹¹⁴, O.A. Ducu^{36,27b}, D. Duda¹¹⁵, A. Dudarev³⁶,
 A.C. Dudder¹⁰⁰, E.M. Duffield¹⁸, M. D'uffizi¹⁰¹, L. Duflot⁶⁵, M. Dührssen³⁶, C. Dülsen¹⁸²,
 M. Dumancic¹⁸⁰, A.E. Dumitriu^{27b}, M. Dunford^{61a}, A. Duperrin¹⁰², H. Duran Yildiz^{4a}, M. Düren⁵⁶,
 A. Durglishvili^{159b}, D. Duschinger⁴⁸, B. Dutta⁴⁶, D. Duvnjak¹, G.I. Dyckes¹³⁶, M. Dyndal³⁶, S. Dysch¹⁰¹,
 B.S. Dziedzic⁸⁵, M.G. Eggleston⁴⁹, T. Eifert⁸, G. Eigen¹⁷, K. Einsweiler¹⁸, T. Ekelof¹⁷², H. El Jarrai^{35f},
 V. Ellajosyula¹⁷², M. Ellert¹⁷², F. Ellinghaus¹⁸², A.A. Elliot⁹³, N. Ellis³⁶, J. Elmsheuser²⁹, M. Elsing³⁶,
 D. Emelianov¹⁴³, A. Emerman³⁹, Y. Enari¹⁶³, M.B. Epland⁴⁹, J. Erdmann⁴⁷, A. Ereditato²⁰,
 P.A. Erland⁸⁵, M. Errenst¹⁸², M. Escalier⁶⁵, C. Escobar¹⁷⁴, O. Estrada Pastor¹⁷⁴, E. Etzion¹⁶¹, H. Evans⁶⁶,
 M.O. Evans¹⁵⁶, A. Ezhilov¹³⁷, F. Fabbri⁵⁷, L. Fabbri^{23b,23a}, V. Fabiani¹¹⁹, G. Facini¹⁷⁸,
 R.M. Fakhrutdinov¹²³, S. Falciano^{73a}, P.J. Falke²⁴, S. Falke³⁶, J. Faltova¹⁴², Y. Fang^{15a}, Y. Fang^{15a},
 G. Fanourakis⁴⁴, M. Fanti^{69a,69b}, M. Faraj^{67a,67c,q}, A. Farbin⁸, A. Farilla^{75a}, E.M. Farina^{71a,71b},
 T. Farooque¹⁰⁷, S.M. Farrington⁵⁰, P. Parthouat³⁶, F. Fassi^{35f}, P. Fassnacht³⁶, D. Fassouliotis⁹,
 M. Faucci Giannelli⁵⁰, W.J. Fawcett³², L. Fayard⁶⁵, O.L. Fedin^{137,0}, W. Fedorko¹⁷⁵, A. Fehr²⁰,
 M. Feickert¹⁷³, L. Feligioni¹⁰², A. Fell¹⁴⁹, C. Feng^{60b}, M. Feng⁴⁹, M.J. Fenton¹⁷¹, A.B. Fenyuk¹²³,
 S.W. Ferguson⁴³, J. Ferrando⁴⁶, A. Ferrante¹⁷³, A. Ferrari¹⁷², P. Ferrari¹²⁰, R. Ferrari^{71a},
 D.E. Ferreira de Lima^{61b}, A. Ferrer¹⁷⁴, D. Ferrere⁵⁴, C. Ferretti¹⁰⁶, F. Fiedler¹⁰⁰, A. Filipčič⁹²,
 F. Filthaut¹¹⁹, K.D. Finelli²⁵, M.C.N. Fiolhais^{139a,139c,a}, L. Fiorini¹⁷⁴, F. Fischer¹¹⁴, J. Fischer¹⁰⁰,
 W.C. Fisher¹⁰⁷, T. Fitschen²¹, I. Fleck¹⁵¹, P. Fleischmann¹⁰⁶, T. Flick¹⁸², B.M. Flierl¹¹⁴, L. Flores¹³⁶,
 L.R. Flores Castillo^{63a}, F.M. Follega^{76a,76b}, N. Fomin¹⁷, J.H. Foo¹⁶⁷, G.T. Forcolin^{76a,76b}, B.C. Forland⁶⁶,
 A. Formica¹⁴⁴, F.A. Förster¹⁴, A.C. Forti¹⁰¹, E. Fortin¹⁰², M.G. Foti¹³⁴, D. Fournier⁶⁵, H. Fox⁹⁰,
 P. Francavilla^{72a,72b}, S. Francescato^{73a,73b}, M. Franchini^{23b,23a}, S. Franchino^{61a}, D. Francis³⁶, L. Franco⁵,
 L. Franconi²⁰, M. Franklin⁵⁹, G. Frattari^{73a,73b}, A.N. Fray⁹³, P.M. Freeman²¹, B. Freund¹¹⁰,
 W.S. Freund^{81b}, E.M. Freundlich⁴⁷, D.C. Frizzell¹²⁸, D. Froidevaux³⁶, J.A. Frost¹³⁴, M. Fujimoto¹²⁶,
 C. Fukunaga¹⁶⁴, E. Fullana Torregrosa¹⁷⁴, T. Fusayasu¹¹⁶, J. Fuster¹⁷⁴, A. Gabrielli^{23b,23a}, A. Gabrielli³⁶,
 S. Gadatsch⁵⁴, P. Gadow¹¹⁵, G. Gagliardi^{55b,55a}, L.G. Gagnon¹¹⁰, G.E. Gallardo¹³⁴, E.J. Gallas¹³⁴,
 B.J. Gallop¹⁴³, R. Gamboa Goni⁹³, K.K. Gan¹²⁷, S. Ganguly¹⁸⁰, J. Gao^{60a}, Y. Gao⁵⁰, Y.S. Gao^{31,l},

F.M. Garay Walls^{146a}, C. García¹⁷⁴, J.E. García Navarro¹⁷⁴, J.A. García Pascual^{15a}, C. Garcia-Argos⁵², M. Garcia-Sciveres¹⁸, R.W. Gardner³⁷, N. Garelli¹⁵³, S. Gargiulo⁵², C.A. Garner¹⁶⁷, V. Garonne¹³³, S.J. Gasiorowski¹⁴⁸, P. Gaspar^{81b}, A. Gaudiello^{55b,55a}, G. Gaudio^{71a}, I.L. Gavrilenko¹¹¹, A. Gavrilyuk¹²⁴, C. Gay¹⁷⁵, G. Gaycken⁴⁶, E.N. Gazis¹⁰, A.A. Geanta^{27b}, C.M. Gee¹⁴⁵, C.N.P. Gee¹⁴³, J. Geisen⁹⁷, M. Geisen¹⁰⁰, C. Gemme^{55b}, M.H. Genest⁵⁸, C. Geng¹⁰⁶, S. Gentile^{73a,73b}, S. George⁹⁴, T. Geralis⁴⁴, L.O. Gerlach⁵³, P. Gessinger-Befurt¹⁰⁰, G. Gessner⁴⁷, S. Ghasemi¹⁵¹, M. Ghasemi Bostanabad¹⁷⁶, M. Ghneimat¹⁵¹, A. Ghosh⁶⁵, A. Ghosh⁷⁸, B. Giacobbe^{23b}, S. Giagu^{73a,73b}, N. Giangiocomi^{23b,23a}, P. Giannetti^{72a}, A. Giannini^{70a,70b}, G. Giannini¹⁴, S.M. Gibson⁹⁴, M. Gignac¹⁴⁵, D.T. Gil^{84b}, B.J. Gilbert³⁹, D. Gillberg³⁴, G. Gilles¹⁸², D.M. Gingrich^{3,am}, M.P. Giordani^{67a,67c}, P.F. Giraud¹⁴⁴, G. Giugliarelli^{67a,67c}, D. Giugni^{69a}, F. Giuli^{74a,74b}, S. Gkaitatzis¹⁶², I. Gkialas^{9,g}, E.L. Gkougkousis¹⁴, P. Gkountoumis¹⁰, L.K. Gladilin¹¹³, C. Glasman⁹⁹, J. Glatzer¹⁴, P.C.F. Glaysher⁴⁶, A. Glazov⁴⁶, G.R. Gledhill¹³¹, I. Gnesi^{41b,b}, M. Goblirsch-Kolb²⁶, D. Godin¹¹⁰, S. Goldfarb¹⁰⁵, T. Golling⁵⁴, D. Golubkov¹²³, A. Gomes^{139a,139b}, R. Goncalves Gama⁵³, R. Gonçalo^{139a,139c}, G. Gonella¹³¹, L. Gonella²¹, A. Gongadze⁸⁰, F. Gonnella²¹, J.L. Gonski³⁹, S. González de la Hoz¹⁷⁴, S. Gonzalez Fernandez¹⁴, R. Gonzalez Lopez⁹¹, C. Gonzalez Renteria¹⁸, R. Gonzalez Suarez¹⁷², S. Gonzalez-Sevilla⁵⁴, G.R. Gonzalvo Rodriguez¹⁷⁴, L. Goossens³⁶, N.A. Gorasia²¹, P.A. Gorbounov¹²⁴, H.A. Gordon²⁹, B. Gorini³⁶, E. Gorini^{68a,68b}, A. Gorišek⁹², A.T. Goshaw⁴⁹, M.I. Gostkin⁸⁰, C.A. Gottardo¹¹⁹, M. Gouighri^{35b}, A.G. Goussiou¹⁴⁸, N. Govender^{33c}, C. Goy⁵, I. Grabowska-Bold^{84a}, E.C. Graham⁹¹, J. Gramling¹⁷¹, E. Gramstad¹³³, S. Grancagnolo¹⁹, M. Grandi¹⁵⁶, V. Gratchev¹³⁷, P.M. Gravila^{27f}, F.G. Gravili^{68a,68b}, C. Gray⁵⁷, H.M. Gray¹⁸, C. Grefe²⁴, K. Gregersen⁹⁷, I.M. Gregor⁴⁶, P. Grenier¹⁵³, K. Grevtsov⁴⁶, C. Grieco¹⁴, N.A. Grieser¹²⁸, A.A. Grillo¹⁴⁵, K. Grimm^{31,k}, S. Grinstein^{14,w}, J.-F. Grivaz⁶⁵, S. Groh¹⁰⁰, E. Gross¹⁸⁰, J. Grosse-Knetter⁵³, Z.J. Grout⁹⁵, C. Grud¹⁰⁶, A. Grummer¹¹⁸, J.C. Grundy¹³⁴, L. Guan¹⁰⁶, W. Guan¹⁸¹, C. Gubbels¹⁷⁵, J. Guenther³⁶, A. Guerguichon⁶⁵, J.G.R. Guerrero Rojas¹⁷⁴, F. Guescini¹¹⁵, D. Guest¹⁷¹, R. Gugel¹⁰⁰, A. Guida⁴⁶, T. Guillemin⁵, S. Guindon³⁶, U. Gul⁵⁷, J. Guo^{60c}, W. Guo¹⁰⁶, Y. Guo^{60a}, Z. Guo¹⁰², R. Gupta⁴⁶, S. Gurbuz^{12c}, G. Gustavino¹²⁸, M. Guth⁵², P. Gutierrez¹²⁸, C. Gutschow⁹⁵, C. Guyot¹⁴⁴, C. Gwenlan¹³⁴, C.B. Gwilliam⁹¹, E.S. Haaland¹³³, A. Haas¹²⁵, C. Haber¹⁸, H.K. Hadavand⁸, A. Hadef^{60a}, M. Haleem¹⁷⁷, J. Haley¹²⁹, J.J. Hall¹⁴⁹, G. Halladjian¹⁰⁷, G.D. Hallewell¹⁰², K. Hamano¹⁷⁶, H. Hamdaoui^{35f}, M. Hamer²⁴, G.N. Hamity⁵⁰, K. Han^{60a,v}, L. Han^{60a}, S. Han¹⁸, Y.F. Han¹⁶⁷, K. Hanagaki^{82,t}, M. Hance¹⁴⁵, D.M. Handl¹¹⁴, M.D. Hank³⁷, R. Hankache¹³⁵, E. Hansen⁹⁷, J.B. Hansen⁴⁰, J.D. Hansen⁴⁰, M.C. Hansen²⁴, P.H. Hansen⁴⁰, E.C. Hanson¹⁰¹, K. Hara¹⁶⁹, T. Harenberg¹⁸², S. Harkusha¹⁰⁸, P.F. Harrison¹⁷⁸, N.M. Hartman¹⁵³, N.M. Hartmann¹¹⁴, Y. Hasegawa¹⁵⁰, A. Hasib⁵⁰, S. Hassani¹⁴⁴, S. Haug²⁰, R. Hauser¹⁰⁷, L.B. Havener³⁹, M. Havranek¹⁴¹, C.M. Hawkes²¹, R.J. Hawkings³⁶, S. Hayashida¹¹⁷, D. Hayden¹⁰⁷, C. Hayes¹⁰⁶, R.L. Hayes¹⁷⁵, C.P. Hays¹³⁴, J.M. Hays⁹³, H.S. Hayward⁹¹, S.J. Haywood¹⁴³, F. He^{60a}, Y. He¹⁶⁵, M.P. Heath⁵⁰, V. Hedberg⁹⁷, S. Heer²⁴, A.L. Heggelund¹³³, C. Heidegger⁵², K.K. Heidegger⁵², W.D. Heidorn⁷⁹, J. Heilman³⁴, S. Heim⁴⁶, T. Heim¹⁸, B. Heinemann^{46,ak}, J.G. Heinlein¹³⁶, J.J. Heinrich¹³¹, L. Heinrich³⁶, J. Hejbal¹⁴⁰, L. Helary⁴⁶, A. Held¹²⁵, S. Hellesund¹³³, C.M. Helling¹⁴⁵, S. Hellman^{45a,45b}, C. Helsens³⁶, R.C.W. Henderson⁹⁰, Y. Heng¹⁸¹, L. Henkelmann³², A.M. Henriques Correia³⁶, H. Herde²⁶, Y. Hernández Jiménez^{33f}, H. Herr¹⁰⁰, M.G. Herrmann¹¹⁴, T. Herrmann⁴⁸, G. Herten⁵², R. Hertenberger¹¹⁴, L. Hervas³⁶, T.C. Herwig¹³⁶, G.G. Hesketh⁹⁵, N.P. Hessey^{168a}, H. Hibi⁸³, A. Higashida¹⁶³, S. Higashino⁸², E. Higón-Rodríguez¹⁷⁴, K. Hildebrand³⁷, J.C. Hill³², K.K. Hill²⁹, K.H. Hiller⁴⁶, S.J. Hillier²¹, M. Hils⁴⁸, I. Hinchliffe¹⁸, F. Hinterkeuser²⁴, M. Hirose¹³², S. Hirose⁵², D. Hirschbuehl¹⁸², B. Hiti⁹², O. Hladík¹⁴⁰, D.R. Hlaluku^{33f}, J. Hobbs¹⁵⁵, N. Hod¹⁸⁰, M.C. Hodgkinson¹⁴⁹, A. Hoecker³⁶, D. Hohn⁵², D. Hohov⁶⁵, T. Holm²⁴, T.R. Holmes³⁷, M. Holzbock¹¹⁴, L.B.A.H. Hommels³², T.M. Hong¹³⁸, J.C. Honig⁵², A. Höngle¹¹⁵, B.H. Hooberman¹⁷³, W.H. Hopkins⁶, Y. Horii¹¹⁷, P. Horn⁴⁸, L.A. Horyn³⁷, S. Hou¹⁵⁸, A. Hoummada^{35a}, J. Howarth⁵⁷, J. Hoya⁸⁹, M. Hrabovsky¹³⁰, J. Hrdinka⁷⁷, J. Hrivnac⁶⁵, A. Hrynevich¹⁰⁹, T. Hrynn'ova⁵, P.J. Hsu⁶⁴, S.-C. Hsu¹⁴⁸, Q. Hu²⁹, S. Hu^{60c}, Y.F. Hu^{15a,15d,ao}, D.P. Huang⁹⁵, Y. Huang^{60a},

Y. Huang^{15a}, Z. Hubacek¹⁴¹, F. Hubaut¹⁰², M. Huebner²⁴, F. Huegging²⁴, T.B. Huffman¹³⁴, M. Huhtinen³⁶, R. Hulskens⁵⁸, R.F.H. Hunter³⁴, P. Huo¹⁵⁵, N. Huseynov^{80,ac}, J. Huston¹⁰⁷, J. Huth⁵⁹, R. Hyneman¹⁵³, S. Hyrych^{28a}, G. Iacobucci⁵⁴, G. Iakovidis²⁹, I. Ibragimov¹⁵¹, L. Iconomidou-Fayard⁶⁵, P. Iengo³⁶, R. Ignazzi⁴⁰, O. Igonkina^{120,y,*}, R. Iguchi¹⁶³, T. Iizawa⁵⁴, Y. Ikegami⁸², M. Ikeno⁸², N. Illic^{119,167,ab}, F. Iltzsche⁴⁸, H. Imam^{35a}, G. Introzzi^{71a,71b}, M. Iodice^{75a}, K. Iordanidou^{168a}, V. Ippolito^{73a,73b}, M.F. Isacson¹⁷², M. Ishino¹⁶³, W. Islam¹²⁹, C. Issever^{19,46}, S. Istin¹⁶⁰, F. Ito¹⁶⁹, J.M. Iturbe Ponce^{63a}, R. Iuppa^{76a,76b}, A. Ivina¹⁸⁰, H. Iwasaki⁸², J.M. Izen⁴³, V. Izzo^{70a}, P. Jacka¹⁴⁰, P. Jackson¹, R.M. Jacobs⁴⁶, B.P. Jaeger¹⁵², V. Jain², G. Jäkel¹⁸², K.B. Jakobi¹⁰⁰, K. Jakobs⁵², T. Jakoubek¹⁸⁰, J. Jamieson⁵⁷, K.W. Janas^{84a}, R. Jansky⁵⁴, M. Janus⁵³, P.A. Janus^{84a}, G. Jarlskog⁹⁷, A.E. Jaspan⁹¹, N. Javadov^{80,ac}, T. Javůrek³⁶, M. Javurkova¹⁰³, F. Jeanneau¹⁴⁴, L. Jeanty¹³¹, J. Jejelava^{159a}, P. Jenni^{52,c}, N. Jeong⁴⁶, S. Jézéquel⁵, H. Ji¹⁸¹, J. Jia¹⁵⁵, H. Jiang⁷⁹, Y. Jiang^{60a}, Z. Jiang¹⁵³, S. Jiggins⁵², F.A. Jimenez Morales³⁸, J. Jimenez Pena¹¹⁵, S. Jin^{15c}, A. Jinaru^{27b}, O. Jinnouchi¹⁶⁵, H. Jivan^{33f}, P. Johansson¹⁴⁹, K.A. Johns⁷, C.A. Johnson⁶⁶, R.W.L. Jones⁹⁰, S.D. Jones¹⁵⁶, T.J. Jones⁹¹, J. Jongmanns^{61a}, J. Jovicevic³⁶, X. Ju¹⁸, J.J. Junggeburth¹¹⁵, A. Juste Rozas^{14,w}, A. Kaczmarska⁸⁵, M. Kado^{73a,73b}, H. Kagan¹²⁷, M. Kagan¹⁵³, A. Kahn³⁹, C. Kahra¹⁰⁰, T. Kaji¹⁷⁹, E. Kajomovitz¹⁶⁰, C.W. Kalderon²⁹, A. Kaluza¹⁰⁰, A. Kamenshchikov¹²³, M. Kaneda¹⁶³, N.J. Kang¹⁴⁵, S. Kang⁷⁹, Y. Kano¹¹⁷, J. Kanzaki⁸², L.S. Kaplan¹⁸¹, D. Kar^{33f}, K. Karava¹³⁴, M.J. Kareem^{168b}, I. Karkanias¹⁶², S.N. Karpov⁸⁰, Z.M. Karpova⁸⁰, V. Kartvelishvili⁹⁰, A.N. Karyukhin¹²³, E. Kasimi¹⁶², A. Kastanas^{45a,45b}, C. Kato^{60d,60c}, J. Katzy⁴⁶, K. Kawade¹⁵⁰, K. Kawagoe⁸⁸, T. Kawaguchi¹¹⁷, T. Kawamoto¹⁴⁴, G. Kawamura⁵³, E.F. Kay¹⁷⁶, S. Kazakos¹⁴, V.F. Kazanin^{122b,122a}, R. Keeler¹⁷⁶, R. Kehoe⁴², J.S. Keller³⁴, E. Kellermann⁹⁷, D. Kelsey¹⁵⁶, J.J. Kempster²¹, J. Kendrick²¹, K.E. Kennedy³⁹, O. Kepka¹⁴⁰, S. Kersten¹⁸², B.P. Kerševan⁹², S. Ketabchi Haghigat¹⁶⁷, M. Khader¹⁷³, F. Khalil-Zada¹³, M. Khandoga¹⁴⁴, A. Khanov¹²⁹, A.G. Kharlamov^{122b,122a}, T. Kharlamova^{122b,122a}, E.E. Khoda¹⁷⁵, A. Khodinov¹⁶⁶, T.J. Khoo⁵⁴, G. Khoriauli¹⁷⁷, E. Khramov⁸⁰, J. Khubua^{159b}, S. Kido⁸³, M. Kiehn³⁶, C.R. Kilby⁹⁴, E. Kim¹⁶⁵, Y.K. Kim³⁷, N. Kimura⁹⁵, A. Kirchhoff⁵³, D. Kirchmeier⁴⁸, J. Kirk¹⁴³, A.E. Kiryunin¹¹⁵, T. Kishimoto¹⁶³, D.P. Kisliuk¹⁶⁷, V. Kitali⁴⁶, C. Kitsaki¹⁰, O. Kivernyk²⁴, T. Klapdor-Kleingrothaus⁵², M. Klassen^{61a}, C. Klein³⁴, M.H. Klein¹⁰⁶, M. Klein⁹¹, U. Klein⁹¹, K. Kleinknecht¹⁰⁰, P. Klimek¹²¹, A. Klimentov²⁹, T. Klingl²⁴, T. Klioutchnikova³⁶, F.F. Klitzner¹¹⁴, P. Kluit¹²⁰, S. Kluth¹¹⁵, E. Kneringer⁷⁷, E.B.F.G. Knoops¹⁰², A. Knue⁵², D. Kobayashi⁸⁸, M. Kobel⁴⁸, M. Kocian¹⁵³, T. Kodama¹⁶³, P. Kodys¹⁴², D.M. Koeck¹⁵⁶, P.T. Koenig²⁴, T. Koffas³⁴, N.M. Köhler³⁶, M. Kolb¹⁴⁴, I. Koletsou⁵, T. Komarek¹³⁰, T. Kondo⁸², K. Köneke⁵², A.X.Y. Kong¹, A.C. König¹¹⁹, T. Kono¹²⁶, V. Konstantinides⁹⁵, N. Konstantinidis⁹⁵, B. Konya⁹⁷, R. Kopeliansky⁶⁶, S. Koperny^{84a}, K. Korcyl⁸⁵, K. Kordas¹⁶², G. Koren¹⁶¹, A. Korn⁹⁵, I. Korolkov¹⁴, E.V. Korolkova¹⁴⁹, N. Korotkova¹¹³, O. Kortner¹¹⁵, S. Kortner¹¹⁵, V.V. Kostyukhin^{149,166}, A. Kotsokechagia⁶⁵, A. Kotwal⁴⁹, A. Koulouris¹⁰, A. Kourkoumeli-Charalampidi^{71a,71b}, C. Kourkoumelis⁹, E. Kourlitis⁶, V. Kouskoura²⁹, R. Kowalewski¹⁷⁶, W. Kozanecki¹⁰¹, A.S. Kozhin¹²³, V.A. Kramarenko¹¹³, G. Kramberger⁹², D. Krasnopevtsev^{60a}, M.W. Krasny¹³⁵, A. Krasznahorkay³⁶, D. Krauss¹¹⁵, J.A. Kremer¹⁰⁰, J. Kretzschmar⁹¹, P. Krieger¹⁶⁷, F. Krieter¹¹⁴, A. Krishnan^{61b}, M. Krivos¹⁴², K. Krizka¹⁸, K. Kroeninger⁴⁷, H. Kroha¹¹⁵, J. Kroll¹⁴⁰, J. Kroll¹³⁶, K.S. Krowpman¹⁰⁷, U. Kruchonak⁸⁰, H. Krüger²⁴, N. Krumnack⁷⁹, M.C. Kruse⁴⁹, J.A. Krzysiak⁸⁵, A. Kubota¹⁶⁵, O. Kuchinskaia¹⁶⁶, S. Kuday^{4b}, D. Kuechler⁴⁶, J.T. Kuechler⁴⁶, S. Kuehn³⁶, T. Kuhl⁴⁶, V. Kukhtin⁸⁰, Y. Kulchitsky^{108,af}, S. Kuleshov^{146b}, Y.P. Kulinich¹⁷³, M. Kuna⁵⁸, T. Kunigo⁸⁶, A. Kupco¹⁴⁰, T. Kupfer⁴⁷, O. Kuprash⁵², H. Kurashige⁸³, L.L. Kurchaninov^{168a}, Y.A. Kurochkin¹⁰⁸, A. Kurova¹¹², M.G. Kurth^{15a,15d}, E.S. Kuwertz³⁶, M. Kuze¹⁶⁵, A.K. Kvam¹⁴⁸, J. Kvita¹³⁰, T. Kwan¹⁰⁴, F. La Ruffa^{41b,41a}, C. Lacasta¹⁷⁴, F. Lacava^{73a,73b}, D.P.J. Lack¹⁰¹, H. Lacker¹⁹, D. Lacour¹³⁵, E. Ladygin⁸⁰, R. Lafaye⁵, B. Laforge¹³⁵, T. Lagouri^{146c}, S. Lai⁵³, I.K. Lakomiec^{84a}, J.E. Lambert¹²⁸, S. Lammers⁶⁶, W. Lampl⁷, C. Lampoudis¹⁶², E. Lançon²⁹, U. Landgraf⁵², M.P.J. Landon⁹³, M.C. Lanfermann⁵⁴, V.S. Lang⁵², J.C. Lange⁵³, R.J. Langenberg¹⁰³, A.J. Lankford¹⁷¹, F. Lanni²⁹, K. Lantzsch²⁴, A. Lanza^{71a},

A. Lapertosa^{55b,55a}, J.F. Laporte¹⁴⁴, T. Lari^{69a}, F. Lasagni Manghi^{23b,23a}, M. Lassnig³⁶, T.S. Lau^{63a},
 A. Laudrain⁶⁵, A. Laurier³⁴, M. Lavorgna^{70a,70b}, S.D. Lawlor⁹⁴, M. Lazzaroni^{69a,69b}, B. Le¹⁰¹,
 E. Le Guirriec¹⁰², A. Lebedev⁷⁹, M. LeBlanc⁷, T. LeCompte⁶, F. Ledroit-Guillon⁵⁸, A.C.A. Lee⁹⁵,
 C.A. Lee²⁹, G.R. Lee¹⁷, L. Lee⁵⁹, S.C. Lee¹⁵⁸, S. Lee⁷⁹, B. Lefebvre^{168a}, H.P. Lefebvre⁹⁴, M. Lefebvre¹⁷⁶,
 C. Leggett¹⁸, K. Lehmann¹⁵², N. Lehmann²⁰, G. Lehmann Miotto³⁶, W.A. Leight⁴⁶, A. Leisos^{162,u},
 M.A.L. Leite^{81c}, C.E. Leitgeb¹¹⁴, R. Leitner¹⁴², D. Lellouch^{180,*}, K.J.C. Leney⁴², T. Lenz²⁴, S. Leone^{72a},
 C. Leonidopoulos⁵⁰, A. Leopold¹³⁵, C. Leroy¹¹⁰, R. Les¹⁰⁷, C.G. Lester³², M. Levchenko¹³⁷, J. Levêque⁵,
 D. Levin¹⁰⁶, L.J. Levinson¹⁸⁰, D.J. Lewis²¹, B. Li^{15b}, B. Li¹⁰⁶, C-Q. Li^{60a}, F. Li^{60c}, H. Li^{60a}, H. Li^{60b},
 J. Li^{60c}, K. Li¹⁴⁸, L. Li^{60c}, M. Li^{15a,15d}, Q. Li^{15a,15d}, Q.Y. Li^{60a}, S. Li^{60d,60c}, X. Li⁴⁶, Y. Li⁴⁶, Z. Li^{60b},
 Z. Li¹³⁴, Z. Li¹⁰⁴, Z. Liang^{15a}, M. Liberatore⁴⁶, B. Liberti^{74a}, A. Liblong¹⁶⁷, K. Lie^{63c}, S. Lim²⁹,
 C.Y. Lin³², K. Lin¹⁰⁷, R.A. Linck⁶⁶, R.E. Lindley⁷, J.H. Lindon²¹, A. Linss⁴⁶, A.L. Lioni⁵⁴, E. Lipeles¹³⁶,
 A. Lipniacka¹⁷, T.M. Liss^{173,al}, A. Lister¹⁷⁵, J.D. Little⁸, B. Liu⁷⁹, B.X. Liu⁶, H.B. Liu²⁹, J.B. Liu^{60a},
 J.K.K. Liu³⁷, K. Liu^{60d,60c}, M. Liu^{60a}, P. Liu^{15a}, X. Liu^{60a}, Y. Liu⁴⁶, Y. Liu^{15a,15d}, Y.L. Liu¹⁰⁶, Y.W. Liu^{60a},
 M. Livan^{71a,71b}, A. Lleres⁵⁸, J. Llorente Merino¹⁵², S.L. Lloyd⁹³, C.Y. Lo^{63b}, E.M. Lobodzinska⁴⁶,
 P. Loch⁷, S. Loffredo^{74a,74b}, T. Lohse¹⁹, K. Lohwasser¹⁴⁹, M. Lokajicek¹⁴⁰, J.D. Long¹⁷³, R.E. Long⁹⁰,
 I. Longarini^{73a,73b}, L. Longo³⁶, K.A. Looper¹²⁷, I. Lopez Paz¹⁰¹, A. Lopez Solis¹⁴⁹, J. Lorenz¹¹⁴,
 N. Lorenzo Martinez⁵, A.M. Lory¹¹⁴, P.J. Lösel¹¹⁴, A. Lösle⁵², X. Lou⁴⁶, X. Lou^{15a}, A. Lounis⁶⁵, J. Love⁶,
 P.A. Love⁹⁰, J.J. Lozano Bahilo¹⁷⁴, M. Lu^{60a}, Y.J. Lu⁶⁴, H.J. Lubatti¹⁴⁸, C. Luci^{73a,73b}, F.L. Lucio Alves^{15c},
 A. Lucotte⁵⁸, F. Luehring⁶⁶, I. Luise¹³⁵, L. Luminari^{73a}, B. Lund-Jensen¹⁵⁴, M.S. Lutz¹⁶¹, D. Lynn²⁹,
 H. Lyons⁹¹, R. Lysak¹⁴⁰, E. Lytken⁹⁷, F. Lyu^{15a}, V. Lyubushkin⁸⁰, T. Lyubushkina⁸⁰, H. Ma²⁹, L.L. Ma^{60b},
 Y. Ma⁹⁵, D.M. Mac Donell¹⁷⁶, G. Maccarrone⁵¹, A. Macchiolo¹¹⁵, C.M. Macdonald¹⁴⁹,
 J.C. MacDonald¹⁴⁹, J. Machado Miguens¹³⁶, D. Madaffari¹⁷⁴, R. Madar³⁸, W.F. Mader⁴⁸,
 M. Madugoda Ralalage Don¹²⁹, N. Madysa⁴⁸, J. Maeda⁸³, T. Maeno²⁹, M. Maerker⁴⁸, V. Magerl⁵²,
 N. Magini⁷⁹, J. Magro^{67a,67c,q}, D.J. Mahon³⁹, C. Maidantchik^{81b}, T. Maier¹¹⁴, A. Maio^{139a,139b,139d},
 K. Maj^{84a}, O. Majersky^{28a}, S. Majewski¹³¹, Y. Makida⁸², N. Makovec⁶⁵, B. Malaescu¹³⁵, Pa. Malecki⁸⁵,
 V.P. Maleev¹³⁷, F. Malek⁵⁸, D. Malito^{41b,41a}, U. Mallik⁷⁸, D. Malon⁶, C. Malone³², S. Maltezos¹⁰,
 S. Malyukov⁸⁰, J. Mamuzic¹⁷⁴, G. Mancini^{70a,70b}, I. Mandić⁹², L. Manhaes de Andrade Filho^{81a},
 I.M. Maniatis¹⁶², J. Manjarres Ramos⁴⁸, K.H. Mankinen⁹⁷, A. Mann¹¹⁴, A. Manousos⁷⁷, B. Mansoulie¹⁴⁴,
 I. Manthos¹⁶², S. Manzoni¹²⁰, A. Marantis^{162,u}, G. Marceca³⁰, L. Marchese¹³⁴, G. Marchiori¹³⁵,
 M. Marcisovsky¹⁴⁰, L. Marcoccia^{74a,74b}, C. Marcon⁹⁷, C.A. Marin Tobon³⁶, M. Marjanovic¹²⁸,
 Z. Marshall¹⁸, M.U.F. Martensson¹⁷², S. Marti-Garcia¹⁷⁴, C.B. Martin¹²⁷, T.A. Martin¹⁷⁸, V.J. Martin⁵⁰,
 B. Martin dit Latour¹⁷, L. Martinelli^{75a,75b}, M. Martinez^{14,w}, P. Martinez Agullo¹⁷⁴,
 V.I. Martinez Outschoorn¹⁰³, S. Martin-Haugh¹⁴³, V.S. Martoiu^{27b}, A.C. Martyniuk⁹⁵, A. Marzin³⁶,
 S.R. Maschek¹¹⁵, L. Masetti¹⁰⁰, T. Mashimo¹⁶³, R. Mashinistov¹¹¹, J. Masik¹⁰¹, A.L. Maslennikov^{122b,122a},
 L. Massa^{23b,23a}, P. Massarotti^{70a,70b}, P. Mastrandrea^{72a,72b}, A. Mastroberardino^{41b,41a}, T. Masubuchi¹⁶³,
 D. Matakias²⁹, A. Matic¹¹⁴, N. Matsuzawa¹⁶³, P. Mättig²⁴, J. Maurer^{27b}, B. Maček⁹²,
 D.A. Maximov^{122b,122a}, R. Mazini¹⁵⁸, I. Maznas¹⁶², S.M. Mazza¹⁴⁵, J.P. Mc Gowan¹⁰⁴, S.P. Mc Kee¹⁰⁶,
 T.G. McCarthy¹¹⁵, W.P. McCormack¹⁸, E.F. McDonald¹⁰⁵, J.A. McFayden³⁶, G. McHedlidze^{159b},
 M.A. McKay⁴², K.D. McLean¹⁷⁶, S.J. McMahon¹⁴³, P.C. McNamara¹⁰⁵, C.J. Nicol¹⁷⁸,
 R.A. McPherson^{176,ab}, J.E. Mdhului^{33f}, Z.A. Meadows¹⁰³, S. Meehan³⁶, T. Megy³⁸, S. Mehlhase¹¹⁴,
 A. Mehta⁹¹, B. Meirose⁴³, D. Melini¹⁶⁰, B.R. Mellado Garcia^{33f}, J.D. Mellenthin⁵³, M. Melo^{28a},
 F. Meloni⁴⁶, A. Melzer²⁴, E.D. Mendes Gouveia^{139a,139e}, L. Meng³⁶, X.T. Meng¹⁰⁶, S. Menke¹¹⁵,
 E. Meoni^{41b,41a}, S. Mergelmeyer¹⁹, S.A.M. Merkt¹³⁸, C. Merlassino¹³⁴, P. Mermod^{54,*}, L. Merola^{70a,70b},
 C. Meroni^{69a}, G. Merz¹⁰⁶, O. Meshkov^{113,111}, J.K.R. Meshreki¹⁵¹, J. Metcalfe⁶, A.S. Mete⁶, C. Meyer⁶⁶,
 J.-P. Meyer¹⁴⁴, M. Michetti¹⁹, R.P. Middleton¹⁴³, L. Mijović⁵⁰, G. Mikenberg¹⁸⁰, M. Mikestikova¹⁴⁰,
 M. Mikuž⁹², H. Mildner¹⁴⁹, A. Milic¹⁶⁷, C.D. Milke⁴², D.W. Miller³⁷, A. Milov¹⁸⁰, D.A. Milstead^{45a,45b},
 R.A. Mina¹⁵³, A.A. Minaenko¹²³, I.A. Minashvili^{159b}, A.I. Mincer¹²⁵, B. Mindur^{84a}, M. Mineev⁸⁰,

Y. Minegishi¹⁶³, L.M. Mir¹⁴, M. Mironova¹³⁴, A. Mirto^{68a,68b}, K.P. Mistry¹³⁶, T. Mitani¹⁷⁹,
 J. Mitrevski¹¹⁴, V.A. Mitsou¹⁷⁴, M. Mittal^{60c}, O. Miu¹⁶⁷, A. Miucci²⁰, P.S. Miyagawa⁹³, A. Mizukami⁸²,
 J.U. Mjörnmark⁹⁷, T. Mkrtchyan^{61a}, M. Mlynarikova¹⁴², T. Moa^{45a,45b}, S. Mobius⁵³, K. Mochizuki¹¹⁰,
 P. Mogg¹¹⁴, S. Mohapatra³⁹, R. Moles-Valls²⁴, K. Mönig⁴⁶, E. Monnier¹⁰², A. Montalbano¹⁵²,
 J. Montejo Berlingen³⁶, M. Montella⁹⁵, F. Monticelli⁸⁹, S. Monzani^{69a}, N. Morange⁶⁵,
 A.L. Moreira De Carvalho^{139a}, D. Moreno^{22a}, M. Moreno Llácer¹⁷⁴, C. Moreno Martinez¹⁴,
 P. Morettini^{55b}, M. Morgenstern¹⁶⁰, S. Morgenstern⁴⁸, D. Mori¹⁵², M. Morii⁵⁹, M. Morinaga¹⁷⁹,
 V. Morisbak¹³³, A.K. Morley³⁶, G. Mornacchi³⁶, A.P. Morris⁹⁵, L. Morvaj¹⁵⁵, P. Moschovakos³⁶,
 B. Moser¹²⁰, M. Mosidze^{159b}, T. Moskalets¹⁴⁴, J. Moss^{31,m}, E.J.W. Moyse¹⁰³, S. Muanza¹⁰², J. Mueller¹³⁸,
 R.S.P. Mueller¹¹⁴, D. Muenstermann⁹⁰, G.A. Mullier⁹⁷, D.P. Mungo^{69a,69b}, J.L. Munoz Martinez¹⁴,
 F.J. Munoz Sanchez¹⁰¹, P. Murin^{28b}, W.J. Murray^{178,143}, A. Murrone^{69a,69b}, J.M. Muse¹²⁸, M. Muškinja¹⁸,
 C. Mwewa^{33a}, A.G. Myagkov^{123,ah}, A.A. Myers¹³⁸, G. Myers⁶⁶, J. Myers¹³¹, M. Myska¹⁴¹,
 B.P. Nachman¹⁸, O. Nackenhorst⁴⁷, A.Nag Nag⁴⁸, K. Nagai¹³⁴, K. Nagano⁸², Y. Nagasaka⁶², J.L. Nagle²⁹,
 E. Nagy¹⁰², A.M. Nairz³⁶, Y. Nakahama¹¹⁷, K. Nakamura⁸², T. Nakamura¹⁶³, H. Nanjo¹³²,
 F. Napolitano^{61a}, R.F. Naranjo Garcia⁴⁶, R. Narayan⁴², I. Naryshkin¹³⁷, T. Naumann⁴⁶, G. Navarro^{22a},
 P.Y. Nechaeva¹¹¹, F. Nechansky⁴⁶, T.J. Neep²¹, A. Negri^{71a,71b}, M. Negrini^{23b}, C. Nellist¹¹⁹, C. Nelson¹⁰⁴,
 M.E. Nelson^{45a,45b}, S. Nemecek¹⁴⁰, M. Nessi^{36,e}, M.S. Neubauer¹⁷³, F. Neuhaus¹⁰⁰, M. Neumann¹⁸²,
 R. Newhouse¹⁷⁵, P.R. Newman²¹, C.W. Ng¹³⁸, Y.S. Ng¹⁹, Y.W.Y. Ng¹⁷¹, B. Ngair^{35f}, H.D.N. Nguyen¹⁰²,
 T. Nguyen Manh¹¹⁰, E. Nibigira³⁸, R.B. Nickerson¹³⁴, R. Nicolaïdou¹⁴⁴, D.S. Nielsen⁴⁰, J. Nielsen¹⁴⁵,
 M. Niemeyer⁵³, N. Nikiforou¹¹, V. Nikolaenko^{123,ah}, I. Nikolic-Audit¹³⁵, K. Nikolopoulos²¹, P. Nilsson²⁹,
 H.R. Nindhito⁵⁴, Y. Ninomiya⁸², A. Nisati^{73a}, N. Nishu^{60c}, R. Nisius¹¹⁵, I. Nitsche⁴⁷, T. Nitta¹⁷⁹,
 T. Nobe¹⁶³, D.L. Noel³², Y. Noguchi⁸⁶, I. Nomidis¹³⁵, M.A. Nomura²⁹, M. Nordberg³⁶, J. Novak⁹²,
 T. Novak⁹², O. Novgorodova⁴⁸, R. Novotny¹⁴¹, L. Nozka¹³⁰, K. Ntekas¹⁷¹, E. Nurse⁹⁵, F.G. Oakham^{34,am},
 H. Oberlack¹¹⁵, J. Ocariz¹³⁵, A. Ochi⁸³, I. Ochoa³⁹, J.P. Ochoa-Ricoux^{146a}, K. O'Connor²⁶, S. Oda⁸⁸,
 S. Odaka⁸², S. Oerdekk⁵³, A. Ogródniak^{84a}, A. Oh¹⁰¹, C.C. Ohm¹⁵⁴, H. Oide¹⁶⁵, M.L. Ojeda¹⁶⁷,
 H. Okawa¹⁶⁹, Y. Okazaki⁸⁶, M.W. O'Keefe⁹¹, Y. Okumura¹⁶³, T. Okuyama⁸², A. Olariu^{27b},
 L.F. Oleiro Seabra^{139a}, S.A. Olivares Pino^{146a}, D. Oliveira Damazio²⁹, J.L. Oliver¹, M.J.R. Olsson¹⁷¹,
 A. Olszewski⁸⁵, J. Olszowska⁸⁵, Ö.O. Öncel²⁴, D.C. O'Neil¹⁵², A.P. O'neill¹³⁴, A. Onofre^{139a,139e},
 P.U.E. Onyisi¹¹, H. Oppen¹³³, R.G. Oreamuno Madriz¹²¹, M.J. Oreglia³⁷, G.E. Orellana⁸⁹,
 D. Orestano^{75a,75b}, N. Orlando¹⁴, R.S. Orr¹⁶⁷, V. O'Shea⁵⁷, R. Ospanov^{60a}, G. Otero y Garzon³⁰,
 H. Otono⁸⁸, P.S. Ott^{61a}, G.J. Ottino¹⁸, M. Ouchrif^{35e}, J. Ouellette²⁹, F. Ould-Saada¹³³, A. Ouraou^{144,*},
 Q. Ouyang^{15a}, M. Owen⁵⁷, R.E. Owen¹⁴³, V.E. Ozcan^{12c}, N. Ozturk⁸, J. Pacalt¹³⁰, H.A. Pacey³²,
 K. Pachal⁴⁹, A. Pacheco Pages¹⁴, C. Padilla Aranda¹⁴, S. Pagan Griso¹⁸, G. Palacino⁶⁶, S. Palazzo⁵⁰,
 S. Palestini³⁶, M. Palka^{84b}, P. Palni^{84a}, C.E. Pandini⁵⁴, J.G. Panduro Vazquez⁹⁴, P. Pani⁴⁶, G. Panizzo^{67a,67c},
 L. Paolozzi⁵⁴, C. Papadatos¹¹⁰, K. Papageorgiou^{9,g}, S. Parajuli⁴², A. Paramonov⁶, C. Paraskevopoulos¹⁰,
 D. Paredes Hernandez^{63b}, S.R. Paredes Saenz¹³⁴, B. Parida¹⁸⁰, T.H. Park¹⁶⁷, A.J. Parker³¹, M.A. Parker³²,
 F. Parodi^{55b,55a}, E.W. Parrish¹²¹, J.A. Parsons³⁹, U. Parzefall⁵², L. Pascual Dominguez¹³⁵, V.R. Pascuzzi¹⁸,
 J.M.P. Pasner¹⁴⁵, F. Pasquali¹²⁰, E. Pasqualucci^{73a}, S. Passaggio^{55b}, F. Pastore⁹⁴, P. Pasuwan^{45a,45b},
 S. Pataraia¹⁰⁰, J.R. Pater¹⁰¹, A. Pathak^{181,i}, J. Patton⁹¹, T. Pauly³⁶, J. Pearkes¹⁵³, B. Pearson¹¹⁵,
 M. Pedersen¹³³, L. Pedraza Diaz¹¹⁹, R. Pedro^{139a}, T. Peiffer⁵³, S.V. Peleganchuk^{122b,122a}, O. Penc¹⁴⁰,
 H. Peng^{60a}, B.S. Peralva^{81a}, M.M. Perego⁶⁵, A.P. Pereira Peixoto^{139a}, L. Pereira Sanchez^{45a,45b},
 D.V. Perepelitsa²⁹, E. Perez Codina^{168a}, F. Peri¹⁹, L. Perini^{69a,69b}, H. Pernegger³⁶, S. Perrella³⁶,
 A. Perrevoort¹²⁰, K. Peters⁴⁶, R.F.Y. Peters¹⁰¹, B.A. Petersen³⁶, T.C. Petersen⁴⁰, E. Petit¹⁰², V. Petousis¹⁴¹,
 A. Petridis¹, C. Petridou¹⁶², F. Petrucci^{75a,75b}, M. Pettee¹⁸³, N.E. Pettersson¹⁰³, K. Petukhova¹⁴²,
 A. Peyaud¹⁴⁴, R. Pezoa^{146d}, L. Pezzotti^{71a,71b}, T. Pham¹⁰⁵, F.H. Phillips¹⁰⁷, P.W. Phillips¹⁴³,
 M.W. Phipps¹⁷³, G. Piacquadio¹⁵⁵, E. Pianori¹⁸, A. Picazio¹⁰³, R.H. Pickles¹⁰¹, R. Piegaia³⁰,
 D. Pietreanu^{27b}, J.E. Pilcher³⁷, A.D. Pilkington¹⁰¹, M. Pinamonti^{67a,67c}, J.L. Pinfole³,

C. Pitman Donaldson⁹⁵, M. Pitt¹⁶¹, L. Pizzimento^{74a,74b}, A. Pizzini¹²⁰, M.-A. Pleier²⁹, V. Plesanovs⁵², V. Pleskot¹⁴², E. Plotnikova⁸⁰, P. Podberezko^{122b,122a}, R. Poettgen⁹⁷, R. Poggi⁵⁴, L. Poggiali¹³⁵, I. Pogrebnyak¹⁰⁷, D. Pohl²⁴, I. Pokharel⁵³, G. Polesello^{71a}, A. Poley^{152,168a}, A. Policicchio^{73a,73b}, R. Polifka¹⁴², A. Polini^{23b}, C.S. Pollard⁴⁶, V. Polychronakos²⁹, D. Ponomarenko¹¹², L. Pontecorvo³⁶, S. Popa^{27a}, G.A. Popeneciu^{27d}, L. Portales⁵, D.M. Portillo Quintero⁵⁸, S. Pospisil¹⁴¹, K. Potamianos⁴⁶, I.N. Potrap⁸⁰, C.J. Potter³², H. Potti¹¹, T. Poulsen⁹⁷, J. Poveda¹⁷⁴, T.D. Powell¹⁴⁹, G. Pownall⁴⁶, M.E. Pozo Astigarraga³⁶, P. Pralavorio¹⁰², S. Prell⁷⁹, D. Price¹⁰¹, M. Primavera^{68a}, M.L. Proffitt¹⁴⁸, N. Proklova¹¹², K. Prokofiev^{63c}, F. Prokoshin⁸⁰, S. Protopopescu²⁹, J. Proudfoot⁶, M. Przybycien^{84a}, D. Pudzha¹³⁷, A. Puri¹⁷³, P. Puzo⁶⁵, D. Pyatiizbyantseva¹¹², J. Qian¹⁰⁶, Y. Qin¹⁰¹, A. Quadt⁵³, M. Queitsch-Maitland³⁶, M. Racko^{28a}, F. Ragusa^{69a,69b}, G. Rahal⁹⁸, J.A. Raine⁵⁴, S. Rajagopalan²⁹, A. Ramirez Morales⁹³, K. Ran^{15a,15d}, D.M. Rauch⁴⁶, F. Rauscher¹¹⁴, S. Rave¹⁰⁰, B. Ravina¹⁴⁹, I. Ravinovich¹⁸⁰, J.H. Rawling¹⁰¹, M. Raymond³⁶, A.L. Read¹³³, N.P. Readoff¹⁴⁹, M. Reale^{68a,68b}, D.M. Rebuzzi^{71a,71b}, G. Redlinger²⁹, K. Reeves⁴³, J. Reichert¹³⁶, D. Reikher¹⁶¹, A. Reiss¹⁰⁰, A. Rej¹⁵¹, C. Rembser³⁶, A. Renardi⁴⁶, M. Renda^{27b}, M.B. Rendel¹¹⁵, A.G. Rennie⁵⁷, S. Resconi^{69a}, E.D. Ressegue¹⁸, S. Rettie⁹⁵, B. Reynolds¹²⁷, E. Reynolds²¹, O.L. Rezanova^{122b,122a}, P. Reznicek¹⁴², E. Ricci^{76a,76b}, R. Richter¹¹⁵, S. Richter⁴⁶, E. Richter-Was^{84b}, M. Ridel¹³⁵, P. Rieck¹¹⁵, O. Rifki⁴⁶, M. Rijssenbeek¹⁵⁵, A. Rimoldi^{71a,71b}, M. Rimoldi⁴⁶, L. Rinaldi^{23b}, T.T. Rinn¹⁷³, G. Ripellino¹⁵⁴, I. Riu¹⁴, P. Rivadeneira⁴⁶, J.C. Rivera Vergara¹⁷⁶, F. Rizatdinova¹²⁹, E. Rizvi⁹³, C. Rizzi³⁶, S.H. Robertson^{104,ab}, M. Robin⁴⁶, D. Robinson³², C.M. Robles Gajardo^{146d}, M. Robles Manzano¹⁰⁰, A. Robson⁵⁷, A. Rocchi^{74a,74b}, E. Rocco¹⁰⁰, C. Roda^{72a,72b}, S. Rodriguez Bosca¹⁷⁴, A.M. Rodríguez Vera^{168b}, S. Roe³⁶, J. Roggel¹⁸², O. Røhne¹³³, R. Röhrlig¹¹⁵, R.A. Rojas^{146d}, B. Roland⁵², C.P.A. Roland⁶⁶, J. Roloff²⁹, A. Romanouk¹¹², M. Romano^{23b,23a}, N. Rompotis⁹¹, M. Ronzani¹²⁵, L. Roos¹³⁵, S. Rosati^{73a}, G. Rosin¹⁰³, B.J. Rosser¹³⁶, E. Rossi⁴⁶, E. Rossi^{75a,75b}, E. Rossi^{70a,70b}, L.P. Rossi^{55b}, L. Rossini⁴⁶, R. Rosten¹⁴, M. Rotaru^{27b}, B. Rottler⁵², D. Rousseau⁶⁵, G. Rovelli^{71a,71b}, A. Roy¹¹, D. Roy^{33f}, A. Rozanov¹⁰², Y. Rozen¹⁶⁰, X. Ruan^{33f}, T.A. Ruggeri¹, F. Rühr⁵², A. Ruiz-Martinez¹⁷⁴, A. Rummller³⁶, Z. Rurikova⁵², N.A. Rusakovich⁸⁰, H.L. Russell¹⁰⁴, L. Rustige^{38,47}, J.P. Rutherford⁷, E.M. Rüttinger¹⁴⁹, M. Rybar¹⁴², G. Rybkin⁶⁵, E.B. Rye¹³³, A. Ryzhov¹²³, J.A. Sabater Iglesias⁴⁶, P. Sabatini⁵³, L. Sabetta^{73a,73b}, S. Sacerdoti⁶⁵, H.F-W. Sadrozinski¹⁴⁵, R. Sadykov⁸⁰, F. Safai Tehrani^{73a}, B. Safarzadeh Samani¹⁵⁶, M. Safdari¹⁵³, P. Saha¹²¹, S. Saha¹⁰⁴, M. Sahinsoy¹¹⁵, A. Sahu¹⁸², M. Saimpert³⁶, M. Saito¹⁶³, T. Saito¹⁶³, H. Sakamoto¹⁶³, D. Salamani⁵⁴, G. Salamanna^{75a,75b}, A. Salnikov¹⁵³, J. Salt¹⁷⁴, A. Salvador Salas¹⁴, D. Salvatore^{41b,41a}, F. Salvatore¹⁵⁶, A. Salvucci^{63a,63b,63c}, A. Salzburger³⁶, J. Samarati³⁶, D. Sammel⁵², D. Sampsonidis¹⁶², D. Sampsonidou¹⁶², J. Sánchez¹⁷⁴, A. Sanchez Pineda^{67a,36,67c}, H. Sandaker¹³³, C.O. Sander⁴⁶, I.G. Sanderswood⁹⁰, M. Sandhoff¹⁸², C. Sandoval^{22b}, D.P.C. Sankey¹⁴³, M. Sannino^{55b,55a}, Y. Sano¹¹⁷, A. Sansoni⁵¹, C. Santoni³⁸, H. Santos^{139a,139b}, S.N. Santpur¹⁸, A. Santra¹⁷⁴, K.A. Saoucha¹⁴⁹, A. Sapronov⁸⁰, J.G. Saraiva^{139a,139d}, O. Sasaki⁸², K. Sato¹⁶⁹, F. Sauerburger⁵², E. Sauvan⁵, P. Savard^{167,am}, R. Sawada¹⁶³, C. Sawyer¹⁴³, L. Sawyer^{96,ag}, I. Sayago Galvan¹⁷⁴, C. Sbarra^{23b}, A. Sbrizzi^{67a,67c}, T. Scanlon⁹⁵, J. Schaarschmidt¹⁴⁸, P. Schacht¹¹⁵, D. Schaefer³⁷, L. Schaefer¹³⁶, S. Schaepe³⁶, U. Schäfer¹⁰⁰, A.C. Schaffer⁶⁵, D. Schaile¹¹⁴, R.D. Schamberger¹⁵⁵, E. Schanet¹¹⁴, C. Scharf¹⁹, N. Scharmburg¹⁰¹, V.A. Schegelsky¹³⁷, D. Scheirich¹⁴², F. Schenck¹⁹, M. Schernau¹⁷¹, C. Schiavi^{55b,55a}, L.K. Schildgen²⁴, Z.M. Schillaci²⁶, E.J. Schioppa^{68a,68b}, M. Schioppa^{41b,41a}, K.E. Schleicher⁵², S. Schlenker³⁶, K.R. Schmidt-Sommerfeld¹¹⁵, K. Schmieden³⁶, C. Schmitt¹⁰⁰, S. Schmitt⁴⁶, J.C. Schmoeckel⁴⁶, L. Schoeffel¹⁴⁴, A. Schoening^{61b}, P.G. Scholer⁵², E. Schopf¹³⁴, M. Schott¹⁰⁰, J.F.P. Schouwenberg¹¹⁹, J. Schovancova³⁶, S. Schramm⁵⁴, F. Schroeder¹⁸², A. Schulte¹⁰⁰, H-C. Schultz-Coulon^{61a}, M. Schumacher⁵², B.A. Schumm¹⁴⁵, Ph. Schune¹⁴⁴, A. Schwartzman¹⁵³, T.A. Schwarz¹⁰⁶, Ph. Schwemling¹⁴⁴, R. Schwienhorst¹⁰⁷, A. Sciandra¹⁴⁵, G. Sciolla²⁶, M. Scornajenghi^{41b,41a}, F. Scuri^{72a}, F. Scutti¹⁰⁵, L.M. Scyboz¹¹⁵, C.D. Sebastiani⁹¹, P. Seema¹⁹, S.C. Seidel¹¹⁸, A. Seiden¹⁴⁵, B.D. Seidlitz²⁹, T. Seiss³⁷, C. Seitz⁴⁶, J.M. Seixas^{81b}, G. Sekhniaidze^{70a}, S.J. Sekula⁴², N. Semprini-Cesari^{23b,23a}, S. Sen⁴⁹,

C. Serfon²⁹, L. Serin⁶⁵, L. Serkin^{67a,67b}, M. Sessa^{60a}, H. Severini¹²⁸, S. Sevova¹⁵³, F. Sforza^{55b,55a},
 A. Sfyrla⁵⁴, E. Shabalina⁵³, J.D. Shahinian¹⁴⁵, N.W. Shaikh^{45a,45b}, D. Shaked Renous¹⁸⁰, L.Y. Shan^{15a},
 M. Shapiro¹⁸, A. Sharma¹³⁴, A.S. Sharma¹, P.B. Shatalov¹²⁴, K. Shaw¹⁵⁶, S.M. Shaw¹⁰¹, M. Shehade¹⁸⁰,
 Y. Shen¹²⁸, A.D. Sherman²⁵, P. Sherwood⁹⁵, L. Shi⁹⁵, S. Shimizu⁸², C.O. Shimmin¹⁸³, Y. Shimogama¹⁷⁹,
 M. Shimojima¹¹⁶, I.P.J. Shipsey¹³⁴, S. Shirabe¹⁶⁵, M. Shiyakova^{80,z}, J. Shlomi¹⁸⁰, A. Shmeleva¹¹¹,
 M.J. Shochet³⁷, J. Shojaii¹⁰⁵, D.R. Shope¹⁵⁴, S. Shrestha¹²⁷, E.M. Shrif^{33f}, E. Shulga¹⁸⁰, P. Sicho¹⁴⁰,
 A.M. Sickles¹⁷³, E. Sideras Haddad^{33f}, O. Sidiropoulou³⁶, A. Sidoti^{23b,23a}, F. Siegert⁴⁸, Dj. Sijacki¹⁶,
 M.Jr. Silva¹⁸¹, M.V. Silva Oliveira³⁶, S.B. Silverstein^{45a}, S. Simion⁶⁵, R. Simoniello¹⁰⁰,
 C.J. Simpson-allsop²¹, S. Simsek^{12b}, P. Sinervo¹⁶⁷, V. Sinetckii¹¹³, S. Singh¹⁵², M. Sioli^{23b,23a}, I. Siral¹³¹,
 S.Yu. Sivoklokov¹¹³, J. Sjölin^{45a,45b}, A. Skaf⁵³, E. Skorda⁹⁷, P. Skubic¹²⁸, M. Slawinska⁸⁵, K. Sliwa¹⁷⁰,
 R. Slovak¹⁴², V. Smakhtin¹⁸⁰, B.H. Smart¹⁴³, J. Smiesko^{28b}, N. Smirnov¹¹², S.Yu. Smirnov¹¹²,
 Y. Smirnov¹¹², L.N. Smirnova^{113,r}, O. Smirnova⁹⁷, E.A. Smith³⁷, H.A. Smith¹³⁴, M. Smizanska⁹⁰,
 K. Smolek¹⁴¹, A. Smykiewicz⁸⁵, A.A. Snesarev¹¹¹, H.L. Snoek¹²⁰, I.M. Snyder¹³¹, S. Snyder²⁹,
 R. Sobie^{176,ab}, A. Soffer¹⁶¹, A. Søgaard⁵⁰, F. Sohns⁵³, C.A. Solans Sanchez³⁶, E.Yu. Soldatov¹¹²,
 U. Soldevila¹⁷⁴, A.A. Solodkov¹²³, A. Soloshenko⁸⁰, O.V. Solovyanov¹²³, V. Solovyev¹³⁷, P. Sommer¹⁴⁹,
 H. Son¹⁷⁰, W. Song¹⁴³, W.Y. Song^{168b}, A. Sopczak¹⁴¹, A.L. Sopio⁹⁵, F. Sopkova^{28b}, S. Sottocornola^{71a,71b},
 R. Soualah^{67a,67c}, A.M. Soukharev^{122b,122a}, D. South⁴⁶, S. Spagnolo^{68a,68b}, M. Spalla¹¹⁵,
 M. Spangenberg¹⁷⁸, F. Spanò⁹⁴, D. Sperlich⁵², T.M. Spieker^{61a}, G. Spigo³⁶, M. Spina¹⁵⁶, D.P. Spiteri⁵⁷,
 M. Spousta¹⁴², A. Stabile^{69a,69b}, B.L. Stamas¹²¹, R. Stamen^{61a}, M. Stamenkovic¹²⁰, E. Stanecka⁸⁵,
 B. Stanislaus¹³⁴, M.M. Stanitzki⁴⁶, M. Stankaityte¹³⁴, B. Stapf¹²⁰, E.A. Starchenko¹²³, G.H. Stark¹⁴⁵,
 J. Stark⁵⁸, P. Staroba¹⁴⁰, P. Starovoitov^{61a}, S. Stärz¹⁰⁴, R. Staszewski⁸⁵, G. Stavropoulos⁴⁴, M. Stegler⁴⁶,
 P. Steinberg²⁹, A.L. Steinhebel¹³¹, B. Stelzer^{152,168a}, H.J. Stelzer¹³⁸, O. Stelzer-Chilton^{168a}, H. Stenzel⁵⁶,
 T.J. Stevenson¹⁵⁶, G.A. Stewart³⁶, M.C. Stockton³⁶, G. Stoica^{27b}, M. Stolarski^{139a}, S. Stonjek¹¹⁵,
 A. Straessner⁴⁸, J. Strandberg¹⁵⁴, S. Strandberg^{45a,45b}, M. Strauss¹²⁸, T. Strebler¹⁰², P. Strizenec^{28b},
 R. Ströhmer¹⁷⁷, D.M. Strom¹³¹, R. Stroynowski⁴², A. Strubig⁵⁰, S.A. Stucci²⁹, B. Stugu¹⁷, J. Stupak¹²⁸,
 N.A. Styles⁴⁶, D. Su¹⁵³, W. Su^{60c,148}, X. Su^{60a}, V.V. Sulin¹¹¹, M.J. Sullivan⁹¹, D.M.S. Sultan⁵⁴,
 S. Sultansoy^{4c}, T. Sumida⁸⁶, S. Sun¹⁰⁶, X. Sun¹⁰¹, K. Suruliz¹⁵⁶, C.J.E. Suster¹⁵⁷, M.R. Sutton¹⁵⁶,
 S. Suzuki⁸², M. Svatos¹⁴⁰, M. Swiatlowski^{168a}, S.P. Swift², T. Swirski¹⁷⁷, A. Sydorenko¹⁰⁰, I. Sykora^{28a},
 M. Sykora¹⁴², T. Sykora¹⁴², D. Ta¹⁰⁰, K. Tackmann^{46,x}, J. Taenzer¹⁶¹, A. Taffard¹⁷¹, R. Tafirout^{168a},
 E. Tagiev¹²³, R. Takashima⁸⁷, K. Takeda⁸³, T. Takeshita¹⁵⁰, E.P. Takeva⁵⁰, Y. Takubo⁸², M. Talby¹⁰²,
 A.A. Talyshев^{122b,122a}, K.C. Tam^{63b}, N.M. Tamir¹⁶¹, J. Tanaka¹⁶³, R. Tanaka⁶⁵, S. Tapia Araya¹⁷³,
 S. Tapprogge¹⁰⁰, A. Tarek Abouelfadl Mohamed¹⁰⁷, S. Tarem¹⁶⁰, K. Tariq^{60b}, G. Tarna^{27b,d},
 G.F. Tartarelli^{69a}, P. Tas¹⁴², M. Tasevsky¹⁴⁰, T. Tashiro⁸⁶, E. Tassi^{41b,41a}, A. Tavares Delgado^{139a},
 Y. Tayalati^{35f}, A.J. Taylor⁵⁰, G.N. Taylor¹⁰⁵, W. Taylor^{168b}, H. Teagle⁹¹, A.S. Tee⁹⁰,
 R. Teixeira De Lima¹⁵³, P. Teixeira-Dias⁹⁴, H. Ten Kate³⁶, J.J. Teoh¹²⁰, S. Terada⁸², K. Terashi¹⁶³,
 J. Terron⁹⁹, S. Terzo¹⁴, M. Testa⁵¹, R.J. Teuscher^{167,ab}, S.J. Thais¹⁸³, N. Themistokleous⁵⁰,
 T. Theveneaux-Pelzer⁴⁶, F. Thiele⁴⁰, D.W. Thomas⁹⁴, J.O. Thomas⁴², J.P. Thomas²¹, E.A. Thompson⁴⁶,
 P.D. Thompson²¹, E. Thomson¹³⁶, E.J. Thorpe⁹³, R.E. Ticse Torres⁵³, V.O. Tikhomirov^{111,ai},
 Yu.A. Tikhonov^{122b,122a}, S. Timoshenko¹¹², P. Tipton¹⁸³, S. Tisserant¹⁰², K. Todome^{23b,23a},
 S. Todorova-Nova¹⁴², S. Todt⁴⁸, J. Tojo⁸⁸, S. Tokár^{28a}, K. Tokushuku⁸², E. Tolley¹²⁷, R. Tombs³²,
 K.G. Tomiwa^{33f}, M. Tomoto¹¹⁷, L. Tompkins¹⁵³, P. Tornambe¹⁰³, E. Torrence¹³¹, H. Torres⁴⁸,
 E. Torró Pastor¹⁴⁸, C. Toscirci¹³⁴, J. Toth^{102,aa}, D.R. Tovey¹⁴⁹, A. Traeet¹⁷, C.J. Treado¹²⁵, T. Trefzger¹⁷⁷,
 F. Tresoldi¹⁵⁶, A. Tricoli²⁹, I.M. Trigger^{168a}, S. Trincatz-Duvoid¹³⁵, D.A. Trischuk¹⁷⁵, W. Trischuk¹⁶⁷,
 B. Trocmé⁵⁸, A. Trofymov⁶⁵, C. Troncon^{69a}, F. Trovato¹⁵⁶, L. Truong^{33c}, M. Trzebinski⁸⁵, A. Trzupek⁸⁵,
 F. Tsai⁴⁶, J.C.-L. Tseng¹³⁴, P.V. Tsiareshka^{108,af}, A. Tsirigotis^{162,u}, V. Tsiskaridze¹⁵⁵, E.G. Tskhadadze^{159a},
 M. Tsopoulou¹⁶², I.I. Tsukerman¹²⁴, V. Tsulaia¹⁸, S. Tsuno⁸², D. Tsybychev¹⁵⁵, Y. Tu^{63b}, A. Tudorache^{27b},
 V. Tudorache^{27b}, T.T. Tulbure^{27a}, A.N. Tuna⁵⁹, S. Turchikhin⁸⁰, D. Turgeman¹⁸⁰, I. Turk Cakir^{4b,s},

R.J. Turner²¹, R. Turra^{69a}, P.M. Tuts³⁹, S. Tzamarias¹⁶², E. Tzovara¹⁰⁰, K. Uchida¹⁶³, F. Ukegawa¹⁶⁹, G. Unal³⁶, M. Unal¹¹, A. Undrus²⁹, G. Unel¹⁷¹, F.C. Ungaro¹⁰⁵, Y. Unno⁸², K. Uno¹⁶³, J. Urban^{28b}, P. Urquijo¹⁰⁵, G. Usai⁸, Z. Uysal^{12d}, V. Vacek¹⁴¹, B. Vachon¹⁰⁴, K.O.H. Vadla¹³³, T. Vafeiadis³⁶, A. Vaidya⁹⁵, C. Valderanis¹¹⁴, E. Valdes Santurio^{45a,45b}, M. Valente⁵⁴, S. Valentini^{23b,23a}, A. Valero¹⁷⁴, L. Valéry⁴⁶, R.A. Vallance²¹, A. Vallier³⁶, J.A. Valls Ferrer¹⁷⁴, T.R. Van Daalen¹⁴, P. Van Gemmeren⁶, S. Van Stroud⁹⁵, I. Van Vulpen¹²⁰, M. Vanadia^{74a,74b}, W. Vandelli³⁶, M. Vandembroucke¹⁴⁴, E.R. Vandewall¹²⁹, A. Vaniachine¹⁶⁶, D. Vannicola^{73a,73b}, R. Vari^{73a}, E.W. Varnes⁷, C. Varni^{55b,55a}, T. Varol¹⁵⁸, D. Varouchas⁶⁵, K.E. Varvell¹⁵⁷, M.E. Vasile^{27b}, G.A. Vasquez¹⁷⁶, F. Vazeille³⁸, D. Vazquez Furelos¹⁴, T. Vazquez Schroeder³⁶, J. Veatch⁵³, V. Vecchio¹⁰¹, M.J. Veen¹²⁰, L.M. Veloce¹⁶⁷, F. Veloso^{139a,139c}, S. Veneziano^{73a}, A. Ventura^{68a,68b}, A. Verbytskyi¹¹⁵, V. Vercesi^{71a}, M. Verducci^{72a,72b}, C.M. Vergel Infante⁷⁹, C. Vergis²⁴, W. Verkerke¹²⁰, A.T. Vermeulen¹²⁰, J.C. Vermeulen¹²⁰, C. Vernieri¹⁵³, M.C. Vetterli^{152,am}, N. Viaux Maira^{146d}, T. Vickey¹⁴⁹, O.E. Vickey Boeriu¹⁴⁹, G.H.A. Viehhauser¹³⁴, L. Vigani^{61b}, M. Villa^{23b,23a}, M. Villaplana Perez³, E.M. Villhauer⁵⁰, E. Vilucchi⁵¹, M.G. Vincter³⁴, G.S. Virdee²¹, A. Vishwakarma⁵⁰, C. Vittori^{23b,23a}, I. Vivarelli¹⁵⁶, M. Vogel¹⁸², P. Vokac¹⁴¹, S.E. von Buddenbrock^{33f}, E. Von Toerne²⁴, V. Vorobel¹⁴², K. Vorobev¹¹², M. Vos¹⁷⁴, J.H. Vossebeld⁹¹, M. Vozak¹⁰¹, N. Vranjes¹⁶, M. Vranjes Milosavljevic¹⁶, V. Vrba^{141,*}, M. Vreeswijk¹²⁰, R. Vuillermet³⁶, I. Vukotic³⁷, S. Wada¹⁶⁹, P. Wagner²⁴, W. Wagner¹⁸², J. Wagner-Kuhr¹¹⁴, S. Wahdan¹⁸², H. Wahlberg⁸⁹, R. Wakasa¹⁶⁹, V.M. Walbrecht¹¹⁵, J. Walder¹⁴³, R. Walker¹¹⁴, S.D. Walker⁹⁴, W. Walkowiak¹⁵¹, V. Wallangen^{45a,45b}, A.M. Wang⁵⁹, A.Z. Wang¹⁸¹, C. Wang^{60a}, C. Wang^{60c}, F. Wang¹⁸¹, H. Wang¹⁸, H. Wang³, J. Wang^{63a}, P. Wang⁴², Q. Wang¹²⁸, R.-J. Wang¹⁰⁰, R. Wang^{60a}, R. Wang⁶, S.M. Wang¹⁵⁸, W.T. Wang^{60a}, W. Wang^{15c}, W.X. Wang^{60a}, Y. Wang^{60a}, Z. Wang¹⁰⁶, C. Wanotayaroj⁴⁶, A. Warburton¹⁰⁴, C.P. Ward³², D.R. Wardrope⁹⁵, N. Warrack⁵⁷, A.T. Watson²¹, M.F. Watson²¹, G. Watts¹⁴⁸, B.M. Waugh⁹⁵, A.F. Webb¹¹, C. Weber²⁹, M.S. Weber²⁰, S.A. Weber³⁴, S.M. Weber^{61a}, A.R. Weidberg¹³⁴, J. Weingarten⁴⁷, M. Weirich¹⁰⁰, C. Weiser⁵², P.S. Wells³⁶, T. Wenaus²⁹, B. Wendland⁴⁷, T. Wengler³⁶, S. Wenig³⁶, N. Wermes²⁴, M. Wessels^{61a}, T.D. Weston²⁰, K. Whalen¹³¹, A.M. Wharton⁹⁰, A.S. White¹⁰⁶, A. White⁸, M.J. White¹, D. Whiteson¹⁷¹, B.W. Whitmore⁹⁰, W. Wiedenmann¹⁸¹, C. Wiel⁴⁸, M. Wielaers¹⁴³, N. Wieseotte¹⁰⁰, C. Wiglesworth⁴⁰, L.A.M. Wiik-Fuchs⁵², H.G. Wilkens³⁶, L.J. Wilkins⁹⁴, H.H. Williams¹³⁶, S. Williams³², S. Willocq¹⁰³, P.J. Windischhofer¹³⁴, I. Wingerter-Seez⁵, E. Winkels¹⁵⁶, F. Winklmeier¹³¹, B.T. Winter⁵², M. Wittgen¹⁵³, M. Wobisch⁹⁶, A. Wolf¹⁰⁰, R. Wölker¹³⁴, J. Wollrath⁵², M.W. Wolter⁸⁵, H. Wolters^{139a,139c}, V.W.S. Wong¹⁷⁵, N.L. Woods¹⁴⁵, S.D. Worm⁴⁶, B.K. Wosiek⁸⁵, K.W. Woźniak⁸⁵, K. Wright⁵⁷, S.L. Wu¹⁸¹, X. Wu⁵⁴, Y. Wu^{60a}, J. Wuerzinger¹³⁴, T.R. Wyatt¹⁰¹, B.M. Wynne⁵⁰, S. Xella⁴⁰, J. Xiang^{63c}, X. Xiao¹⁰⁶, X. Xie^{60a}, I. Xiotidis¹⁵⁶, D. Xu^{15a}, H. Xu^{60a}, H. Xu^{60a}, L. Xu²⁹, T. Xu¹⁴⁴, W. Xu¹⁰⁶, Z. Xu^{60b}, Z. Xu¹⁵³, B. Yabsley¹⁵⁷, S. Yacoob^{33a}, K. Yajima¹³², D.P. Yallup⁹⁵, N. Yamaguchi⁸⁸, Y. Yamaguchi¹⁶⁵, A. Yamamoto⁸², M. Yamatani¹⁶³, T. Yamazaki¹⁶³, Y. Yamazaki⁸³, J. Yan^{60c}, Z. Yan²⁵, H.J. Yang^{60c,60d}, H.T. Yang¹⁸, S. Yang^{60a}, T. Yang^{63c}, X. Yang^{60b,58}, Y. Yang¹⁶³, Z. Yang^{106,60a}, W.-M. Yao¹⁸, Y.C. Yap⁴⁶, Y. Yasu⁸², E. Yatsenko^{60c}, H. Ye^{15c}, J. Ye⁴², S. Ye²⁹, I. Yeletskikh⁸⁰, M.R. Yexley⁹⁰, E. Yigitbasi²⁵, P. Yin³⁹, K. Yorita¹⁷⁹, K. Yoshihara⁷⁹, C.J.S. Young³⁶, C. Young¹⁵³, J. Yu⁷⁹, R. Yuan^{60b,h}, X. Yue^{61a}, M. Zaazoua^{35f}, B. Zabinski⁸⁵, G. Zacharis¹⁰, E. Zaffaroni⁵⁴, J. Zahreddine¹³⁵, A.M. Zaitsev^{123,ah}, T. Zakareishvili^{159b}, N. Zakharchuk³⁴, S. Zambito³⁶, D. Zanzi³⁶, D.R. Zaripovas⁵⁷, S.V. Zeißner⁴⁷, C. Zeitnitz¹⁸², G. Zemaityte¹³⁴, J.C. Zeng¹⁷³, O. Zenin¹²³, T. Ženiš^{28a}, D. Zerwas⁶⁵, M. Zgubič¹³⁴, B. Zhang^{15c}, D.F. Zhang^{15b}, G. Zhang^{15b}, J. Zhang⁶, K. Zhang^{15a}, L. Zhang^{15c}, L. Zhang^{60a}, M. Zhang¹⁷³, R. Zhang¹⁸¹, S. Zhang¹⁰⁶, X. Zhang^{60c}, X. Zhang^{60b}, Y. Zhang^{15a,15d}, Z. Zhang^{63a}, Z. Zhang⁶⁵, P. Zhao⁴⁹, Z. Zhao^{60a}, A. Zhemchugov⁸⁰, Z. Zheng¹⁰⁶, D. Zhong¹⁷³, B. Zhou¹⁰⁶, C. Zhou¹⁸¹, H. Zhou⁷, M.S. Zhou^{15a,15d}, M. Zhou¹⁵⁵, N. Zhou^{60c}, Y. Zhou⁷, C.G. Zhu^{60b}, C. Zhu^{15a,15d}, H.L. Zhu^{60a}, H. Zhu^{15a}, J. Zhu¹⁰⁶, Y. Zhu^{60a}, X. Zhuang^{15a}, K. Zhukov¹¹¹, V. Zhulanov^{122b,122a}, D. Ziemińska⁶⁶, N.I. Zimine⁸⁰, S. Zimmermann^{52,*}, Z. Zinonos¹¹⁵, M. Ziolkowski¹⁵¹, L. Živković¹⁶, G. Zobernig¹⁸¹, A. Zoccoli^{23b,23a}, K. Zoch⁵³, T.G. Zorbas¹⁴⁹, R. Zou³⁷, L. Zwalski³⁶.

- ¹Department of Physics, University of Adelaide, Adelaide; Australia.
- ²Physics Department, SUNY Albany, Albany NY; United States of America.
- ³Department of Physics, University of Alberta, Edmonton AB; Canada.
- ^{4(a)}Department of Physics, Ankara University, Ankara; ^(b)Istanbul Aydin University, Application and Research Center for Advanced Studies, Istanbul; ^(c)Division of Physics, TOBB University of Economics and Technology, Ankara; Turkey.
- ⁵LAPP, Univ. Savoie Mont Blanc, CNRS/IN2P3, Annecy ; France.
- ⁶High Energy Physics Division, Argonne National Laboratory, Argonne IL; United States of America.
- ⁷Department of Physics, University of Arizona, Tucson AZ; United States of America.
- ⁸Department of Physics, University of Texas at Arlington, Arlington TX; United States of America.
- ⁹Physics Department, National and Kapodistrian University of Athens, Athens; Greece.
- ¹⁰Physics Department, National Technical University of Athens, Zografou; Greece.
- ¹¹Department of Physics, University of Texas at Austin, Austin TX; United States of America.
- ^{12(a)}Bahcesehir University, Faculty of Engineering and Natural Sciences, Istanbul; ^(b)Istanbul Bilgi University, Faculty of Engineering and Natural Sciences, Istanbul; ^(c)Department of Physics, Bogazici University, Istanbul; ^(d)Department of Physics Engineering, Gaziantep University, Gaziantep; Turkey.
- ¹³Institute of Physics, Azerbaijan Academy of Sciences, Baku; Azerbaijan.
- ¹⁴Institut de Física d'Altes Energies (IFAE), Barcelona Institute of Science and Technology, Barcelona; Spain.
- ^{15(a)}Institute of High Energy Physics, Chinese Academy of Sciences, Beijing; ^(b)Physics Department, Tsinghua University, Beijing; ^(c)Department of Physics, Nanjing University, Nanjing; ^(d)University of Chinese Academy of Science (UCAS), Beijing, China.
- ¹⁶Institute of Physics, University of Belgrade, Belgrade; Serbia.
- ¹⁷Department for Physics and Technology, University of Bergen, Bergen; Norway.
- ¹⁸Physics Division, Lawrence Berkeley National Laboratory and University of California, Berkeley CA; United States of America.
- ¹⁹Institut für Physik, Humboldt Universität zu Berlin, Berlin; Germany.
- ²⁰Albert Einstein Center for Fundamental Physics and Laboratory for High Energy Physics, University of Bern, Bern; Switzerland.
- ²¹School of Physics and Astronomy, University of Birmingham, Birmingham; United Kingdom.
- ^{22(a)}Facultad de Ciencias y Centro de Investigaciones, Universidad Antonio Nariño, Bogotá; ^(b)Departamento de Física, Universidad Nacional de Colombia, Bogotá, Colombia; Colombia.
- ^{23(a)}INFN Bologna and Universita' di Bologna, Dipartimento di Fisica; ^(b)INFN Sezione di Bologna; Italy.
- ²⁴Physikalisches Institut, Universität Bonn, Bonn; Germany.
- ²⁵Department of Physics, Boston University, Boston MA; United States of America.
- ²⁶Department of Physics, Brandeis University, Waltham MA; United States of America.
- ^{27(a)}Transilvania University of Brasov, Brasov; ^(b)Horia Hulubei National Institute of Physics and Nuclear Engineering, Bucharest; ^(c)Department of Physics, Alexandru Ioan Cuza University of Iasi, Iasi; ^(d)National Institute for Research and Development of Isotopic and Molecular Technologies, Physics Department, Cluj-Napoca; ^(e)University Politehnica Bucharest, Bucharest; ^(f)West University in Timisoara, Timisoara; Romania.
- ^{28(a)}Faculty of Mathematics, Physics and Informatics, Comenius University, Bratislava; ^(b)Department of Subnuclear Physics, Institute of Experimental Physics of the Slovak Academy of Sciences, Kosice; Slovak Republic.
- ²⁹Physics Department, Brookhaven National Laboratory, Upton NY; United States of America.
- ³⁰Departamento de Física, Universidad de Buenos Aires, Buenos Aires; Argentina.
- ³¹California State University, CA; United States of America.

- ³²Cavendish Laboratory, University of Cambridge, Cambridge; United Kingdom.
- ³³^(a)Department of Physics, University of Cape Town, Cape Town;^(b)iThemba Labs, Western Cape;^(c)Department of Mechanical Engineering Science, University of Johannesburg, Johannesburg;^(d)National Institute of Physics, University of the Philippines Diliman;^(e)University of South Africa, Department of Physics, Pretoria;^(f)School of Physics, University of the Witwatersrand, Johannesburg; South Africa.
- ³⁴Department of Physics, Carleton University, Ottawa ON; Canada.
- ³⁵^(a)Faculté des Sciences Ain Chock, Réseau Universitaire de Physique des Hautes Energies - Université Hassan II, Casablanca;^(b)Faculté des Sciences, Université Ibn-Tofail, Kénitra;^(c)Faculté des Sciences Semlalia, Université Cadi Ayyad, LPHEA-Marrakech;^(d)Moroccan Foundation for Advanced Science Innovation and Research (MASCIR), Rabat;^(e)LPMR, Faculté des Sciences, Université Mohamed Premier, Oujda;^(f)Faculté des sciences, Université Mohammed V, Rabat; Morocco.
- ³⁶CERN, Geneva; Switzerland.
- ³⁷Enrico Fermi Institute, University of Chicago, Chicago IL; United States of America.
- ³⁸LPC, Université Clermont Auvergne, CNRS/IN2P3, Clermont-Ferrand; France.
- ³⁹Nevis Laboratory, Columbia University, Irvington NY; United States of America.
- ⁴⁰Niels Bohr Institute, University of Copenhagen, Copenhagen; Denmark.
- ⁴¹^(a)Dipartimento di Fisica, Università della Calabria, Rende;^(b)INFN Gruppo Collegato di Cosenza, Laboratori Nazionali di Frascati; Italy.
- ⁴²Physics Department, Southern Methodist University, Dallas TX; United States of America.
- ⁴³Physics Department, University of Texas at Dallas, Richardson TX; United States of America.
- ⁴⁴National Centre for Scientific Research "Demokritos", Agia Paraskevi; Greece.
- ⁴⁵^(a)Department of Physics, Stockholm University;^(b)Oskar Klein Centre, Stockholm; Sweden.
- ⁴⁶Deutsches Elektronen-Synchrotron DESY, Hamburg and Zeuthen; Germany.
- ⁴⁷Lehrstuhl für Experimentelle Physik IV, Technische Universität Dortmund, Dortmund; Germany.
- ⁴⁸Institut für Kern- und Teilchenphysik, Technische Universität Dresden, Dresden; Germany.
- ⁴⁹Department of Physics, Duke University, Durham NC; United States of America.
- ⁵⁰SUPA - School of Physics and Astronomy, University of Edinburgh, Edinburgh; United Kingdom.
- ⁵¹INFN e Laboratori Nazionali di Frascati, Frascati; Italy.
- ⁵²Physikalisches Institut, Albert-Ludwigs-Universität Freiburg, Freiburg; Germany.
- ⁵³II. Physikalisches Institut, Georg-August-Universität Göttingen, Göttingen; Germany.
- ⁵⁴Département de Physique Nucléaire et Corpusculaire, Université de Genève, Genève; Switzerland.
- ⁵⁵^(a)Dipartimento di Fisica, Università di Genova, Genova;^(b)INFN Sezione di Genova; Italy.
- ⁵⁶II. Physikalisches Institut, Justus-Liebig-Universität Giessen, Giessen; Germany.
- ⁵⁷SUPA - School of Physics and Astronomy, University of Glasgow, Glasgow; United Kingdom.
- ⁵⁸LPSC, Université Grenoble Alpes, CNRS/IN2P3, Grenoble INP, Grenoble; France.
- ⁵⁹Laboratory for Particle Physics and Cosmology, Harvard University, Cambridge MA; United States of America.
- ⁶⁰^(a)Department of Modern Physics and State Key Laboratory of Particle Detection and Electronics, University of Science and Technology of China, Hefei;^(b)Institute of Frontier and Interdisciplinary Science and Key Laboratory of Particle Physics and Particle Irradiation (MOE), Shandong University, Qingdao;^(c)School of Physics and Astronomy, Shanghai Jiao Tong University, Key Laboratory for Particle Astrophysics and Cosmology (MOE), SKLPPC, Shanghai;^(d)Tsung-Dao Lee Institute, Shanghai; China.
- ⁶¹^(a)Kirchhoff-Institut für Physik, Ruprecht-Karls-Universität Heidelberg, Heidelberg;^(b)Physikalisches Institut, Ruprecht-Karls-Universität Heidelberg, Heidelberg; Germany.
- ⁶²Faculty of Applied Information Science, Hiroshima Institute of Technology, Hiroshima; Japan.
- ⁶³^(a)Department of Physics, Chinese University of Hong Kong, Shatin, N.T., Hong Kong;^(b)Department

of Physics, University of Hong Kong, Hong Kong;^(c)Department of Physics and Institute for Advanced Study, Hong Kong University of Science and Technology, Clear Water Bay, Kowloon, Hong Kong; China.

⁶⁴Department of Physics, National Tsing Hua University, Hsinchu; Taiwan.

⁶⁵IJCLab, Université Paris-Saclay, CNRS/IN2P3, 91405, Orsay; France.

⁶⁶Department of Physics, Indiana University, Bloomington IN; United States of America.

^{67(a)}INFN Gruppo Collegato di Udine, Sezione di Trieste, Udine;^(b)ICTP, Trieste;^(c)Dipartimento Politecnico di Ingegneria e Architettura, Università di Udine, Udine; Italy.

^{68(a)}INFN Sezione di Lecce;^(b)Dipartimento di Matematica e Fisica, Università del Salento, Lecce; Italy.

^{69(a)}INFN Sezione di Milano;^(b)Dipartimento di Fisica, Università di Milano, Milano; Italy.

^{70(a)}INFN Sezione di Napoli;^(b)Dipartimento di Fisica, Università di Napoli, Napoli; Italy.

^{71(a)}INFN Sezione di Pavia;^(b)Dipartimento di Fisica, Università di Pavia, Pavia; Italy.

^{72(a)}INFN Sezione di Pisa;^(b)Dipartimento di Fisica E. Fermi, Università di Pisa, Pisa; Italy.

^{73(a)}INFN Sezione di Roma;^(b)Dipartimento di Fisica, Sapienza Università di Roma, Roma; Italy.

^{74(a)}INFN Sezione di Roma Tor Vergata;^(b)Dipartimento di Fisica, Università di Roma Tor Vergata, Roma; Italy.

^{75(a)}INFN Sezione di Roma Tre;^(b)Dipartimento di Matematica e Fisica, Università Roma Tre, Roma; Italy.

^{76(a)}INFN-TIFPA;^(b)Università degli Studi di Trento, Trento; Italy.

⁷⁷Institut für Astro- und Teilchenphysik, Leopold-Franzens-Universität, Innsbruck; Austria.

⁷⁸University of Iowa, Iowa City IA; United States of America.

⁷⁹Department of Physics and Astronomy, Iowa State University, Ames IA; United States of America.

⁸⁰Joint Institute for Nuclear Research, Dubna; Russia.

^{81(a)}Departamento de Engenharia Elétrica, Universidade Federal de Juiz de Fora (UFJF), Juiz de Fora;^(b)Universidade Federal do Rio De Janeiro COPPE/EE/IF, Rio de Janeiro;^(c)Instituto de Física, Universidade de São Paulo, São Paulo; Brazil.

⁸²KEK, High Energy Accelerator Research Organization, Tsukuba; Japan.

⁸³Graduate School of Science, Kobe University, Kobe; Japan.

^{84(a)}AGH University of Science and Technology, Faculty of Physics and Applied Computer Science, Krakow;^(b)Marian Smoluchowski Institute of Physics, Jagiellonian University, Krakow; Poland.

⁸⁵Institute of Nuclear Physics Polish Academy of Sciences, Krakow; Poland.

⁸⁶Faculty of Science, Kyoto University, Kyoto; Japan.

⁸⁷Kyoto University of Education, Kyoto; Japan.

⁸⁸Research Center for Advanced Particle Physics and Department of Physics, Kyushu University, Fukuoka ; Japan.

⁸⁹Instituto de Física La Plata, Universidad Nacional de La Plata and CONICET, La Plata; Argentina.

⁹⁰Physics Department, Lancaster University, Lancaster; United Kingdom.

⁹¹Oliver Lodge Laboratory, University of Liverpool, Liverpool; United Kingdom.

⁹²Department of Experimental Particle Physics, Jožef Stefan Institute and Department of Physics, University of Ljubljana, Ljubljana; Slovenia.

⁹³School of Physics and Astronomy, Queen Mary University of London, London; United Kingdom.

⁹⁴Department of Physics, Royal Holloway University of London, Egham; United Kingdom.

⁹⁵Department of Physics and Astronomy, University College London, London; United Kingdom.

⁹⁶Louisiana Tech University, Ruston LA; United States of America.

⁹⁷Fysiska institutionen, Lunds universitet, Lund; Sweden.

⁹⁸Centre de Calcul de l’Institut National de Physique Nucléaire et de Physique des Particules (IN2P3), Villeurbanne; France.

⁹⁹Departamento de Física Teorica C-15 and CIAFF, Universidad Autónoma de Madrid, Madrid; Spain.

- ¹⁰⁰Institut für Physik, Universität Mainz, Mainz; Germany.
- ¹⁰¹School of Physics and Astronomy, University of Manchester, Manchester; United Kingdom.
- ¹⁰²CPPM, Aix-Marseille Université, CNRS/IN2P3, Marseille; France.
- ¹⁰³Department of Physics, University of Massachusetts, Amherst MA; United States of America.
- ¹⁰⁴Department of Physics, McGill University, Montreal QC; Canada.
- ¹⁰⁵School of Physics, University of Melbourne, Victoria; Australia.
- ¹⁰⁶Department of Physics, University of Michigan, Ann Arbor MI; United States of America.
- ¹⁰⁷Department of Physics and Astronomy, Michigan State University, East Lansing MI; United States of America.
- ¹⁰⁸B.I. Stepanov Institute of Physics, National Academy of Sciences of Belarus, Minsk; Belarus.
- ¹⁰⁹Research Institute for Nuclear Problems of Byelorussian State University, Minsk; Belarus.
- ¹¹⁰Group of Particle Physics, University of Montreal, Montreal QC; Canada.
- ¹¹¹P.N. Lebedev Physical Institute of the Russian Academy of Sciences, Moscow; Russia.
- ¹¹²National Research Nuclear University MEPhI, Moscow; Russia.
- ¹¹³D.V. Skobeltsyn Institute of Nuclear Physics, M.V. Lomonosov Moscow State University, Moscow; Russia.
- ¹¹⁴Fakultät für Physik, Ludwig-Maximilians-Universität München, München; Germany.
- ¹¹⁵Max-Planck-Institut für Physik (Werner-Heisenberg-Institut), München; Germany.
- ¹¹⁶Nagasaki Institute of Applied Science, Nagasaki; Japan.
- ¹¹⁷Graduate School of Science and Kobayashi-Maskawa Institute, Nagoya University, Nagoya; Japan.
- ¹¹⁸Department of Physics and Astronomy, University of New Mexico, Albuquerque NM; United States of America.
- ¹¹⁹Institute for Mathematics, Astrophysics and Particle Physics, Radboud University/Nikhef, Nijmegen; Netherlands.
- ¹²⁰Nikhef National Institute for Subatomic Physics and University of Amsterdam, Amsterdam; Netherlands.
- ¹²¹Department of Physics, Northern Illinois University, DeKalb IL; United States of America.
- ^{122(a)}Budker Institute of Nuclear Physics and NSU, SB RAS, Novosibirsk; ^(b)Novosibirsk State University Novosibirsk; Russia.
- ¹²³Institute for High Energy Physics of the National Research Centre Kurchatov Institute, Protvino; Russia.
- ¹²⁴Institute for Theoretical and Experimental Physics named by A.I. Alikhanov of National Research Centre "Kurchatov Institute", Moscow; Russia.
- ¹²⁵Department of Physics, New York University, New York NY; United States of America.
- ¹²⁶Ochanomizu University, Otsuka, Bunkyo-ku, Tokyo; Japan.
- ¹²⁷Ohio State University, Columbus OH; United States of America.
- ¹²⁸Homer L. Dodge Department of Physics and Astronomy, University of Oklahoma, Norman OK; United States of America.
- ¹²⁹Department of Physics, Oklahoma State University, Stillwater OK; United States of America.
- ¹³⁰Palacký University, Joint Laboratory of Optics, Olomouc; Czech Republic.
- ¹³¹Institute for Fundamental Science, University of Oregon, Eugene, OR; United States of America.
- ¹³²Graduate School of Science, Osaka University, Osaka; Japan.
- ¹³³Department of Physics, University of Oslo, Oslo; Norway.
- ¹³⁴Department of Physics, Oxford University, Oxford; United Kingdom.
- ¹³⁵LPNHE, Sorbonne Université, Université de Paris, CNRS/IN2P3, Paris; France.
- ¹³⁶Department of Physics, University of Pennsylvania, Philadelphia PA; United States of America.
- ¹³⁷Konstantinov Nuclear Physics Institute of National Research Centre "Kurchatov Institute", PNPI, St. Petersburg; Russia.

¹³⁸Department of Physics and Astronomy, University of Pittsburgh, Pittsburgh PA; United States of America.

^{139(a)}Laboratório de Instrumentação e Física Experimental de Partículas - LIP, Lisboa; ^(b)Departamento de Física, Faculdade de Ciências, Universidade de Lisboa, Lisboa; ^(c)Departamento de Física, Universidade de Coimbra, Coimbra; ^(d)Centro de Física Nuclear da Universidade de Lisboa, Lisboa; ^(e)Departamento de Física, Universidade do Minho, Braga; ^(f)Departamento de Física Teórica y del Cosmos, Universidad de Granada, Granada (Spain); ^(g)Dep Física and CEFITEC of Faculdade de Ciências e Tecnologia, Universidade Nova de Lisboa, Caparica; ^(h)Instituto Superior Técnico, Universidade de Lisboa, Lisboa; Portugal.

¹⁴⁰Institute of Physics of the Czech Academy of Sciences, Prague; Czech Republic.

¹⁴¹Czech Technical University in Prague, Prague; Czech Republic.

¹⁴²Charles University, Faculty of Mathematics and Physics, Prague; Czech Republic.

¹⁴³Particle Physics Department, Rutherford Appleton Laboratory, Didcot; United Kingdom.

¹⁴⁴IRFU, CEA, Université Paris-Saclay, Gif-sur-Yvette; France.

¹⁴⁵Santa Cruz Institute for Particle Physics, University of California Santa Cruz, Santa Cruz CA; United States of America.

^{146(a)}Departamento de Física, Pontificia Universidad Católica de Chile, Santiago; ^(b)Universidad Andres Bello, Department of Physics, Santiago; ^(c)Instituto de Alta Investigación, Universidad de Tarapacá, Arica; ^(d)Departamento de Física, Universidad Técnica Federico Santa María, Valparaíso; Chile.

¹⁴⁷Universidade Federal de São João del Rei (UFSJ), São João del Rei; Brazil.

¹⁴⁸Department of Physics, University of Washington, Seattle WA; United States of America.

¹⁴⁹Department of Physics and Astronomy, University of Sheffield, Sheffield; United Kingdom.

¹⁵⁰Department of Physics, Shinshu University, Nagano; Japan.

¹⁵¹Department Physik, Universität Siegen, Siegen; Germany.

¹⁵²Department of Physics, Simon Fraser University, Burnaby BC; Canada.

¹⁵³SLAC National Accelerator Laboratory, Stanford CA; United States of America.

¹⁵⁴Department of Physics, Royal Institute of Technology, Stockholm; Sweden.

¹⁵⁵Departments of Physics and Astronomy, Stony Brook University, Stony Brook NY; United States of America.

¹⁵⁶Department of Physics and Astronomy, University of Sussex, Brighton; United Kingdom.

¹⁵⁷School of Physics, University of Sydney, Sydney; Australia.

¹⁵⁸Institute of Physics, Academia Sinica, Taipei; Taiwan.

^{159(a)}E. Andronikashvili Institute of Physics, Iv. Javakhishvili Tbilisi State University, Tbilisi; ^(b)High Energy Physics Institute, Tbilisi State University, Tbilisi; Georgia.

¹⁶⁰Department of Physics, Technion, Israel Institute of Technology, Haifa; Israel.

¹⁶¹Raymond and Beverly Sackler School of Physics and Astronomy, Tel Aviv University, Tel Aviv; Israel.

¹⁶²Department of Physics, Aristotle University of Thessaloniki, Thessaloniki; Greece.

¹⁶³International Center for Elementary Particle Physics and Department of Physics, University of Tokyo, Tokyo; Japan.

¹⁶⁴Graduate School of Science and Technology, Tokyo Metropolitan University, Tokyo; Japan.

¹⁶⁵Department of Physics, Tokyo Institute of Technology, Tokyo; Japan.

¹⁶⁶Tomsk State University, Tomsk; Russia.

¹⁶⁷Department of Physics, University of Toronto, Toronto ON; Canada.

^{168(a)}TRIUMF, Vancouver BC; ^(b)Department of Physics and Astronomy, York University, Toronto ON; Canada.

¹⁶⁹Division of Physics and Tomonaga Center for the History of the Universe, Faculty of Pure and Applied Sciences, University of Tsukuba, Tsukuba; Japan.

- ¹⁷⁰Department of Physics and Astronomy, Tufts University, Medford MA; United States of America.
- ¹⁷¹Department of Physics and Astronomy, University of California Irvine, Irvine CA; United States of America.
- ¹⁷²Department of Physics and Astronomy, University of Uppsala, Uppsala; Sweden.
- ¹⁷³Department of Physics, University of Illinois, Urbana IL; United States of America.
- ¹⁷⁴Instituto de Física Corpuscular (IFIC), Centro Mixto Universidad de Valencia - CSIC, Valencia; Spain.
- ¹⁷⁵Department of Physics, University of British Columbia, Vancouver BC; Canada.
- ¹⁷⁶Department of Physics and Astronomy, University of Victoria, Victoria BC; Canada.
- ¹⁷⁷Fakultät für Physik und Astronomie, Julius-Maximilians-Universität Würzburg, Würzburg; Germany.
- ¹⁷⁸Department of Physics, University of Warwick, Coventry; United Kingdom.
- ¹⁷⁹Waseda University, Tokyo; Japan.
- ¹⁸⁰Department of Particle Physics and Astrophysics, Weizmann Institute of Science, Rehovot; Israel.
- ¹⁸¹Department of Physics, University of Wisconsin, Madison WI; United States of America.
- ¹⁸²Fakultät für Mathematik und Naturwissenschaften, Fachgruppe Physik, Bergische Universität Wuppertal, Wuppertal; Germany.
- ¹⁸³Department of Physics, Yale University, New Haven CT; United States of America.
- ^a Also at Borough of Manhattan Community College, City University of New York, New York NY; United States of America.
- ^b Also at Centro Studi e Ricerche Enrico Fermi; Italy.
- ^c Also at CERN, Geneva; Switzerland.
- ^d Also at CPPM, Aix-Marseille Université, CNRS/IN2P3, Marseille; France.
- ^e Also at Département de Physique Nucléaire et Corpusculaire, Université de Genève, Genève; Switzerland.
- ^f Also at Departament de Fisica de la Universitat Autònoma de Barcelona, Barcelona; Spain.
- ^g Also at Department of Financial and Management Engineering, University of the Aegean, Chios; Greece.
- ^h Also at Department of Physics and Astronomy, Michigan State University, East Lansing MI; United States of America.
- ⁱ Also at Department of Physics and Astronomy, University of Louisville, Louisville, KY; United States of America.
- ^j Also at Department of Physics, Ben Gurion University of the Negev, Beer Sheva; Israel.
- ^k Also at Department of Physics, California State University, East Bay; United States of America.
- ^l Also at Department of Physics, California State University, Fresno; United States of America.
- ^m Also at Department of Physics, California State University, Sacramento; United States of America.
- ⁿ Also at Department of Physics, King's College London, London; United Kingdom.
- ^o Also at Department of Physics, St. Petersburg State Polytechnical University, St. Petersburg; Russia.
- ^p Also at Department of Physics, University of Fribourg, Fribourg; Switzerland.
- ^q Also at Dipartimento di Matematica, Informatica e Fisica, Università di Udine, Udine; Italy.
- ^r Also at Faculty of Physics, M.V. Lomonosov Moscow State University, Moscow; Russia.
- ^s Also at Giresun University, Faculty of Engineering, Giresun; Turkey.
- ^t Also at Graduate School of Science, Osaka University, Osaka; Japan.
- ^u Also at Hellenic Open University, Patras; Greece.
- ^v Also at IJCLab, Université Paris-Saclay, CNRS/IN2P3, 91405, Orsay; France.
- ^w Also at Institutio Catalana de Recerca i Estudis Avancats, ICREA, Barcelona; Spain.
- ^x Also at Institut für Experimentalphysik, Universität Hamburg, Hamburg; Germany.
- ^y Also at Institute for Mathematics, Astrophysics and Particle Physics, Radboud University/Nikhef, Nijmegen; Netherlands.
- ^z Also at Institute for Nuclear Research and Nuclear Energy (INRNE) of the Bulgarian Academy of

Sciences, Sofia; Bulgaria.

aa Also at Institute for Particle and Nuclear Physics, Wigner Research Centre for Physics, Budapest; Hungary.

ab Also at Institute of Particle Physics (IPP); Canada.

ac Also at Institute of Physics, Azerbaijan Academy of Sciences, Baku; Azerbaijan.

ad Also at Instituto de Fisica Teorica, IFT-UAM/CSIC, Madrid; Spain.

ae Also at Istanbul University, Dept. of Physics, Istanbul; Turkey.

af Also at Joint Institute for Nuclear Research, Dubna; Russia.

ag Also at Louisiana Tech University, Ruston LA; United States of America.

ah Also at Moscow Institute of Physics and Technology State University, Dolgoprudny; Russia.

ai Also at National Research Nuclear University MEPhI, Moscow; Russia.

aj Also at Physics Department, An-Najah National University, Nablus; Palestine.

ak Also at Physikalisches Institut, Albert-Ludwigs-Universität Freiburg, Freiburg; Germany.

al Also at The City College of New York, New York NY; United States of America.

am Also at TRIUMF, Vancouver BC; Canada.

an Also at Universita di Napoli Parthenope, Napoli; Italy.

ao Also at University of Chinese Academy of Sciences (UCAS), Beijing; China.

* Deceased